Developing concepts for the mine planning of deep-sea poly-metallic nodules

L.J. Zoetmulder

Master of Science Thesis
European Mining Course

October 19, 2020

TU Delft
Allseas

Developing concepts for the mine planning of deep-sea polymetallic nodules

by

L.J. Zoetmulder

Master of Science Thesis
to obtain the degree of Master of Science at
Delft University of Technology,
RWTH Aachen University,
Aalto University.
To be defended on October 19, 2020 at 15:00 PM.

Student number:	4223772	
Project duration:	February 17, 2020 – September 17, 2020	
Supervisor:	Dr. M.W.N. Buxton,	TU Delft
Thesis Committee:	Dr. M. Soleymani Shishvan,	TU Delft
	Dr. S.E. Volkmann,	Allseas
	Dr. B. Yenigul,	Allseas
	Prof. B. G. Lottermoser,	RWTH Aachen
	Prof. J. Leveinen,	Aalto University

TU Delft Allseas

Abstract

Over the last decade, interest in deep-sea mining of Polymetallic Nodules (PN) has reignited. It is driven by an increasing demand of metals that are critical for the digital economy and modern technologies such as batteries. Methods for resource estimation of PN are known and commercially available. There is however no standard method of a planning a deep-sea mining operation. This is an essential step to define mineable reserves. To address this problem, an existing concept has been applied in this thesis. This planning concept was inspired by agriculture and subdivides a mining license area into large scale mining sites, which are in turn subdivided into smaller, continuously mineable areas called mining fields. The subdivision is illustrated in figure 1. The contribution of this thesis is the development of a methodology for this concept. The concept was applied to a framework based upon a license area in the Clarion-Clipperton Zone (CCZ) in the Pacific Ocean.

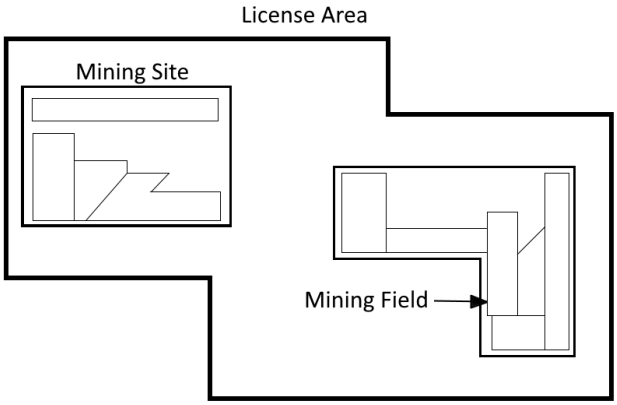

Figure 1: Schematic illustration of a deep-sea mine plan. After [Volkmann, 2018].

The mining will be done using a Nodule Collector (NC), which is a self-propelled machine that continuously gathers PN on the ocean floor and transports them upwards to a vessel at the ocean surface. Certain areas are deemed constrained by slopes or nodule types. Mining sites wherein the NC will operate were outlined within the license area using those constraints and Nodule Abundance (NA). Within the mining sites, a new metric was introduced for assessing the mineability for the NC: the Straight-Line Distance (SLD).

The next step down from mining sites are the mining fields. The operation of the NC within them is approximated by two different driving patterns. Different field shapes are also analyzed, along with the impact of obstacles inside the field. Different methods of creating fields inside the mining sites were considered. The procedure relied upon the SLD to define the boundaries between fields. Two sets of field are created: with elongated shape and compact shape. The best set of fields was selected using the approximation of NC operation.

Lastly, a method for determining the sequence of fields is developed that uses a Genetic Algorithm (GA) as optimization method. It takes into account constraints for mining rate, operational hours, nodule targets and travelling time.

The methods outlined in this thesis are flexible and can be applied in a variety of circumstances. The selection of mineable areas turns out to be the must crucial step. The subsequent delineation of mining fields and sequencing does not make or break the profitability of the operation, although they are essential steps for the definition of mineable reserves.

Acknowledgements

First of all, I would like to thank Allseas. This thesis would not have been possible without their support. They provided me with the data, the workplace, and the guidance that was needed. In particular I would like to thank Sebastian Volkmann, whose vision stands at the base of the work. My gratitude for the weekly meetings, the constructive criticism, and long discussions that covered everything from my thesis to the industry. In addition, I would also like to thank Martin Tan for a fruitful cooperation, and for building the model used in chapter 6.

The contributions of all the thesis committee members are acknowledged and highly appreciated. Buket Yenigul and Wouter Duijnstee from Allseas, your knowledge and feedback have been indispensible. From the TU Delft, Mike Buxton has been a real guide and provided the mining industry perspective. Masoud Soleymani Shishvan has taught me much of what I know about optimization, and was there in the end again to provide useful feedback on the algorithm used in chapter 8.

The biggest thank you goes to my friends and family. I have spent quite a long time at university, and they never stopped supporting me. Finally, all the work is dedicated to my loving girlfriend, who has to listen to me talk about mining, and still refuses to leave me.

Lucas Zoetmulder
October, 2020

Contents

Acronyms

AUV Autonomous Underwater Vehicle. 11, 19

CCZ Clarion-Clipperton Zone. iii, 1, 7–10, 17, 70

DNT Discounted Nodule Tonnage. 57, 58

GA Genetic Algorithm. iii, 14, 56–59

ISA International Seabed Authority. 2

KPI Key Performance Indicator. 3, 4, 17, 33, 37, 39–41, 45, 49, 50, 54, 63

MBES Multibeam Echosounder. 11, 19

MR Mining Rate. 34, 35

MSV Mining Support Vessel. 4, 12, 17

NA Nodule Abundance. iii, 10–12, 18, 19, 22, 35–37, 61

NC Nodule Collector. iii, 2–4, 12–14, 17, 18, 21, 23, 26, 30, 31, 33–37, 39–42, 45, 50, 52, 54, 56, 57, 59, 61, 63, 64

OK Ordinary Kriging. 12, 21, 63

OPPS Open-Pit Production Scheduling. 14, 55, 60, 63, 64

PMT Pilot Mining Test. 17, 19, 29, 31, 58, 59

PN Polymetallic Nodules. iii, 1, 2, 4, 7–12, 15, 17, 21, 24, 39, 57, 70

PR Production Rate. 34–37, 40, 41, 47, 54, 57, 58, 60, 61, 63

SLD Straight-Line Distance. iii, 4, 21, 26–31, 33, 35, 36, 45–47, 49, 51, 52, 54, 61, 63, 64, 71–80

SMU Smallest Mineable Unit. 2, 12, 24, 26

TSP Travelling Salesman Problem. 55, 56, 60, 63

VTS Vertical Transport System. 2, 13, 17

1

Introduction

Polymetallic Nodules (PN) are found at the bottom of the global oceans. They are about the size of potatoes and are composed of mainly iron and manganese oxides. They lie loosely in the sediments on the ocean floor, covering areas larger than the Netherlands. PN grow extremely slowly, acquiring various metals from ocean and/or pore water over millions of years. Some of these metals are of economic interest, notably nickel, cobalt, copper and manganese [Volkmann, 2018][Hein et al., 2020]. A select few are also defined by the European Commission to be critical for modern technologies and the digital economy [EC, 2017]. For example, applications such as electric vehicles and sustainable energy generation. The demand for these critical materials contained in PN, mainly cobalt and rare earths, is predicted to increase [Monnet and Ait Abderrahim, 2016].

High concentrations of PN have been found in the Clarion-Clipperton Zone (CCZ), located in the North-East Pacific Ocean, shown in figure 1.1 [ISA, 2010]. According to Hein et al. [2013], the grades and tonnages of the nodules in the CCZ are moderately well known, and the amount of cobalt, nickel and manganese contained in the nodules exceeds the land-based reserves by a significant amount.

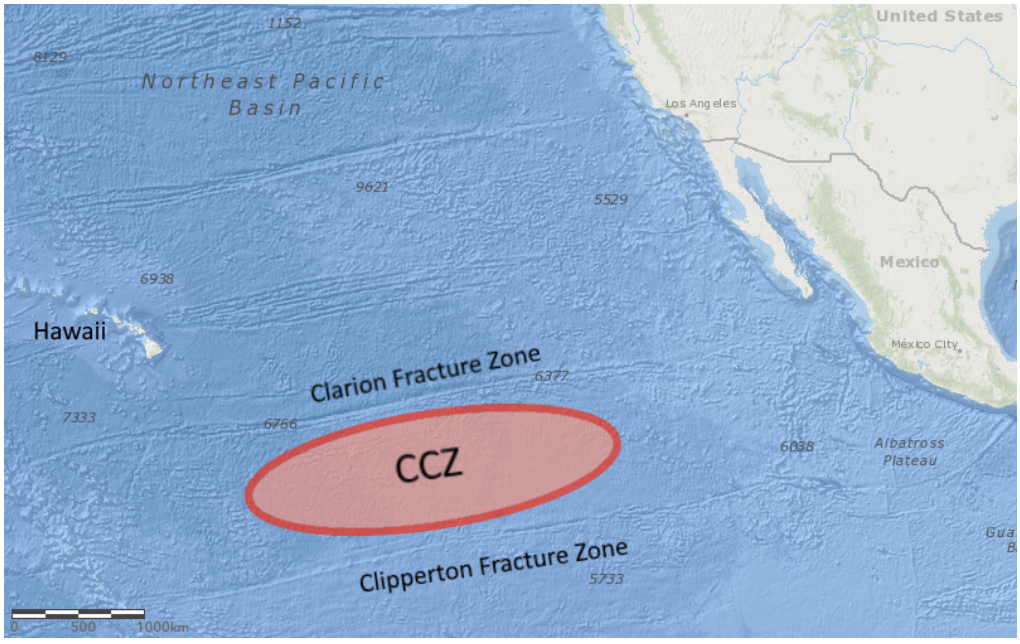

Figure 1.1: The Clarion-Clipperton Zone (CCZ) is located between two fracture zones in the North Pacific Ocean. Map adapted from basemap of ESRI [2020].

PN are found mostly within the first 10cm of the sediment layer and can be approximated as a two-dimensional resource [AMC, 2019]. This makes them different from traditional land-based resources that have an extra dimension because they are found at depth. Mining PN therefore requires a different approach

than terrestrial mines. Earlier, the size of the nodules was described as potato-like. It is no surprise then that the proposed mining method takes inspiration from agriculture. A Nodule Collector (NC) drives over the seabed and can be seen as a harvester of crops (nodules), covering the surface area of the (mining) field until the harvest is complete.

Mining systems are currently being developed by various companies and partnerships. Specifics vary, but the basic idea behind the system is similar and shown in figure 1.2. From a vessel at the ocean surface, a Vertical Transport System (VTS) extends down to the ocean floor. There, the Nodule Collector (NC) picks up the PN and sends them upward through the VTS. They can then be shipped to on-land processing facilities where the valuable metals can be extracted from the nodules.

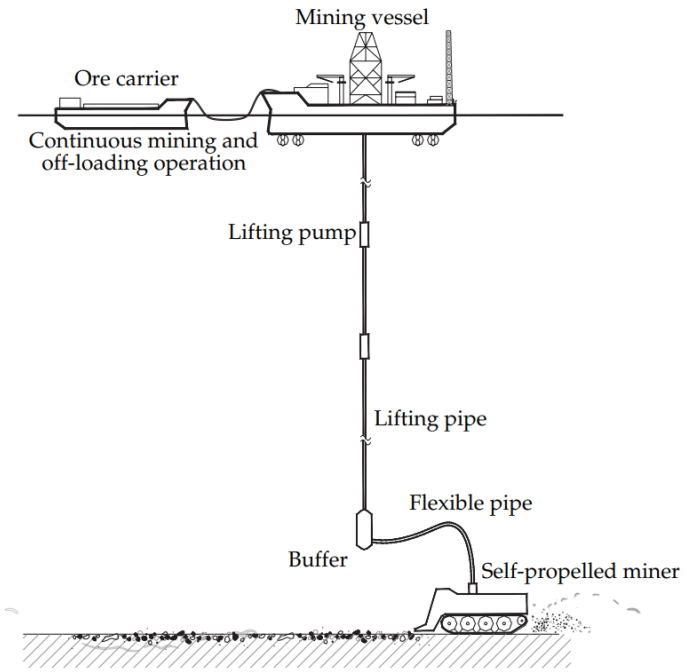

Figure 1.2: Mining concept. Adapted from Lee et al. [2012].

As technical development still ongoing, no deep-sea mining operations have started anywhere in the world and no exploitation licenses have been granted for mining PN [ISA, 2018*b*]. However, the International Seabed Authority (ISA) has so far supplied 22 different countries with a total of 29 contracts for mineral exploration. The exploration is the first step towards mining the PN deposits. Using the results from the exploration, the grades and tonnages of PN can be estimated and the PN can be classified as a resource. The part of the resource that is economically mineable, is called the reserve [CIM, 2014]. There are several criteria before a reserves can be defined. First, the resource needs to be of an adequate level of confidence. Then, to determine if the resource is profitable, a mining plan must be made that considers "modifying factors". These relate to for example environmental, processing or mining factors.

1.1. Problem Statement

Methods for resource estimation of polymetallic nodules are commercially available [Ecorys, 2014]. However, there is currently no standard method for planning a deep-sea mining operation even though this is an essential step for defining reserves [Volkmann, 2018].

According to Ecorys [2014], long-term mine planning is at the lowest technological readiness level and mine planning standards have to be developed and implemented. Because of the differences between deep-sea mining and conventional land-based mining, the planning standards also require a new definition of the Smallest Mineable Unit (SMU), which is the smallest volume of material on which ore waste classification is determined [Poniewierski, 2019]. The problem that this thesis aims to address is thus the absence of a planning methodology for mining polymetallic nodules.

Volkmann [2018] proposed that mine planning will use continuously mineable areas, called "fields", which

can be harvested in a similar pattern as crops in an agricultural field. Still, further research is required concerning field planning, mining pattern and time to mine.

In this thesis, that concept is built upon. Different methods of identifying "good" fields are tested. For that purpose, Key Performance Indicators (KPIs) are introduced. They quantify various aspects related to the amount of nodules that can be mined in a certain amount of time. After the fields are made, different in-field driving patterns are considered for the development of a mine plan and mining sequence. Although the mining plan will be heavily influenced by the final capabilities of the mining system, having a mining plan is very useful for the following reasons:

- It will clarify what the mining system needs to be capable of and give feedback to how the technological development of the mining system should proceed.
- It helps estimation of economic potential within an area. Having a higher certainty of the total amount of nodules that can be mined will lower the investment risks that are associated with deep-sea mining.

1.2. Approach

1.2.1. Objective and Research Questions

The objective of this thesis is to further develop mine planning for mining polymetallic nodules. Therefore, the main research question is: *"How can the mining fields and mining sequence for the mining of deep-sea manganese nodules be planned?"*. The secondary objective is to do a sensitivity analysis of selected operational parameters of the collector in order to determine how their changes affect affect the operation. The following research questions will be answered to reach the objectives:

1. *How can high quality mining areas be identified?*
2. *How can mining sites be selected?*
3. *What are the KPIs of a mining field?*
4. *What are the important parameters for making fields with good KPIs within a site?*
5. *What is the effect of different driving patters on the field KPIs?*
6. *What are the sensitivity of Nodule Collector (NC) parameters with regards to mining KPIs?*
7. *How can land-based mine planning methods be adapted to suit deep-sea mine planning planning?*
8. *Which strategies and/or methods for mine planning can be used to incorporate all relevant aspects?*
9. *Which aspects are most important when deciding upon a mining sequence for the fields?*

1.2.2. Scope

Mine planning is a very broad field. For the thesis objective, only the following aspects are inside the scope:

1. Sequencing and planning path in between fields.
2. Mine planning taking into account selected parameters:
    - Production and capacity targets and constraints.
    - Maneuverability of the collector.
    - Not traversable areas due to slope angle.
    - Quality of the resource. Nodule abundance, nodule size, surface coverage.
    - Field sequence and travel times.
3. Adapting optimization method for use in deep-sea mine planning.

Anything that is not mentioned in the list above is outside the scope of this thesis. Explicitly excluded are the following out-of-scope items:

1. Determining mechanical parameters of mining systems. The design of the collector and other equipment is not dealt with and initial operational parameters are taken from literature or company designs. The objective of the thesis is only to advice which operational parameters are important to consider.

2. No detailed evaluation of path planning. Instead, this thesis will approximate modes of operation for the collector. Excluded are any path calculations of obstacle avoidance, headland turning patterns, effects of lane overlapping and Mining Support Vessel (MSV) maneuvering.
3. No evaluation of preparing the seabed before the mining operation.
4. Mining-related aspects are in-scope, but the other modifying factors for resources and reserves are not. These modifying factors are: metallurgical, economical, marketing legal, social, governmental and environmental.
5. Environmental aspects are out-of-scope. They are one of the modifying factors to quantify reserves. They are of enormous importance and there is a lot of discussion about the impacts of deep-sea mining [DSMC and MiningWatch, 2020]. However, because environmental impacts of deep-sea mining potentially comprises so many different aspects and a lot of unknowns, they cannot be included in the scope of this thesis.

1.3. Thesis Outline

The thesis is built up in sequential steps, outlined below and in figure 1.3.

Chapter 2 The literature is covered for state-of-the-art in deep-sea mining, resource modelling of PN, and mine planning for PN. A brief overview of topics in agricultural planning and field shape analysis that is relevant for deep-sea mine planning will also be given.

Chapter 3 The license area under consideration will be introduced and relevant characteristics discussed. A smaller section of the license area gets special interest as it is the location of the pilot mining test.

Chapter 4 The license area is analyzed using several methods. From a technical report, a resource assessment is recreated, and areas are identified as mineable or constrained. From the various mining constraints, the license area is divided up into several mining sites. Next, A method is proposed to determine the Straight-Line Distance (SLD); the length of a straight path that could be driven by the NC. This serves as a tool for analysis in the next chapters.

Chapter 5 Using the SLD tool, the two main driving patterns for the NC are approximated for assessment of mining fields. This way, KPIs for the mining fields can be calculated for use in following chapters.

Chapter 6 A second approach is tested for the calculation of field KPIs. For this, a comparison is made between deep-sea mining fields and agricultural fields, specifically the shapes of fields. Correlations between field shapes and KPIs are analysed. The impact of obstacles in the field is assessed.

Chapter 7 Using the Straight-Line Distance (SLD) developed in the chapter five, two methods for making mining fields are applied. The first makes long strips, the second makes compact shapes. Both sets of fields are evaluated using both driving methods.

Chapter 8 Using the fields from the chapter four, a mining sequence is made. Time dependent parameters are included such as yearly nodule targets, travel time between fields and discounting.

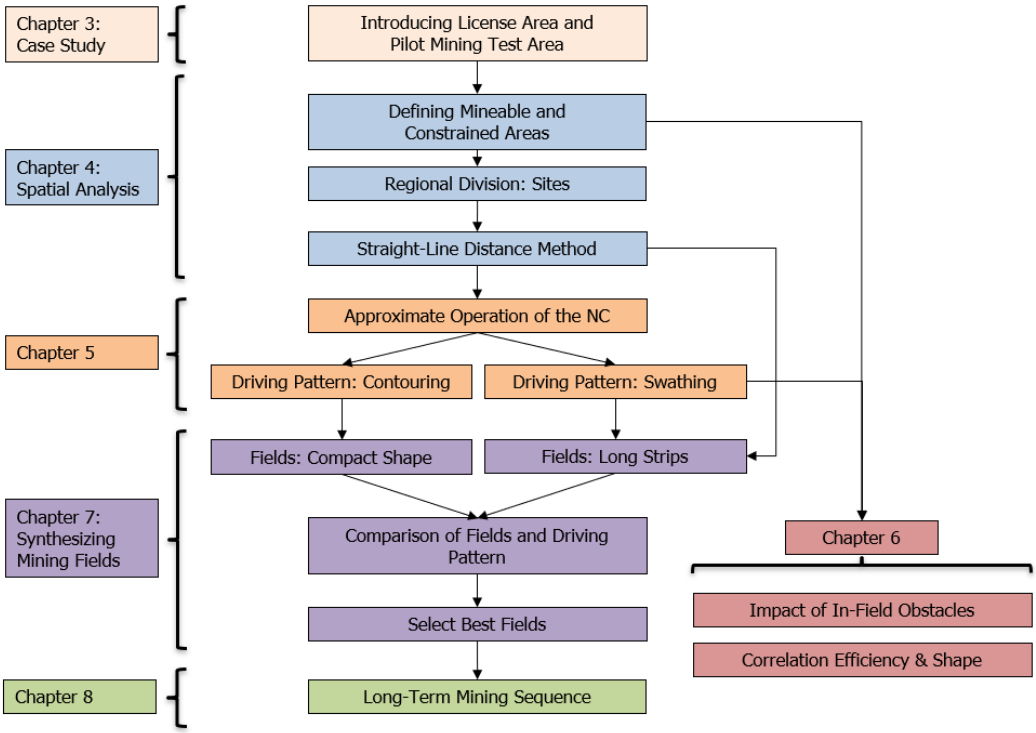

Figure 1.3: Overview of the steps taken in this thesis.

2

Literature Review

In this chapter the most important concepts for this thesis are reviewed from literature. First the historical background is given as context to the current state of affairs. The properties of Polymetallic Nodules (PN) are reviewed to understand the objectives of the mining operation. To understand the data sets that the thesis is built upon, the exploration methods for PN are reviewed, along with the resource modelling process that is used.

To support the development of a planning method in this thesis, the conventional and state-of-the-art methods are reviewed for terrestrial open pit mines. The mining methods for PN are then reviewed, along with suggested methods for planning its operations. Because those methods take inspiration from agriculture, some relevant aspects are reviewed as well.

2.1. Brief History and Recent Interest

The existence of deep-sea minerals was discovered during the expedition of the H.M.S. challenger in the 1870's [Sharma, 2017*b*]. Almost 100 years after the discovery, Mero [1965], predicted that there was an inexhaustible supply of manganese, cobalt, nickel and copper lying on the ocean floor.

This prediction fueled an initial phase of investigation of deep-sea mining from 1972 to 1982. This phase was financed by national agencies, with the United States and the Soviet Union funding most of the expeditions [Glasby, 2000]. These investigations focused on the Clarion-Clipperton Zone (CCZ), located in the pacific ocean. Several pilot mining test were performed and mining was proven to be possible in 1978 when a consortium managed to pump up 800 tons of nodules [Sparenberg, 2019]. However, as global prices of nickel dropped in the 80's, costs turned out to be too high to compete with land-based mining. More than US$ 650 million (in 1982 dollars) was spent on developing technologies and exploring for deep-sea manganese nodules, but in the end no economically feasible mining projects were undertaken [Broadus, 1987].

The information obtained from this large exploration phase has led to a good understanding of PN with the environmental conditions and fundamental processes required for nodule formation well known today [Kuhn et al., 2017]. This existing and accessible knowledge base has helped develop a new phase of interest in deep-sea mining. Between 2011 and 2015, 25 private contractors have obtained exploration licenses for PN in the Clarion-Clipperton Zone (CCZ) [Sharma, 2017*b*], shown in figure 2.1. This interest has been spurred by growing metal prices as well as a perceived growing shortage of certain minerals in terrestrial mining that are needed for modern technologies such as batteries. Hein et al. [2020] compiled data from various sources and calculated the quantities of metals in PN in the CCZ and compared them to terrestrial resources and reserves, table 2.1. The table shows how very large quantities of metals can be found in the CCZ, with some far exceeding terrestrial reserves.

Some of the metals present in the CCZ are also of strategic importance. The European Union, along with several other countries such as the USA, have defined a ranking of critical raw materials that are required for the economy, digital technologies and the energy transition. Their criticality depends on how essential they are, but also the supply risk based on their source. The materials in table 2.1 that the EU defines as critical are predominantly cobalt, but also rare earths, vanadium and tungsten [EC, 2017]. The US considers cobalt, manganese, rare earth elements, tellurium, titanium, vanadium, and zirconium as critical raw materials [Schulz et al., 2017].

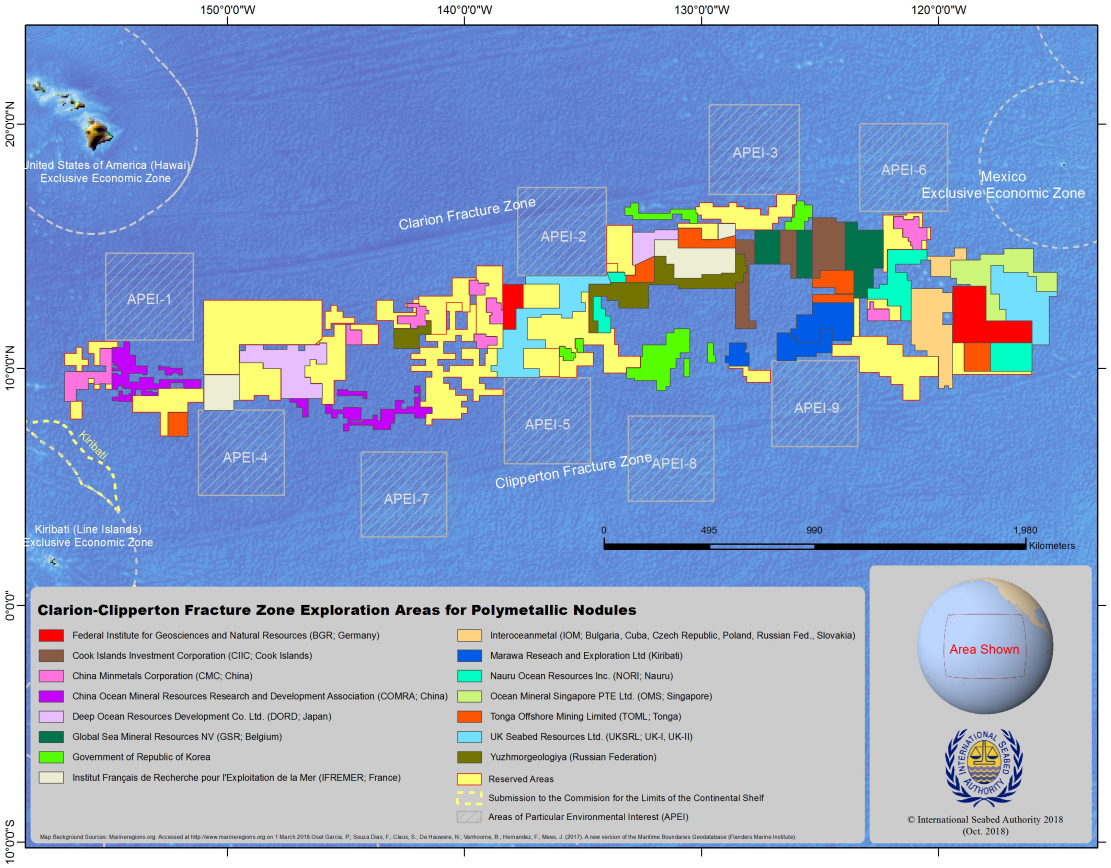

Figure 2.1: All exploration licenses in the CCZ, governed by the ISA. Each license covers an area of 75,000 m^2 [ISA, 2018a].

2.2. Properties of Nodules

According to Kuhn et al. [2017], Polymetallic Nodules (PN), or sometimes called 'Manganese Nodules', can be found in the top sediment layer of all major oceans around 4000–6000 m water depth. A map of all areas that contain the conditions for the nodules to grow is attached in figure A.1. The most well known areas with PN are in the CCZ, Peru Basin, Penrhyn Basin, and the Central Indian Ocean Basin [Hein et al., 2020].

PN are comparable in size to potatoes, have a dry bulk density between 1 to 2.4g/cm^3, and can reach a size of up to 15cm in diameter, although in the CCZ the diameter typically ranges from 2-8cm. PN are created by chemical processes that precipitate concentric layers around a nucleus, for example a shark's tooth [Hein et al., 2020]. The precipitation happens under specific ocean floor sediment and sea water conditions at very slow rate of a few millimeters per million years. Historically, it had been said that the PN were essentially a sustainable resource, growing at a rate faster than humans would be able to exploit [Mero, 1965]. In reality, the growth rates are negligible compared to economical mining rates.

The layers of the PN are alternating iron-rich and manganese-rich. The slight electric charge of the iron (FeOOH) or the manganese (MnO_2) molecules at the surface of these layers attracts ions of the opposite charge that are dissolved in the sea water, such as Cu^{2+}, Ni^{2+} or Co^{2+}. This way, elements that are present in trace amounts in the sea water are enriched over time in the structure of the nodules [Hein et al., 2020]. Because the chemical processes that form the nodules are so dependent on the specific conditions at the sea floor, the nodules have a different composition depending on the area. The mean chemical composition of the nodules in the CCZ are shown in table 2.2.

2.3. Classification of Resources and Reserves

To create certainty for investors and prevent fraud, mining companies are bound to adhere to regulations when it comes to reporting information about the mining projects to investors on the stock exchange [Bickford, 2013]. Examples of such regulations are the NI 43-101 in Canada, or the JORC Code for Australia and

Table 2.1: Global tonnage of metals contained in PN in the CCZ compared to terrestial deposits. Table from [Hein et al., 2020]. [a] Calculated on the basis of an estimation by ISA [2010] of 21.1 billion metric tons of CCZ nodules in place on the seafloor and the mean chemical composition compiled in Hein et al. [2020]. [b] Reserve base is the measured plus indicated resource that includes resources that are currently economic (reserves), marginally economic and some that are currently sub-economic. [c] Terrestrial resource is a concentration of a naturally occurring material in or on the Earth's crust that is in such a form and amount that economic extraction is currently or potentially feasible. [d]: Rare Earth Elements

Element	**Total CCZ nodule resource[a] (Mt)**	**Global terrestrial reserve base [b] (Mt)**	**Global terrestrial resource[c] (Mt)**	**Example metal uses**
Manganese	5992	5200	ND	Steel, batteries
Nickel	274	150	ND	Stainless steel, superalloys, wind turbines, batteries
Copper	226	1000	5600	Electrical, electronic, most high-tech products
Titanium	67	900	1200	Aerospace, superalloys
Cobalt	44	13	ND	Batteries, superalloys, electromagnets
Total REE[d]	15.1	128	ND	Turbines, high-tech smartphones etc.
Molybdenum	12	19	25.4	Steel for strength and hardness
Vanadium	9.4	38	63	Steel alloys, jet engines
Zirconium	6.5	77	ND	Nuclear industry
Thallium	4.2	0.0007	0.65	Photoresistors, infrared optics
Lithium	2.8	11	62	Batteries, aircraft
Yttrium	2.0	0.6	ND	Red phosphor for televisions
Arsenic	1.4	1.6	ND	Semiconductors
Tungsten	1.3	6.3	ND	High-strength steel, superalloys, electrodes
Tellurium	0.08	0.05	ND	Solar cells, superalloys

New Zealand. According to the definitions in the NI 43-101, reports of mineral deposits can be classified as follows [CIM, 2014]:

- **Mineral Resources.** A Mineral Resource is a concentration or occurrence of solid material of economic interest in or on the Earth's crust in such form, grade or quality and quantity that there are reasonable prospects for eventual economic extraction. Mineral Resources can be subdivided into three more categories according to CIM [2014]:
  - **Inferred Resources**. Lowest level of confidence, below indicated or measured resources. Geological evidence is sufficient to imply but not verify geological and grade or quality continuity. Inferred resources cannot be converted to a reserve.
  - **Indicated Resources**. Confidence level above inferred. Geological evidence is sufficient to assume geological and grade or quality continuity. The indicated resources can be used to support mine planning, and can be converted to probable reserves only.
  - **Measured Resources**. High level of confidence. Geological evidence is sufficient to confirm geological and grade or quality continuity.
- **Mineral Reserves**. A Mineral Reserve is the economically mineable part of a Mineral Resource. It can be subdivided into two more categories:
  - **Probable Reserves**. Mineable part of an indicated, and in some cases measured reserve.
  - **Proven Reserves**. Mineable part of measured reserves.

Table 2.2: The chemical composition of nodules in the CCZ and in the license area, which is located inside the CCZ. Data for CCZ from Hein et al. [2013], Mewes et al. [2014], and Hein and Koschinsky [2014], compiled by Hein et al. [2020]. License area data from AMC [2019].

Element	Unit	CCZ	License Area
Manganese	(wt%)	28.4	31.2
Iron	(wt%)	6.16	
Nickel	(wt%)	1.30	1.36
Copper	(wt%)	1.07	1.15
Titanium	(wt%)	0.32	
Cobalt	(wt%)	0.21	0.13
Molybdenum	(ppm)	590	
Total REE	(ppm)	717	
Vanadium	(ppm)	445	
Zirconium	(ppm)	307	
Thallium	(ppm)	199	
Lithium	(ppm)	131	
Yttrium	(ppm)	96	
Arsenic	(ppm)	67	
Tungsten	(ppm)	62	

Because the final goal of any mining business is to be profitable, as many resources as possible must be converted to reserves. To convert a resource to an economically mineable reserve, additional modifying factors need to be studied. These factors include, but are not restricted to; mining, processing, metallurgical, infrastructure, economic, marketing, legal, environmental, social and governmental factors [CIM, 2014]. When all of these factors are considered in a study by qualified person, it is possible to quantify mineable reserves. In figure 2.2, an overview is given of the classification categories and modifying factors.

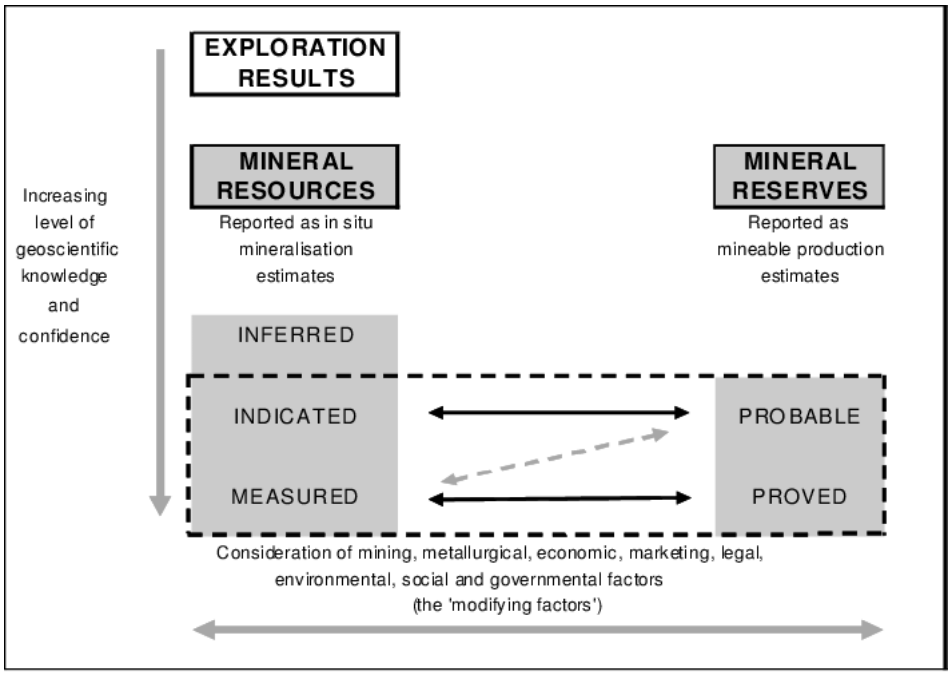

Figure 2.2: Resource and reserve classification and modifying factors [Green and Vogt, 2009]

2.4. Exploration Methods

At the top of figure 2.2, there are the exploration results. For exploration of PN, the most important attribute of nodules besides the metal content is the Nodule Abundance (NA) [Hein et al., 2020]. This is a measurement

for the weight of nodules per unit area, usually reported as $wet\ kgm^{-2}$. To determine the nodule abundance in an area, box cores have been used to collect samples from the sea floor. These devices drive a hollow tube into the seabed to recover material from a fixed area. Free-fall Grab Samplers are also used to sample a fixed area, but do so using a clamshell bucket. According to Lee et al. [2008], the grab samplers often underestimate the NA compared to box corers. They found that an overall correction factor of 1.4 could be applied.

Another commonly used method to determine the NA uses photographs of the sea floor. They are taken by cameras fixed on the box corers and grab samplers, or can be taken by a Autonomous Underwater Vehicle (AUV). On the photos the individual nodules can be seen. An example of such a photo from AMC [2019] is shown in figure 2.3. From each nodule, the axis length is determined, which is correlated to the weight of the nodules. Also the percentage of sea floor coverage can be correlated to photos of box cored areas [Mucha and Wasilewska-Błaszczyk, 2020]. The main advantage of photographs is the speed and the large coverage. Large amount of photos can be analyzed with the use of automated image processing. Neural networks can very reliably estimate the nodule abundance compared to visual inspection of the photographs [Sharma et al., 2010]. However, some issues can arise with quality, lighting or angle of the photographs. Even when using high quality photos, they are still susceptible to under representing the true NA when used only by themselves because nodules may be (partly) covered by sediments. Therefore, box coring needs to be done as clarification of photograph coverage.

From the photographs, AMC [2019] classify the nodules into three broad categories, shown in table 2.3. The areas with the smaller size of type 1 nodules with higher surface coverage and nodule abundance are seen as potential mining areas. Type 2 and 3 are characterized by lower nodule abundance and larger nodules that have sediment in between them. The mining system must be designed for efficient pickup and transport of the optimum nodule size [Sharma, 2017*a*].

Lastly, Multibeam Echosounder (MBES) can be used for identifying areas with PN. MBES is a type of sonar. Sound waves are emitted from a system at sea level. The waves reflect off the ocean floor to give backscatter data and provides information on the seabed structure. According to Knobloch et al. [2017], a higher backscatter value essentially indicates harder material. A higher value can therefore be used to identify areas with nodules present instead of the softer sediments. His research uses a neural network to give estimates of the nodule abundance using backscatter data with a resolution of 100m and boxcore samples. The method shows good results compared to kriging and can be used for resource assessment. AMC [2019] uses the backscatter data to identify areas with less nodule coverage (and thus more sediment), which show correlation with the different nodule types from table 2.3. They assume that nodule types 2 and 3 are not mineable.

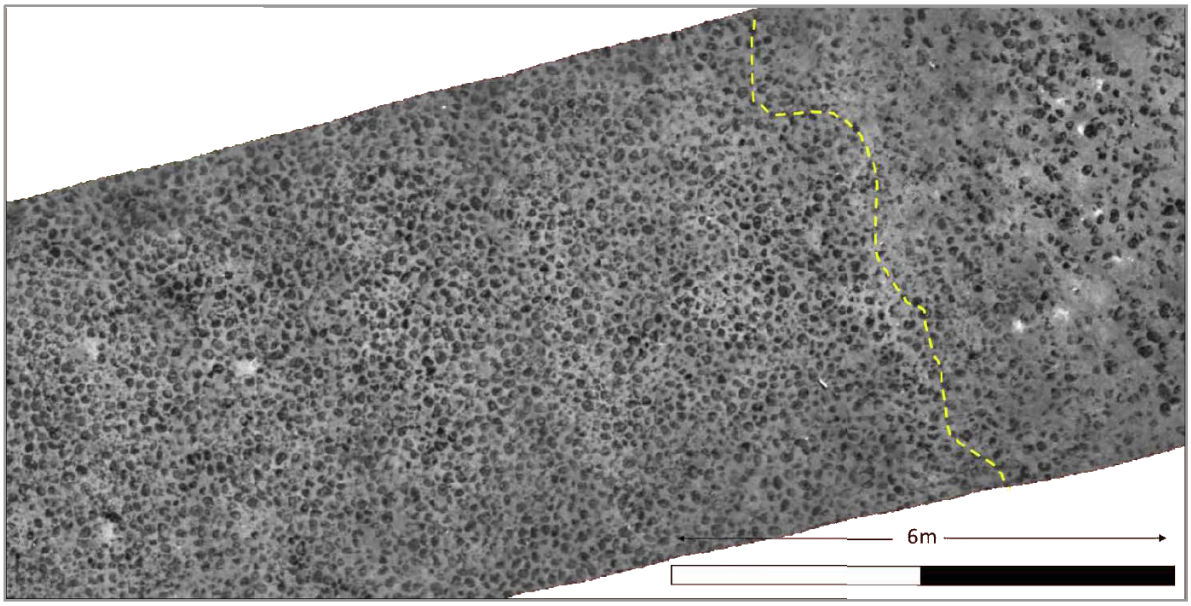

Figure 2.3: Photographs from the seafloor made by a UAV traverse. The dashed line indicates a change from nodule facies type 2 (left) to nodule facies type 3 (right). From AMC [2019].

Table 2.3: The three nodule types and their defining features. From AMC [2019] based on guidelines from ISA [2010] and earlier work from AMC [2016].

Type	Description	Surface Coverage	Size (cm)	Note
1	Densely packed / interconnected	>50%	1 - 10 (uncertain)	Low to moderate confidence in camera imagery to resolve individual nodules
2	Mostly individually / locally interconnected	~20 - 40%	5 - 20	Moderate to high confidence in camera imagery to resolve individual nodules
3	Mostly individual / sparse	~10 - 20%	5 - 20	Moderate to high confidence in camera imagery to resolve individual nodules

2.5. Resource Modelling for Polymetallic Nodules

For the modelling of polymetallic nodules, a procedure based on Ordinary Kriging (OK) is commonly used to interpolate the exploration data for polymetallic nodules, for example in Rahn et al. [2019], AMC [2019] or Golder [2013]. The estimations follow the procedures established in the mining industry, albeit to model a 2D resource instead of a 3D one. Once the exploration data is validated and verified to be accurate, the following steps are used for the resource assessment:

1. **Defining resource domains**. According to AMC [2019], within the license area there is one type of large-scale geological feature that controls the distribution of Nodule Abundance (NA): sea mounts. Slope angles below 15 degrees do not affect the NA, although they affect the ability to collect the nodules [Yamazaki and Sharma, 2000].
2. **Data preparation**. This includes statistical analysis, declustering, and removing outliers.
3. **Variography**. For the purpose of interpolating the data, a description of the spatial variability of the attribute (for example the NA or Co grade) is needed. The variability is found by calculating the semi-variance between pairs of sample points a certain lag distance apart, plotted in a (semi-)variogram. From this experimental variogram, a variogram model can then be fitted that approximates the variability of the attribute [Goovaerts et al., 1997].
4. **Geological block model**. The area to be modelled is discretized into blocks of a fixed size. In the next steps, the information about the resource will be interpolated to these blocks. For conventional terrestrial mining operations, the block size depends on the Smallest Mineable Unit (SMU) [Leuangthong et al., 2003]. In some resource estimations, the sampling interval from borehole data is used. For mining PN, procedures for estimating the SMU are not established. Resource assessments therefore use sizes based on sample spacing intervals.
5. **Nodule Abundance and Grade estimation**. Ordinary Kriging (OK) is used to interpolate the attributes to the block model. OK is a least-squares linear regression algorithm that can estimate an attribute at unsampled locations [Goovaerts et al., 1997], assuming that this attribute is stationary. The interpolation process uses the semi-variogram model.
6. **Model validation**. This consists of at least visual inspection along with quantitative assessment, such as comparison with a different interpolation method like Inverse Distance Weighting (IDW). Commonly also swath plots, and QQ/PP plots are used.

2.6. Mining Methods for Polymetallic Nodules

The common aspect of every deep-sea mining method is the MSV. Such a vessel is the base of the operation and supports the NC [Volkmann, 2018]. An example of the MSV is shown in figure 2.4.

Mining concepts that have been successfully tested in the 1980's all use a self propelled NC that brought the nodules to the surface using an airlift or hydraulic pumping system [Golder, 2013]. More recently, Allseas have announced mining trails in 2021 [Allseas, 2020] using a self propelled collector. Similarly, a Belgian company has announced successful testing of their active collector and upcoming mining tests [GSR, 2020*b*] [GSR, 2020*a*].

Figure 2.4: The mining support vessel recently purchased by Allseas.

For transporting the nodules upwards, a VTS is needed. For this thesis a continuous supply of material from the NC is assumed. According to Ecorys [2014], two methods for vertical transport can be used: either an airlift or hydraulic pumping method. The principle behind the air lift is compressed air that is injected into the pipe. This induces a vertical flow. The downside is the power required to transport the air downwards and prevent clogging. The method that has been applied is the hydraulic pump, with has a proven track record in drilling operations for the oil and gas industry. Hydraulic pumping has also been successfully tested to work in a more shallow environment by Nautilus Minerals [White et al., 2011].

For gathering the nodules from the seabed, mining concepts that have been successfully tested in the 1980's all use a self propelled NC [Golder, 2013]. The self propelled NC collects the nodules from the seabed and separates them from the sediments. Pre-processing steps such as crushing can potentially also be applied. The advantages are high selectivity and control. The complexity of the system makes them a big engineering challenge [Agarwal et al., 2012].

2.7. Mine Planning

Once the resource model is made and there are at least indicated resources, mine planning can start. The mine planning problem can be defined as finding the sequence of material extraction that maximizes the present value of the mining project.

For terrestrial mine planning, the base of the process is the block model as created in the resource assessment. Using economical data for metal prices, mining costs, and processing costs, the value of the material inside the block and the costs of mining and processing it are estimated. It must then be decided for every block if it needs to be removed, whether it be as waste, or as ore. The decision is not simple because the extraction of each block influences the blocks around it. For example, to excavate one block, the blocks above it must have already been removed beforehand. The final result of mine planning is the sequence in which the blocks are excavated.

Traditionally, the planning process for open pit mines starts by defining a small pit with the highest possible value. The edges of the pit are then expanded until the edge of profitability is reached. This is the Ultimate Pit-Limit (UPL) process pioneered by Lerchs and Grossman [1965]. The sequential expansions of the pit boundaries can be used to define sequences or pushbacks [Shishvan and Sattarvand, 2015].

In the planning process for terrestrial mines, many constraints have to be obeyed. These include physical constraints related to the geology and slope angles, and precedence constraints (blocks can only be extracted if the blocks above it have been mined). There are also operational constraints related to mining limitations, and processing limitations [Franco-Sepulveda et al., 2019]. Exact approaches to optimization of the mine planning can run into the limits of what is computationally possible due to the large number of constraints,

along with the large block models required to represent the mines. This has driven researchers to find new algorithms that are less complex, with high computational efficiency and allow incorporation of all mining complexities into the constraints [Shishvan and Sattarvand, 2015].

Recently, metaheuristics have attracted attention to address these problems. Metaheuristics are optimization algorithms whose operation is inspired by processes found in nature [Dullaert et al., 2007]. Most forms of metaheuristic algorithms use stochastics and do not guarantee a globally optimal solution. Instead, the aim is to find a solution that is sufficiently good for the problem.

Many different metaheuristic methods have been applied to the Open-Pit Production Scheduling (OPPS) problem. The first Genetic Algorithm (GA) was developed by Denby and Schofield [1994] and revisited by Alipour et al. [2017]. In this method, a large group of potential solutions (the 'population') is selectively bred over generations for their solution quality (the 'fitness') to end up with good solutions. Other population-based metaheuristics applied to mining are the Ant Colony Optimization (ACO) [Shishvan and Sattarvand, 2015] or the Particle Swarm Optimization (PSO) [Khan and Niemann-Delius, 2015] among many others.

A different approach to metaheuristics are the single-solution methods, where a single solution is improved over iterations. Examples applied to the OPPS problem are Simulated Annealing (SA) [Kumral and Dowd, 2005] or Tabu Search (TS) [Lamghari and Dimitrakopoulos, 2012].

Both population-based approaches and single-solution methods have their downsides. Population-based methods risk not converging close to the best solution, where single-solution methods risk getting stuck in a local optimum. In combating these disadvantages, it has been tried to use the two methods in sequence; first using a population-based method and improving the solution using single-solution methods. Alternatively, there are hyperheuristics, wherein a heuristic method is used to decide the next adequate search step [Lamghari and Dimitrakopoulos, 2020].

2.7.1. Mine Planning for Polymetallic Nodules

To plan out the areas that the NC is going to mine, research by Volkmann [2018] proposes a mining method that divides an area on multiple levels. The highest level is the license area, which is the area that mining rights have been acquired inside. The license area can cover hundreds of square kilometers.

The next level down from the license area, are *mine sites*. The sites are defined by [UNOET, 1987] as "an area of the ocean floor where under specific conditions, a single mining operation can take place for a period of time". There can be multiple mine sites per license area.

The smallest unit are the *mining fields*. These are alike to agricultural fields and defined by [Volkmann, 2018] as "A continuously mineable area described by a boundary, which defines the "in-field" reserve." Again, there can be multiple mining fields per mine site. This division is summarized into figure 2.5. The NC will be mining one field to completion before moving on to the next.

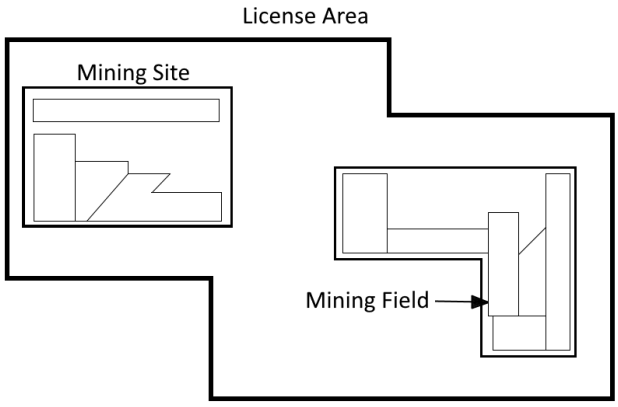

Figure 2.5: Schematic illustration of a deep-sea mine plan. After [Volkmann, 2018].

2.7.2. Planning Methods from Agriculture

The planning methodology described in the previous section takes inspiration from agriculture. The major difference between farming and mining PN is that field boundaries in farming are more restricted and often predetermined. In mining PN the boundaries and methods to define field boundaries are yet to be determined. There is a large body of knowledge on detailed path planning for coverage purposes like robotics and drones, but none of those relate the path of the robot to the area boundaries.

Oksanen and Visala [2009] have developed two algorithms for determining the near-optimal path of agricultural equipment in a field. The path is defined as the path that takes the least time for turning and maneuvering relative to productive harvesting. A path that in total takes less maneuvering time, is more efficient at covering the field. He then related that efficiency to the shape of the field and found a correlation between field shapes and efficiency.

Park et al. [2011] investigated in-field driving patterns for mining PN and suggests two methods of pathing: swathing and contouring. The two methods are shown in figure 2.6.To plan the two methods they suggest using a cellular decomposition approach for path planning. Such a method is used by Oksanen and Visala [2009] in his planning approach for agricultural machines. These two driving patterns will be further examined in this thesis in chapter 5.

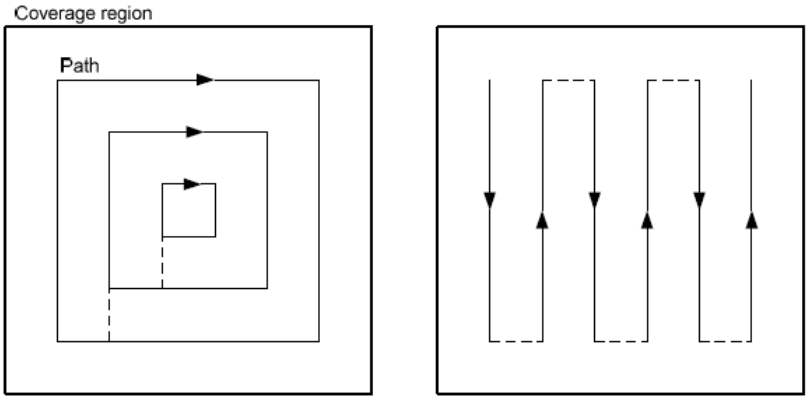

Figure 2.6: Two driving patterns to cover a region with PN. Left: contouring, right: swathing. Figure from Park et al. [2011]

3

Case Study Framework

In this chapter the framework for all further analysis in this thesis is introduced. This framework is based upon information from the license area that is available in public literature. Using the information from the literature study, the bathymetry and exploration done in the license area are explored in more detail. The mining methods described in the literature study will also be expanded by quantifying relevant parameters of the NC. A smaller section of the license area gets special interest as it is the location of the pilot mining test. The framework laid out in this chapter will provide the basis for the resource assessment and identification of mineable areas in chapter 4. The parameters of the NC will be used in all assessments of driving patterns and KPI calculations, for example production rates and nodule tonnages.

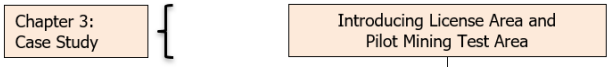

Figure 3.1: The thesis overview for chapter 3. The full overview is shown in figure 1.3

3.1. Description of License area and Pilot Mining Test Area

The license area lies inside the Clarion-Clipperton Zone (CCZ) [AMC, 2019]. The bathymetry inside this area is indicated in figure 3.2 has an average depth of around 4100m below sea level.

The CCZ is an area in the pacific ocean bounded by two fracture zones, with in-between them the abyssal plains. On these plains, seamounts can be found that are several hundred meters high with their directionality roughly orthogonal to the fracture zones bounding the CCZ. They are believed to be caused by seafloor spreading [ISA, 2010]. On figure 3.2, indicating the bathymetry of the license area, the seamounts can be seen. Their directionality is striking north to NNW, which agrees with the overall directionality of the seamounts inside the CCZ. Additional structures in the license area are extinct volcanoes, rising 500 to 2000m above the seafloor.

First mining test are planned for after this thesis is complete. They will take place inside a smaller area (the 'Pilot Mining Test (PMT) area') inside the license area, indicated in figure 3.2. The PMT area is 15 by 10km and has mostly low slope angles below 4 degrees. Mining trails inside there can be used to verify assumptions made in this thesis and check the validity of the results, which is important for future work. In the final results, special attention will therefore be given to this particular area.

3.2. Description of the Mining System

The thesis is based upon the mining system built by Allseas. It uses a self-propelled NC that can maneuver on the seafloor. It collects PN continuously, which are then transferred to the VTS to take them to the MSV. Because nodules are mostly found within the first 10cm of sediments, the system targets only the top of the sediments [AMC, 2019]. It is also built to mine only nodule type 1. For that reason, areas with nodule type 2 & 3 are considered unmineable in this thesis. Test still have to be performed and development is ongoing. It is possible that nodule type 2 & 3 will be suitable for mining in the future, but not at the time of writing.

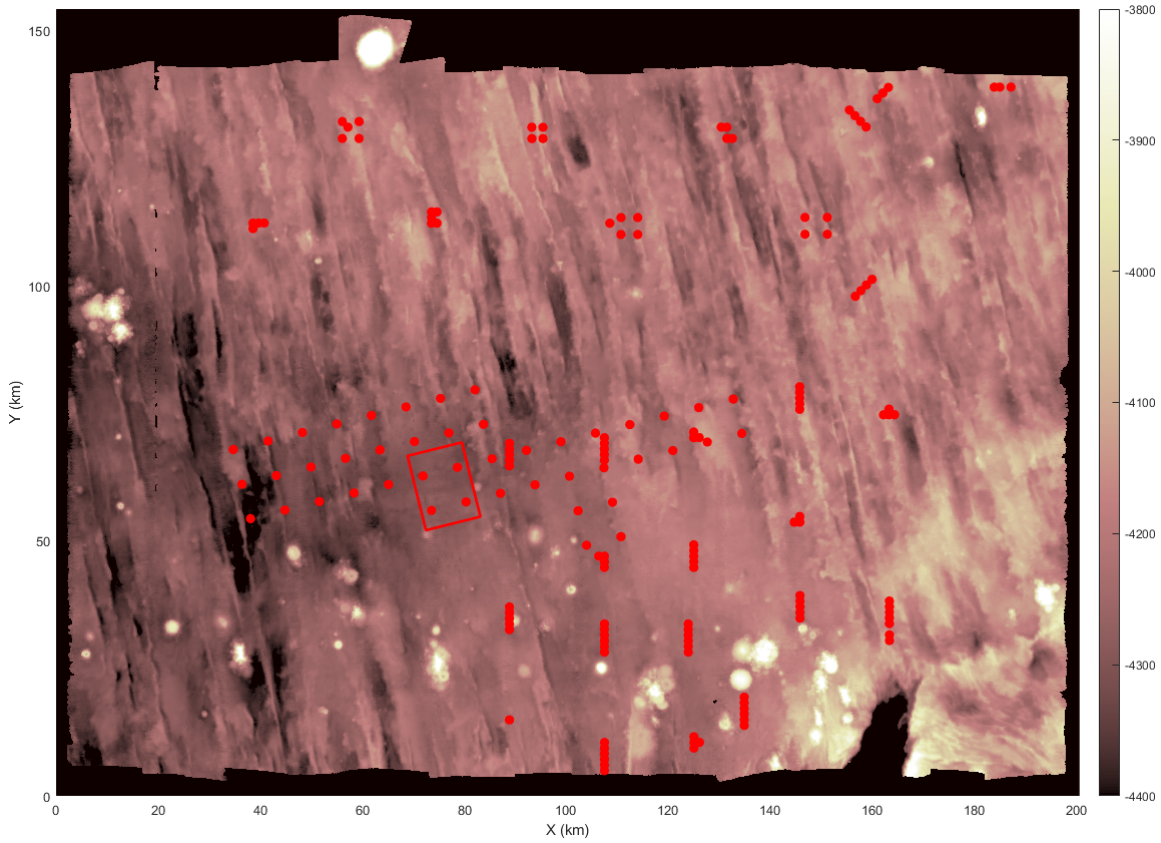

Figure 3.2: The bathymetry of the license area with a resolution of 50m by 50m per pixel. The depth is capped at a minimum of -3800 and a maximum of -4400. The major geological structures in the area have more or less the same strike azimuth of 354. The white circular areas are rising up above the seafloor and are believed to be extinct volcanoes. In red, the pilot mining test area is indicated as a square. The red circles indicate locations of box cores or grab samples that supply the NA information for this thesis.

It is assumed that only one single NC will be used in the mining operation. The operational parameters of the NC are listed in table 3.1. They are either estimated or taken from AMC [2019].

Table 3.1: Parameters of the NC that are under consideration for this thesis. Indicated are also the base specifications that of the NC for calculations and sensitivity analyses. Values of the parameters of the NC are either estimated or taken from AMC [2019].

Symbol	Name	Unit	Base Case
w_{nc}	Width of the NC	m	13
v_{nc}	Speed of the NC	m/s	0.5
MR	Mining Rate	m^2/s	6.5
η_c	Collecting efficiency	%	80
R_t	Turning Radius of the NC	m	30

3.3. Sources of Input Data

For this thesis and case study, data was available from Allseas.

1. Nodule Abundance samples. These are the samples used in the preliminary economic assessment of the license area [AMC, 2019]. Contained in the dataset are 204 boxcore samples, indicated as red circles in figure 3.2. They consist of the following:

   (a) 159 historical samples. These were mostly collected using free-fall grab samplers and a few using box cores (precise counts are unavailable). The nominal sample spacing is 20 by 20 km although

some samples are co-located for estimation of the nugget effect. The grab samplers had an approximate area between 0.25 to $0.5 m^2$ with some $1 m^2$. To correct for the underestimation of NA by the grab samplers, a correction factor can be used [Lee et al., 2008]. However, because that factor lacks precision for individual samples, it was not applied in the AMC technical report. Therefore also not be applied in this thesis.

(b) 45 samples taken in 2018, collected using box coring with an area of $0.75 m^2$. These samples have a sample spacing of 7 by 7 km, which is closer than the historical samples. In the AMC [2019] report, this sample spacing was used to define the indicated resources. The samples were selected without reference to any of the detailed geophysical data to avoid any bias. 4 of these samples are located within the PMT area.

Data that was used in the economic assessment, but that was not available for this thesis are 29 nodule abundance estimates from seafloor photographs. Those 29 photographs have a sample spacing of 3.5 km and are the basis of the measured resource estimation. Because that data is not available, the measured resource estimation is not used in this thesis.

2. Bathymetry of the license area with a 50 m resolution using a MBES mounted below the hull of the vessel. According to AMC [2019], this data lacks the resolution to confirm the suitability of specific areas for mining, particularly regarding definition of small-scale topographic features and confirmation of appropriate geological substrate. A survey using a AUV has the appropriate resolution for this.

   The limitations of the data cause that only large scale features can be delineated in this thesis. An investigation with regards to avoiding obstacles is made to account for smaller scale features.

3. Raster data of the license area containing information on different nodule types. This data was based on the same MBES as the bathymetry. The method of collecting nodule type data was discussed in section 2.4. The resolution is 50m.

4

Spatial Analysis

4.1. Introduction

In chapter 3, the license area and it's framework were introduced. Using the data described in chapter 3, a resource assessment is made. It recreates results from the economic assessment of this area from AMC [2019]. The resulting resources, combined with the operational parameters of the NC from chapter 3, serve as a basis for analyzing which parts of the license area are suitable for mining. The steps taken in this chapter are as follows:

- Recreate the spatial distribution of nodule abundances using ordinary kriging.
- Analyze the bathymetry of the area for the slope constraints of the NC.
- Divide the license area into different mining sites.
- Introducing a new way of determining the mineability of an area: the Straight-Line Distance (SLD).

The results from defining mining sites and the SLD inside them will be used in the chapters following this one. They allow analysis to be focused on a smaller section of entire license area. The thesis outline for chapter 4 can be seen in figure 4.1.

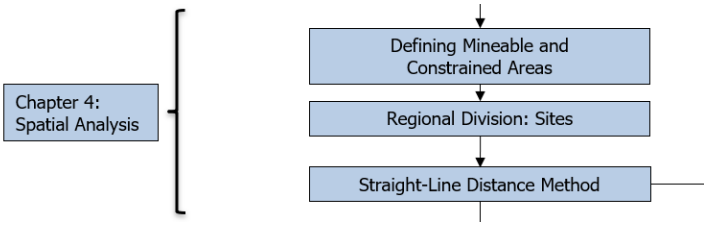

Figure 4.1: The thesis overview for chapter 4. The full overview is shown in figure 1.3

4.2. Objectives and Research Questions

The objective of this chapter is to provide the spatial analysis that can be used to identify high quality mining areas and serve as a base for the rest of the thesis. The research question that will be answered in this chapter are:

- *How can high quality mining areas be identified?*
- *How can mining sites be selected?*

4.3. Assessing Resources Using Ordinary Kriging

Ordinary Kriging (OK) is a common method to estimate resources for Polymetallic Nodules (PN) that has been used by [AMC, 2019], [AMC, 2016], and [Rahn et al., 2019]. The method requires that the variability of the resources is described in a variogram model. This model is based on the experimental variogram built from the exploration data. The sample variogram is calculated through equation 4.1, in which N(h) is the number

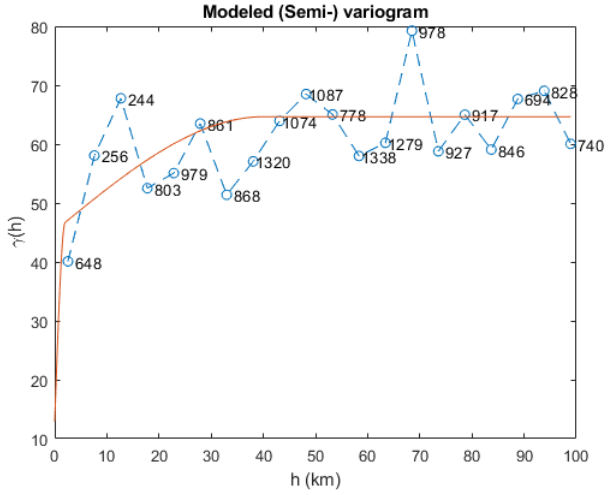

Figure 4.2: Omni-directional experimental variogram (blue) of NA samples. The fitted variogram model is indicated in red. The numbers indicate the number of data pairs used for that point. The variogram is not normalized. Variogram MATLAB function made by Schwanghart [2020].

of points located a distance h apart, and $z(u_\alpha)$ is the value of the attribute at location u_α. The experimental variogram resulting from the NA samples is shown in blue in figure 4.2.

$$\gamma(h) = \frac{1}{2N(h)} \sum_{\alpha=1}^{N(h)} [z(u_\alpha) - z(u_\alpha + h)]^2 \tag{4.1}$$

In the economic assessment of the area from [AMC, 2019], a variogram was fitted to the boxcore data and photographs of the sea floor. The (normalized) variogram contained the following three structures:

- Nugget effect with sill 0.2.
- Spherical variogram model with sill 0.5 and range of 2 km.
- Spherical variogram model with sill 0.3 and range of 40 km.

For this thesis, not the exact same data is available for the construction of the experimental variogram. Still, the same variogram model is used. The experimental and modeled semi-variogram are shown together in figure 4.2. The model used in the report matches with the data and no adjustments were deemed necessary.

After the variogram model was made, the following steps were undertaken to recreate the resource assessment. The steps are the same as the steps from the technical report [AMC, 2019].

1. The block model was constructed in 2D. Parent block sizes were 14km by 14km, which was considered enough for inferred mineral resources. In the areas with sample spacing of 7km the parent blocks were subdivided into blocks of 3.5 by 3.5 km, which is enough for indicated mineral resources. There is no exploration data available with closer sample spacing, so no further divisions of parent blocks were made.
2. Polygons were used for the areas with certain sample spacing. Outside the limit of sampling, abundance was set to the mean value: 15.14 kg/m^s.
3. An elliptical search area was used for selecting interpolation points. The radii of the ellipse were 60 by 30 km with the long axis oriented 75° east. This direction is parallel to the sampling grid in which the boxcore data was collected. Search quadrants were used with a maximum of 4 per quadrant. For the complete search area, a minimum of 4 samples was required.
4. The nodule abundance was interpolated using Ordinary Kriging with the omni-directional variogram model.

In the technical report, the sample spacing polygons were used to differentiate between the different resource levels (measured, indicated, inferred). A quantitative comparison between the resulting block model nodule tonnage in each of the polygons is shown in table 4.1. A visual comparison between the block models can be seen in figure 4.3. The polygons are also shown.

Table 4.1: Comparison between reproduced OK block model and report, with the difference indicated in the last column.

Resource level	Preliminary Economic Assessment [Mt]	OK results [Mt]	Difference [%]
Measured	4	4.18	4.4
Indicated	34	31.09	-9.4
Inferred	244	231.91	-5.2

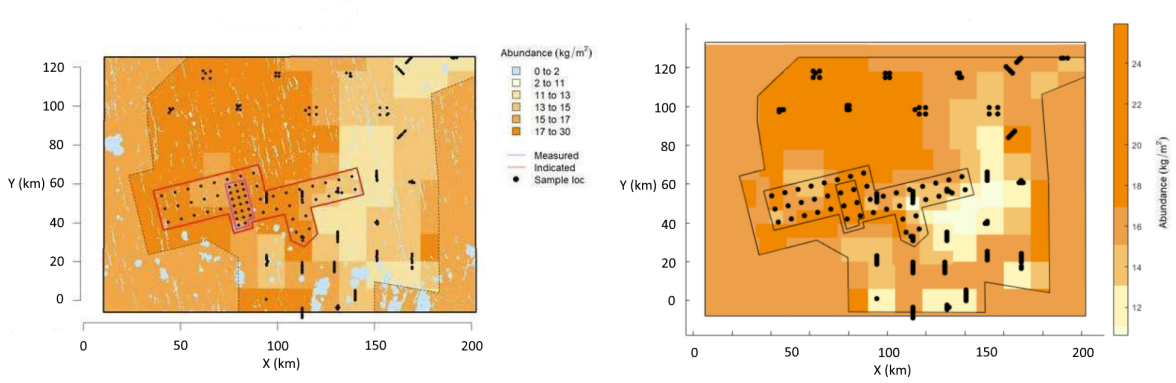

Figure 4.3: A visual comparison between the resource assessment of the technical report (left) and the recreation of the same block model for the purposes of this thesis (right). Black dots are sample locations. In the left figure the different resource classification levels are indicated with coloured polygons. Purple for measured resource, red for indicated resources. The black polygon shows the interpolation limit, outside of that the nodule abundance was set to the mean.

4.4. Identifying Slope Constrained Areas

To go from the resource assessment towards a mineable reserve, the modifying factors must be applied. The first is mining aspects: it must be known which areas are accessible to the NC. Using assumptions from AMC [2019], the NC has a limitation when it comes to driveable slope angles. When the terrain slope angle exceeds the threshold of 8°, it is considered hard constrained. To identify hard constrained areas, the bathymetry of the license area is used, shown in figure 3.2. Using MATLAB's gradient function, the slope at each raster point is determined from the depth difference in X and Y directions. From there, a binary image is created. At each raster point, a black pixel indicates a hard-constrained area, while a white pixel indicates a mineable area.

In the method adopted from Volkmann [2018], mining takes place in mining fields, which are continuous areas. As a first step to identify continuous areas, neighborhood filters are applied to the binary image. The goal of using these filters is that areas with fewer obstacles can be clearly identified and separated from the areas with many obstacles and large geological features such as ridges or volcanoes. An additional important aspect of the filter is that it will also filter out pixels that are perceived to be noise.

The neighborhood filter works by defining a search area around a selected raster point. The selected raster point is in the center of the search area. Each pixel inside the search area is then considered. If the percentage of black pixels exceeds the threshold, then the selected raster point is unmineable. Conversely. if the percentage of black pixels does not reach the threshold, the pixel is mineable.

The neighborhood filter has several settings which need to be adjusted for the specific case. For this thesis, a slope threshold of 8° has been assumed based on AMC [2019]. In the case that the collector has a different slope constraint, the settings can be adjusted. The search area of the neighborhood filter can have various shapes, which will yield different results. Differences with regards to removal of noise and identification of continuous areas were assessed visually. The correct settings for 8° were determined to be the following. The result of the filter for a smaller cutout area is depicted in figure 4.4.

- Ellipsoidal search area with axis ratio of 2:1.
- Long axis length of 700m (radius of 350m)
- Long axis pointing in the same direction as the geological structures in the area: azimuth 354.
- Threshold of maximum 35% black pixels (at least 65% white pixels) to be considered mineable.

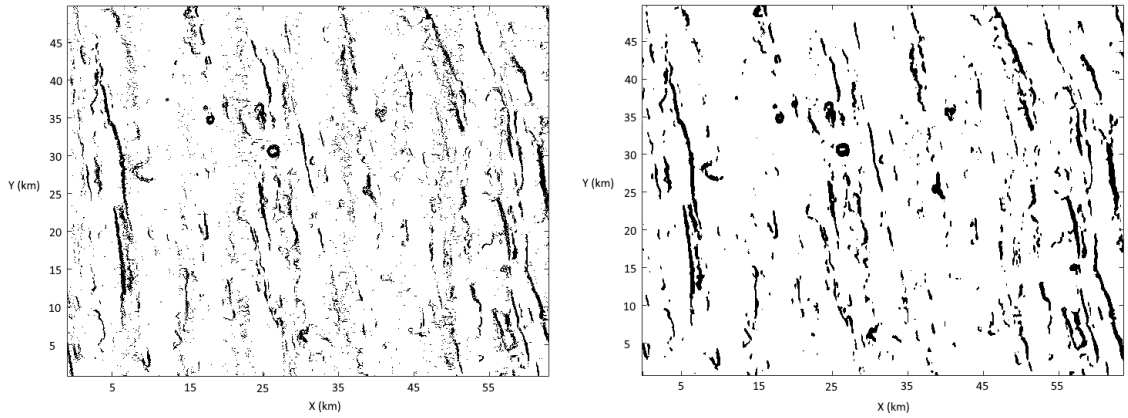

Figure 4.4: Cutout of a smaller area. Black pixels indicate areas with a slope that exceeds the 8° threshold. On the left the unfiltered area. On the right the neighborhood filter is applied. Vertical bands of pixels that are perceived as noise have been removed. Areas with a high density of black areas have been joined together.

4.5. Procedure for Delineating Sites

The main research question of this thesis asks how mining fields can be planned. Following the methodology of Volkmann [2018], large scale mining sites should be defined before the smaller mining fields can be defined, as was shown schematically in figure 2.5.

Because of this hierarchy, mining fields will never cross the boundaries of a mining site. A very important consideration when making mine sites is therefore that the site boundaries should not (or as little as possible) cross areas that would be suitable for mining continuously in a mining field.

Besides that, the following aspects are taken into account for the delineation of mine sites:

- Areas with nodule type 2 & 3 which are considered not mineable with current technology.
- Geological structures that define the constraining slopes.
- The estimation variance from the Ordinary Kriging block model. This is closely linked to the interpolation and resource limits, depicted earlier in figure 4.3.
- Nodule abundances depicted in figure 4.3.
- Bathymetry and roughness of the terrain.

The sites were drawn and adjusted by hand until a satisfactory result was obtained. The resulting mine sites are depicted in figure 4.5 where a colour scheme is used to indicate the motivation behind the different boundaries. The statistics per site are listed in table 4.2.

First, the areas with nodule type 2 & 3 were delineated, keeping in mind the directionality of the geological features. The result of this are the main boundaries of site 1, 2, 3, 6 and 8. The interpolation limits and estimation variance were used to outline areas were exploration data was limited. This resulted in the main boundaries of sites 11, 12, and 14. Areas with low nodule abundance were then grouped, resulting in sites 10 and 11. Lastly, the bathymetry of the terrain were taken into account to delineate impassable geological structures. For some site boundaries, multiple factors were of importance. The boundaries of site 5 for example were mainly influenced by presence of unmineable nodule types and high estimation variance. The boundaries were then chosen to be on top of geological structures. For all boundaries, the directionality of the area was taken into account.

4.6. Determination of Straight-Line Distance

As discussed in section 2.7, it is common procedure to divide the deposit into blocks. When taking the same approach for mining of PN, an issue appears. The size of the blocks normally depends for a large part on the Smallest Mineable Unit (SMU), the smallest volume of material on which ore waste classification can be determined [Leuangthong et al., 2003]. As discussed in the problem statement in section 1.1, the SMU is not defined for deep-sea mining of PN [Ecorys, 2014]. The SMU depends on a lot of factors, among which the

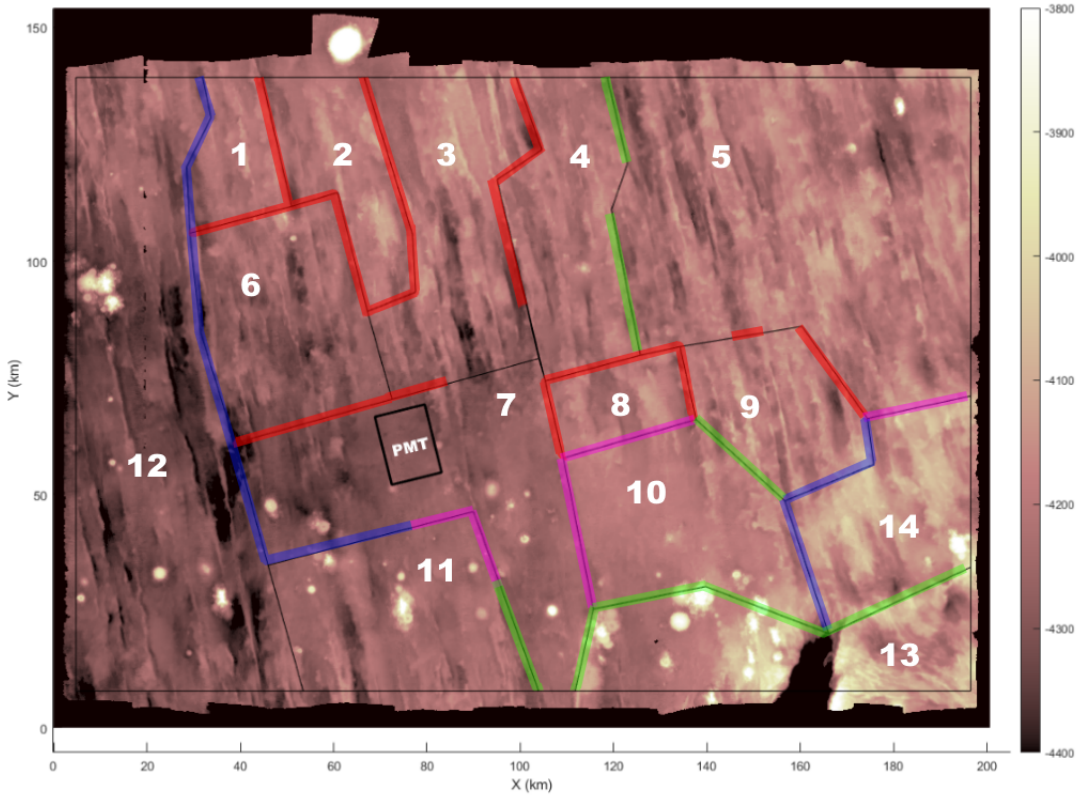

Figure 4.5: The resulting large scale sites in the license area, overlaid on the bathymetry. Numbers indicating the site number for future reference. The primary motivation for a boundary is indicated by a colour scheme: red boundaries are based on nodule type, blue are based on the interpolation limits and estimation variance, green are based on the geological structures, and purple are based on nodule abundance. The remaining boundaries are made connecting the others, keeping in mind the general directionality of the structures in the area.

Table 4.2: Statistics from each site shown in figure 4.5. Specifically for the Pilot Mining Test Area (which lies within site 7) the statistics are also shown.

Site	**Area** [km^2]	**Area Percentage Mineable Nodules Type 1 [%]**	**Area Percentage Slopes >8 [%]**	**Area Percentage Nodule Type 2 & 3 [%]**	**Average NA All Nodule Types** [kg/m^2]	**NA Estimation Standard Deviation**
1	528.6	80.2	5.4	14.4	21.9	7.8
2	881.7	84.7	4.3	11.0	20.5	6.2
3	1817.2	77.7	9.7	12.6	18.5	3.8
4	1350.0	75.9	5.4	18.7	17.1	3.7
5	4628.6	75.1	6.8	18.1	15.8	6.0
6	1592.9	54.0	6.5	39.5	16.5	3.8
7	2560.2	88.1	4.1	7.8	17.0	3.6
8	493.3	83.2	3.7	13.1	13.8	2.5
9	995.7	89.0	10.6	0.4	12.6	2.6
10	1571.6	94.6	5.2	0.2	13.1	2.5
11	1607.6	92.0	8.0	0.0	15.0	7.6
12	4318.9	81.8	8.4	9.8	16.6	8.7
13	1564.4	79.1	20.9	0.0	15.4	7.9
14	1283.5	91.5	8.3	0.2	17.2	6.8
PMT	165	91.5	0.3	8.2	19.1	6.2

selectivity of the mining equipment. It is assumed that the maneuverability of the NC is limited, and that it will mostly travel in a straight line, whether it is driving in a swathing or contouring pattern as discussed in section 2.7.2. That means that blocks are not suitable as a SMU and base for reserve assessment.

A new approximation of the selectivity of the mining operation is therefore needed. To assess which areas would be suitable to traverse with the NC, a new idea is introduced: the Straight-Line Distance (SLD). It is simply said: the longest distance that the collector can drive in a straight line until it comes across an non-traversable area. The SLD is calculated at a single point for a single direction. To give examples, a demonstration of SLD is shown in figure 7.2, where a top-down view of a sample area with black boundaries is shown.

- In figure 4.6a the SLD is plotted at every point for a single direction: 135 degrees north. Three points are indicated in red: for point 1, the SLD is relatively short in this direction because it is in a corner. Point 2 and 3, the SLDs are similar because of they are both constrained by the same boundaries at $y = 180$ and $y = 100$.

- In figure 4.6b again the SLD is plotted, but this time all directions are compared and only the value of the longest SLD is shown. Of the three points indicated, point 1 and 2 now share the same value, because they are both on the longest diagonal. The value at point 3 is lower. Note that for almost all points, the values are higher than in figure 4.6a.

- In figure 4.6c the opposite of figure 4.6b is shown. For every point, all directions are compared, and only the shortest SLD is plotted. For point 1, the shortest SLD is a line between the two closest sides, which is similar to the SLD plotted for point 1 in figure 4.6a. Point 2 and 3 share the same value, since at both points, the shortest SLD possible is between the two opposing boundaries of the sample area.

For the operation of the NC, it is interesting to know which direction gives the longest SLD on average. For this, all points are compared in each direction. The results can be plotted in a rose diagram. For the sample area in figure 7.2, the rose diagram is shown in figure 4.7a. The longest SLD is shown to go from right to left (90 degrees north), which makes intuitive sense as the boundaries of the sample area are the longest in that direction. The SLD in the best direction is plotted in figure 4.7b. It can be seen that the bottom area shows a higher SLD in that direction than the top area. This indicates that in the bottom area, the NC is able to drive straight for longer, which is beneficial.

Another noticeable result is that areas with the a low minimum value (in any direction) can indicate bottlenecks, or passages between areas that have less obstacles. In figure 4.6c, this can be seen by the area between Y-coordinates 80 - 100. These are areas that are likely to be avoided by the NC.

4.6.1. Methodology

The exact procedure used in this thesis for determining the SLD at each raster point is as follows:

1. Select one raster point that is not hard-constrained.
2. Select one direction/azimuth. At this point create two parallel lines in the chosen direction. They are at equal distance above and below the point.
3. Evaluate constraints of all raster points inside the two lines.
4. Calculate distance to the nearest hard-constrained raster points on either side of the selected raster point. This distance is the Straight-Line Distance (SLD). Assign the total distance to each not-constrained raster point between the two lines.
5. Repeat for each direction and each raster point until every raster point is assigned a value.

4.6.2. Straight-Line Distance Results for Mine Sites

The SLD procedure is applied to one of the mine sites that were delineated in section 4.5: site 3, as shown in figure 4.5. The constrained areas of site 3 are shown in figure 4.8. The maximum, mean and minimum SLD are shown in figure 4.9. A larger version of the same plots can be found in the appendix figures B.1 to B.3.

For site 3, the average SLD in each direction can now be determined. In figure 4.10 the average SLD is shown in a rose diagram, for two options:

1. Nodule type 2 & 3 (red area figure 4.8) are hard-constrained and not traversable. Also the slopes and site boundaries are a constrained. This corresponds to figure 4.9.
2. All nodule types are traversable. Only the black areas in figure 4.8 are a constraint.

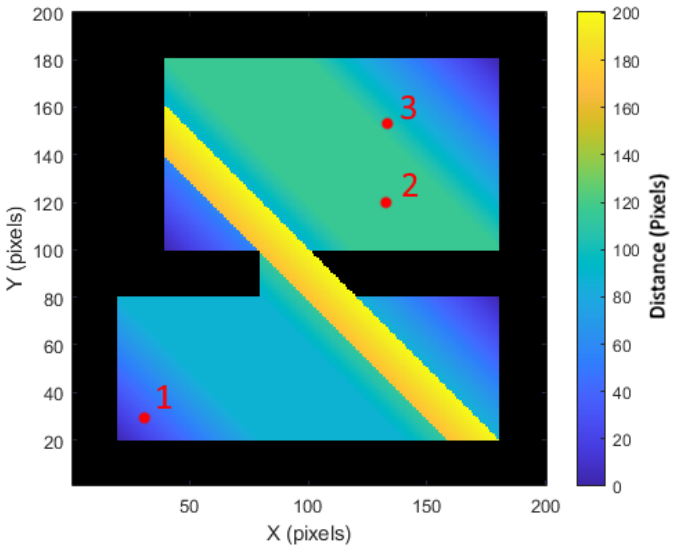

(a) The SLD in the arbitrary direction of 135 degrees north of every point in the field

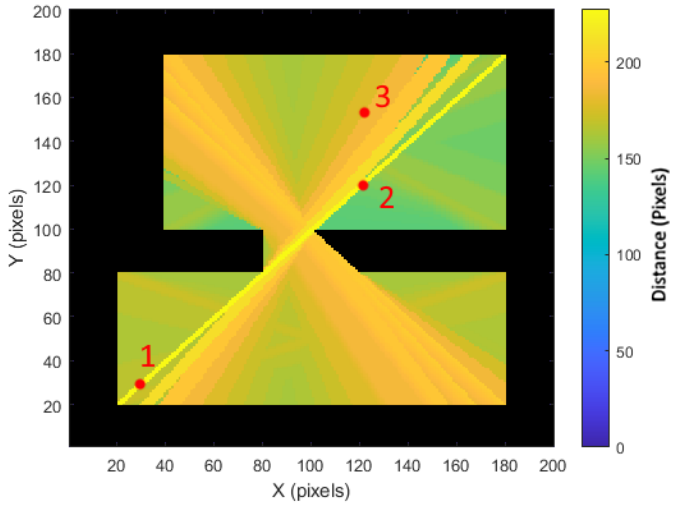

(b) The highest SLD value at every point when comparing all directions.

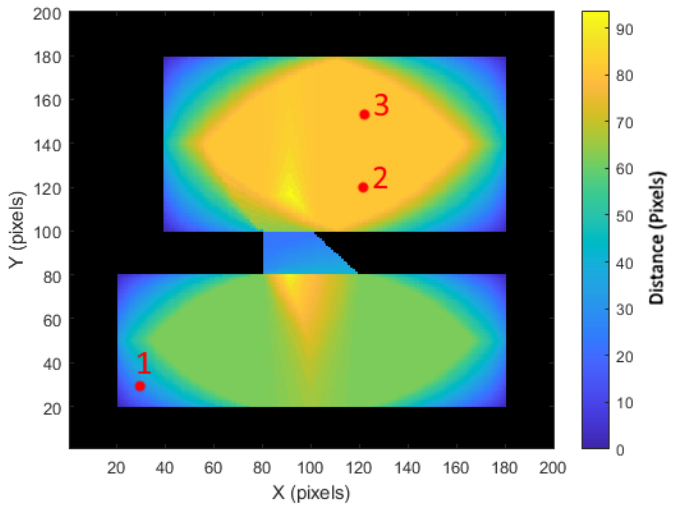

(c) The lowest SLD value at every point when comparing all directions

Figure 4.6: Demonstration of SLD in a sample area. Boundaries of the area indicated in black. All distances indicated by number of pixels. The same three points are indicated in red in all three plots

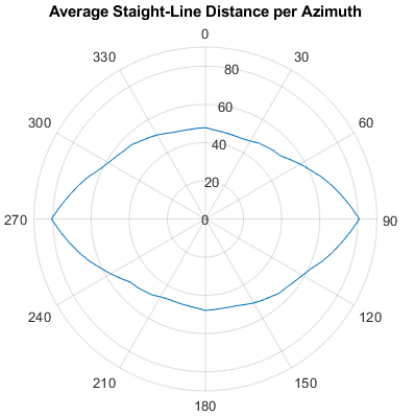

(a) Rose diagram indicating for every direction the average SLD for all points in the sample area shown in figure 7.2.

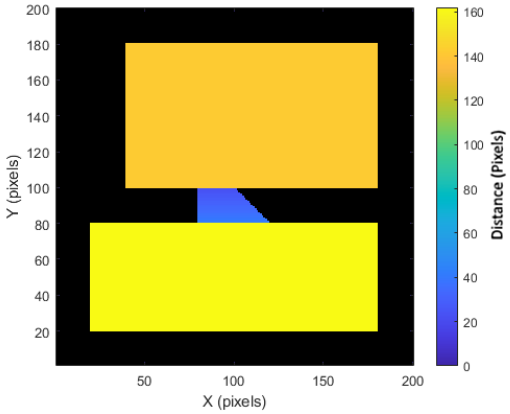

(b) The SLD in the best direction as determined by figure 4.7a.

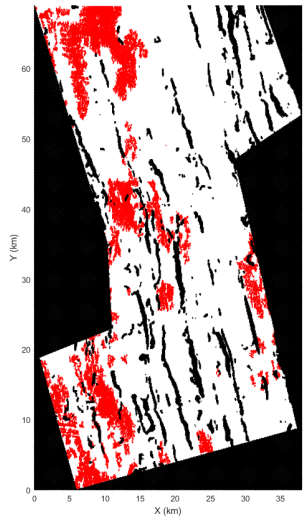

Figure 4.8: The constrained areas in site 3. Areas outside the boundaries of the site are shown in black. Areas that have a slope above the traversable threshold are also black. Areas with nodule types that are currently unmineable are indicated in red.

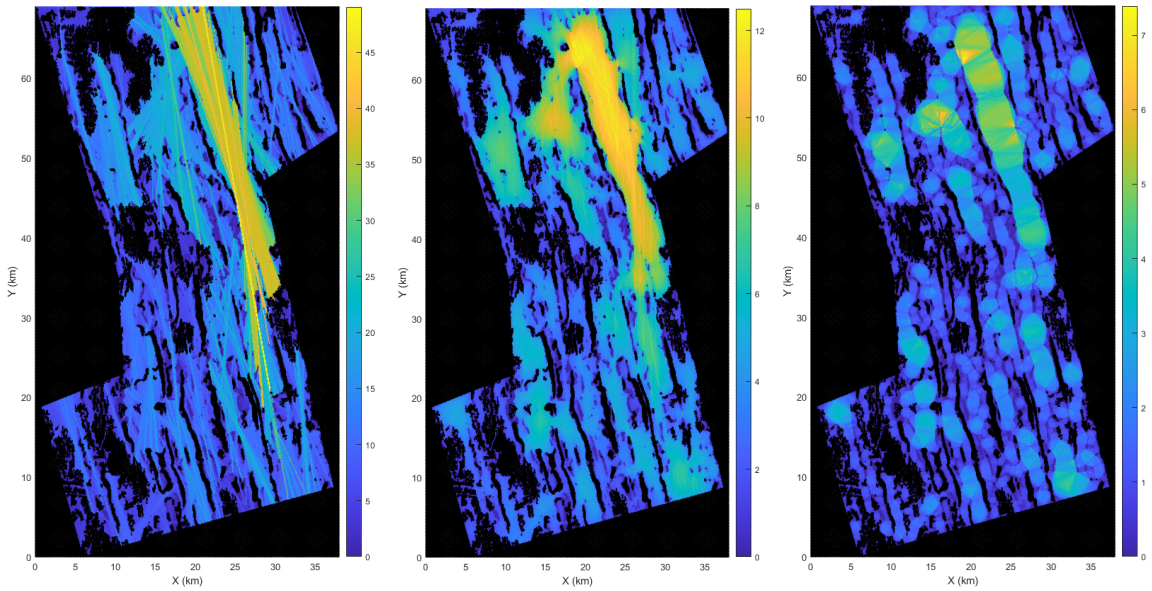

Figure 4.9: The maximum SLD (left), the mean SLD (middle), and minimum SLD (right) in each direction. Distances in kilometers. A larger version of the same plots can be found in the appendix figures B.1 to B.3.

The results show that an azimuth of 345 has the longest average length. This corresponds to the general direction of the geological features observed in figures 4.8 and 4.9. It also shows that the average length is lower when the nodule type is a constraint. In the appendix, plots corresponding to figure 4.8 to figure 4.10 are added for several sites: site 5 (figures B.7 - B.9), site 7 (figures B.10 - B.12), site 8 (figures B.14 - B.15), and the PMT area (figures B.4 - B.6). The results all show the same pattern: the longest average SLD is parallel to the geological features.

4.7. Discussion

4.7.1. Ordinary Kriging

For the variogram fitting, the model that was used has a relatively low nugget effect (20%) and large continuity (40km) compared to literature [Mucha et al., 2013][AMC, 2016][Singh and Sudhakar, 2017]. Singh and Sudhakar [2017] determined an average nugget variance of 43% for study areas in the CCZ (from 9636 samples).

Differences in the block model tonnages can be attributed to various aspects:

- The nodule abundance data that was derived from photographs, which was included in the technical report, but not available for this thesis.
- In the technical report the historical data was excluded within the 7km sample spacing area for in the interpolation process. Those were included in this thesis, which may account for the slightly lower indicated resources.
- Furthermore, nodules within areas with slopes over 8° were excluded from the resource. There might be small differences between the technical report and this thesis that are related to different filters used to filter the noise from the bathymetry data. There are not many structures with slopes over 8° inside the indicated and measured resource ares. Therefore, the differences should be small and should mainly affect the inferred resources.

Overall the quality of the kriging should be more than good enough for the purposes of this thesis.

4.7.2. Slope Constraints

The resolution of the bathymetry data (50m) is larger than the dimensions of the collector. It is possible that (parts of) pixels are wrongly classified. They are either inaccessible while they should be accessible (case 1)

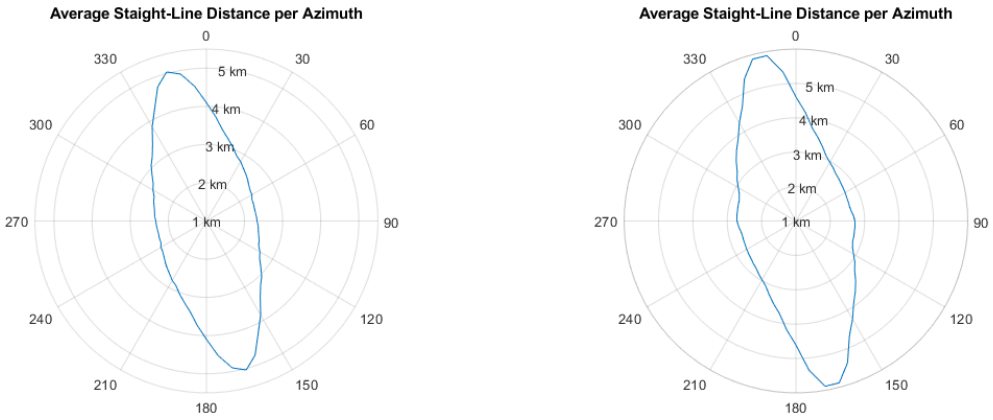

Figure 4.10: Two rose diagrams showing the average SLD for each azimuth for site 3. On the left, the rose diagram for site 3 includes a hard-constraint for the nodule types. On the right, the rose diagram assumes that all nodule types are traversable.

or accessible while they should be inaccessible (case 2).

Case 1 Since the only areas that are classified as inaccessible are the large scale geological features, this should occur there. In that case, the boundary of the inaccessible area is wrong.

Case 2 Smaller geological features are not clearly visible using a 50m resolution. The pixels that contain them are therefore classified as accessible. It is very likely that smaller obstacles will be relevant for the performance of the mining operation. That would also make it relevant for determining site or field boundaries. Because of the available resolution of the data, this aspect has not been included in this thesis. However, in upcoming chapter 6, the impact of obstacles on the performance of the NC is analyzed, which can help mine planning when higher resolution data is available.

If higher resolution data is available, the neighborhood filter has to be modified. This filter is in this thesis mainly used to filter out noise. However, it effectively also decides the type of obstacle that is a hard-constraint. Obstacles that are by themselves will be filtered out if they are not large (one pixel for example) because they show up in the same way that noise does.

4.7.3. Site Selection

It should be clear that the considerations discussed previously have a direct impact on the delineation of the mine sites. For example, in the case the resource boundaries change, this will change the delineation of the site boundaries. The current sites are therefore only a show of methodology. Using the same methodology it would be possible to include different parameters into the site definition, for example soil quality.

A feature of mining sites is that each site will be completely mined before moving on to the next. Smaller mining sites would therefore lend itself to higher selectivity, certainly if more parameters are included into making the sites. For making smaller sites the main constraint becomes more challenging: mine sites boundaries shouldn't cross possible mining fields.

One approach that would allow this main constraint to be fulfilled, is to leave out sites from the hierarchy and directly delineate continuous mining fields. This approach is unfortunately not possible in this thesis due to computational constraints to do with the algorithms used to delineate mining fields. A big reason to make mining sites before moving on to mining fields, is therefore the practical computational aspect.

4.7.4. Straight-Line Distance

The methodology described in section 4.6.1 is quite computationally intensive, depending on the size of the input raster, the number of direction and how constrained the area in the raster is. For that reason, two steps have been taken: Firstly, the resolution of the data was reduced from 50m per pixel (from the bathymetry) to 100m per pixel. Furthermore, the SLD has been calculated in steps of 5 degrees. The results can therefore contain some artifacts. This can be seen in figure 4.6b, where the longest diagonal shown behaves in a step-like pattern.

In more open areas with less slope constraints, such as site 7 shown in figure B.11 or the PMT area figure B.6, the results suffer a bit more. Especially the results from the minimum SLD suffer because it responds strongly to singular obstacles in an open area. Overall, by determining the SLD in 5 degree steps, the accuracy of the results for the longest SLD are slightly limited, and the minimum SLD seems mostly applicable to more constrained areas.

The computational power required for the algorithm also meant that the SLD was not calculated on the scale of the license area, although this might have proven useful in determining mine site boundaries.

Overall, the SLD is suitable as a method to identify areas suitable for mining. However, the pixels that are seen as a hard-constrained need to be carefully considered, as discussed in section about slope constraints.

4.8. Conclusion

At the start of this chapter two research questions were asked:

- *How can high quality mining areas be identified?*
- *How can mining sites be selected?*

Mining areas can be identified by their attributes. From this chapter, those attributes are:

- **Resource level**. Higher resource level means higher confidence. Indicated and measured resources can potentially be converted to reserves.
- **Nodule abundance.** Higher nodule abundance makes it more likely that the resource is economically mineable.
- **Long Straight-Line Distance (SLD).** When comparing two areas for their SLD, the area that has the higher SLD in one direction is of higher quality.
- **High minimum Straight-Line Distance (SLD).** The minimum SLD indicates bottlenecks, which are areas that should be avoided by the NC.
- **Slope constraints.** The area cannot be inside an area constrained by slopes, as determined by the bathymetry and neighborhood filter.
- **Nodule type**. Nodule type 2 and 3 are considered not mineable.

Mining sites should be selected by taking into account that mining fields cannot cross site boundaries. Therefore the boundaries can be next to restrictive areas:

- Areas that are constrained because of high slopes.
- Areas with nodule type 2 and 3.
- Areas with lower resource levels that cannot be converted into mineable reserves.
- Areas with low nodule abundance that cannot profitably be mined.

5

Approximating Driving Patterns

5.1. Introduction

In chapter 4, mining sites were introduced. Eventually, these will be further subdivided into mining fields in chapter 7. Before mining fields are made, the operation of the NC must be approximated inside mining fields. The NC can operate using the two driving patterns for the NC that were introduced in the literature study: swathing and contouring. In this chapter they are discussed in detail. Approximations for the two driving patterns make use of the SLD method described in chapter 4 and the operational parameters for the NC as outlined in chapter 3. The overview of this chapter is shown in figure 5.1

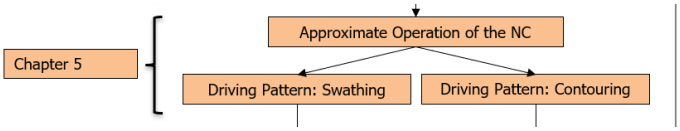

Figure 5.1: The thesis overview for chapter 5. The full overview is shown in figure 1.3

5.2. Objective and Research Questions

The objective of this chapter is to determine KPIs that are relevant for creating mining fields by approximating the operation of the NC. Such KPIs must be within the scope of this thesis. Most likely they will be directly related to nodule production.

The research questions that will be answered in this chapter are:

1. *What are the KPIs of a mining field?*
2. *How can these KPIs be calculated?*

5.3. Types of Driving Patterns

It is assumed that the way the Nodule Collector (NC) is driven on the fields matters for the mining operation. In the ideal case, a detailed simulation would be run for every field, however, a detailed planning of the collector path is outside the scope of this thesis. Therefore, the driving methods will be approximated so that the best driving method and the best fields can be decided upon. Two different methods of operating the nodule collector are compared that were suggested in Park et al. [2011]. A third method is a combination of the first two:

1. **Swathing**. The swathing pattern consists of straight, parallel driving lanes called swaths. For each swath, the collector drives in a straight line until the end of the field is reached. A 180-degree turn is made to turn towards the next swath, parallel to the previous swath. This procedure is repeated until the field is completely covered. For an example, see figure 5.2. For each swath there is some time related to the maneuvering time of the 180-degree turn, which is assumed to be unproductive time. Therefore, an ideal operational scenario would minimize the unproductive time (spent maneuvering), relative to productive driving time (driving straight).

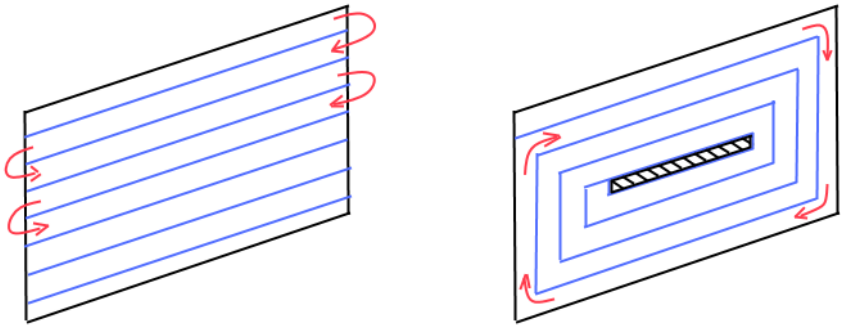

Figure 5.2: The same area covered using two different pathing patterns. On the left: swathing. On the right: contouring, which leaves a small part in the center of the field unmined. The patterns would be applied inside fields such as the ones indicated in figure 2.5.

2. **Contouring**. The contouring pattern is created by the NC rounding the field, making an inward spiral following the the edges of the field. For an example, see figure 5.2. Assumed is that the nodule collector has a certain turning radius. This means that some area can be lost in corners and the innermost part of the spiral where turns are too sharp for the turning radius of the NC. It is also assumed that there is time penalty for each loop around the field to account for the turns that must be made.
3. **Combined method**. Because contouring leaves an inner section of the field unmined, a third method is to do contouring and finish the innermost section using swathing.

5.4. Introducing Production Rate

The Production Rate (PR) is the weight of nodules per unit time that is collected from the sea floor. This is an important metric for the mining operation for economical considerations and it allows the mining operation to set targets on a timely basis, but also per field or site. For example tonnage per year, per field, or per site.

The Production Rate (PR) can also be used to judge the quality of mining areas by the rates that can be achieved there. To determine how good a field is, and how it compares to other fields, the average PR is calculated. It takes three aspects into account:

1. **Nodule tonnage**. Mainly dependent on the area that the field is covering and the nodule abundance inside the field. However, there is also a difference between swathing and contouring since swathing covers the entire field and contouring leaves parts unmined, thus changing the area covered.
2. **Mining Time**. The larger a field, the more time it will take to mine the field. The mining time depends on the surface area of the field, and the rate that this area is mined. This is called the Mining Rate (MR), determined by the speed and width of the NC. See equation 5.1.
3. **Unproductive Time**. Time is also influenced by the driving pattern inside the field. Swathing or contouring both add additional time, albeit in different ways. In the upcoming sections, the approximations for the maneuvering time for both driving methods are detailed.

5.5. Approximating Swathing Pattern

First, the number of swaths is determined. This is done by using the width of the field in the direction orthogonal to the driving direction, or the *effective width* (w_f). Since the fields and areas in this thesis consist of raster points, calculating the effective width from the raster points is done by determining the minimum bounding rectangle using an algorithm from Diener [2020]. The shortest side of the rectangle is used as the effective width.

The number of swaths corresponds to the number of times that the nodule collector has to maneuver at the end of each lane. Several assumptions are made:

1. The nodule collector drives in a straight line with a constant speed in a certain direction.

Table 5.1: Input parameters for calculations in chapter 5 with units and their base case for sensitivity calculations.

Symbol	Name	Unit	Base Case
w_{nc}	Width of the NC	m	13
v_{nc}	Speed of the NC	m/s	0.5
MR	Mining Rate	m^2/s	6.5
T_{man}	Time for maneuvering to the next lane	s	30
η_c	Collecting efficiency	%	80
S_l	Spacing between lanes	m	0
R_t	Turning Radius of the NC	m	30
SLD	Straight-Line Distance	m	
PR	Production Rate	kg/s	
η_{Af}	Area Coverage Efficiency	%	
η_{swath}	Swathing Efficiency	%	
T_f	Time spent in-field	s	
A_f	Area of the field	m^2	
w_f	effective width of the field	m	
N_f	Nodule Tonnage in the Field	t	
N_{loops}	Number of loops for contouring a field	–	

2. At the end of each lane the collector maneuvers to the next lane, and this takes a constant amount of time. This time is assumed to be unproductive.
3. The driving lanes (swaths) within the field are side-by-side and therefore parallel to the other lanes.
4. There are no lanes in line of each other. Because if the opposite is true, the approximation underestimates the number of lanes.
5. The spacing between each lane is constant.

We can determine the time it takes for the collector to cover an area by using the speed (v_{nc}) and the effective width (w_{nc}) of the NC, to determine the Mining Rate (MR) in m^2/s, equation 5.1.

$$MR = v_{nc} * w_{nc} \tag{5.1}$$

The area coverage efficiency for fields (η_{Af}) is introduced as the percentage of the field that is mined, which for swathing depends on the spacing between lanes (S_l).

$$\eta_{Af} = \frac{A_{mined}}{A_f} = \frac{w_{nc}}{w_{nc} + S_l} \tag{5.2}$$

Then the in-field time (T_f) is determined, which is a sum of productive mining time, and the unproductive time depending on the number of swaths.

$$T_f = \frac{A_f * \eta_{Af}}{MR} + \frac{w_f * T_{man}}{w_{nc} + S_l} \tag{5.3}$$

The nodule tonnage is approximated by multiplying the nodule tonnage in the field (N_f) with the area and collecting efficiencies. The in-field time together with the tonnage of the nodules mined gives the PR in kg/s. All parameters that are used in the calculation are shown in table 5.1.

$$PR_{field} = \frac{N_f * \eta_c * \eta_{Af}}{T_f} * 10^3 \tag{5.4}$$

5.6. Production Rate Targets Using Swathing

The Straight-Line Distance (SLD) approximates the length of a swath at each point. Since the Nodule Abundance (NA) has also been approximated at each point using kriging, it is possible to determine the PR that

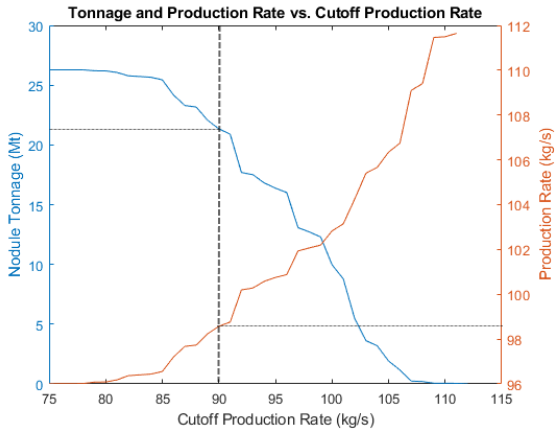

(a) The Production Rate (PR) is shown as a cutoff. The PR is calculated using equation 5.6, nodule abundance from kriging, and input parameters from table 5.1.

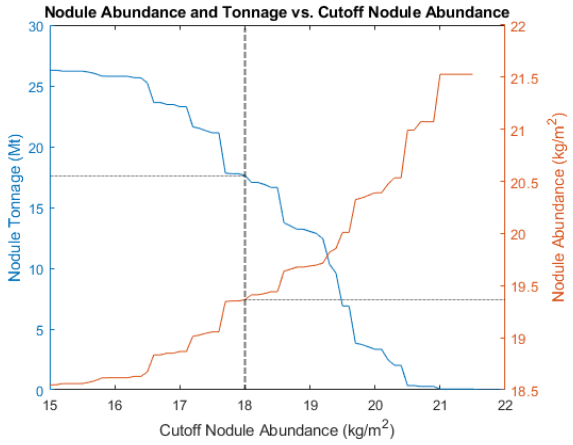

(b) The nodule abundance is shown as a cutoff. The resulting tonnage is shown for areas above the cutoff.

Figure 5.3: Both graphs show data from site 3, using the Straight-Line Distance (SLD) displayed on the left in figure 7.2. On both x-axes a cutoff value is displayed. The corresponding points on the y-axis are obtained when excluding areas that are below the cutoff.

can be achieved there. For the calculation, the *Swathing Efficiency* (η_{swath}) is introduced, shown in equation 5.5, which is the productive time as a percentage of the total time.

$$\eta_{swath} = 1 - \frac{T_{man}}{T_{man} + \frac{SLD}{v_{nc}}} \tag{5.5}$$

To determine the PR using equation 5.6 it is also necessary to know other parameters of the Nodule Collector (NC), listed in table 5.1.

$$PR_{swath} = NA * MR * \eta_c * \eta_{swath} \tag{5.6}$$

A *target PR*, or *cutoff PR* can be defined if the mining operation needs a certain PR to be achieved at all times. Since the PR can be estimated for each point using equation 5.6, areas where this PR can not be achieved can be excluded. Those areas are below the cutoff. From the remaining areas that are above the cutoff, the nodule tonnage can be calculated. The result can be summarized in a graph, shown for site 3 in figure 5.3a.

As an example, lines are indicated in figure 5.3a for a PR cutoff of 90 kg/s. All raster points where the calculated PR is below the cutoff, are excluded. This results in a total nodule tonnage of around 21.3 Mt, indicated on the left y-axis. The nodules are mined at an average PR of around 98.5 kg/s, indicated on the right y-axis. Assuming around 7000 operational hours per year site 3 would then take around 8.5 years to mine.

A similar graph is shown in figure 5.3b, which displays the NA as a cutoff. This is similar to the grade-tonnage curve seen in terrestrial mining. As an example, a NA cutoff of 18 kg/m^2 gives a total tonnage of around 17.5 Mt, which is mined at an average NA of around 19.4 kg/m^2.

5.7. Approximating Contouring Pattern

The field is based on raster points. For the approximation of the contouring mode of operation, these raster points are converted to a polygon around the boundaries of the field. The field polygon is made up of vertices and edges. To approximate the operation of the NC, the following assumptions are made:

1. The NC drives inside the field at a constant speed, following the edges of the field polygon and making turns at each vertex. It continues parallel to the inside of it's own track to make loops around field.
2. The NC must make a turn at each vertex of the polygon. This turn is possible or not depending on the turning radius of the NC.
3. For each loop around the field, time is added for maneuvering.

An algorithm was made based on parts of the approach developed by [Oksanen and Visala, 2009]. The algorithm uses the polygon of the field. For every loop, a buffer is created on the inside of the edges of the

polygon. The buffer represents the path the nodule collector takes and is the width of the harvester plus the lane spacing. Each time a buffer is created, the turns at the vertices are checked. When the turns are too tight for the NC, the mining stops, leaving the inner section unmined. The total number of loops (N_{loops}) equals the number of times a buffer could be created.

The PR can then be calculated similarly to the swathing approximation in section 5.5. First, the area coverage efficiency (η_{Af}) is determined from the unmined area in the middle of the field using equation 5.7.

$$\eta_{Af} = \frac{A_{mined}}{A_f} = \frac{w_{nc}}{w_{nc} + S_l} \tag{5.7}$$

This efficiency is used to determine the time spent mining in the field, equation 5.8. For each loop, additional unproductive time is added, equal to twice the unproductive time per swath (T_t). This was chosen because maneuvering to the next lane is essentially a 180 degree turning maneuver and each loop includes sums to a 360 degree turn.

$$T_f = \frac{A_f * \eta_{Af}}{MR} + 2T_t * N_{loops} \tag{5.8}$$

The PR can then be determined using the mined nodule tonnage, which is approximated the same way as for swathing.

$$PR_{field} = \frac{N_f * \eta_c * \eta_{Af}}{T_f} \tag{5.9}$$

5.8. Combining Contouring and Swathing

The approximations for contouring were made in section 5.7. For each field, a part would be left unmined. If this part is assumed to be not-mineable using contouring, perhaps it would be worthwhile to mine it using swathing. The approximations for swathing were made in section 5.5. Using the width of the unmined polygon, the same swathing assumptions are applied. This driving pattern is called the combined method and will be considered as a third option besides swathing and contouring.

5.9. Discussion

The approximation of the swathing pattern does not take into account many things that could be considered, but are left out within the scope of this thesis:

- Varying conditions on the ocean floor that impact the operation, such as soil types and quality, obstacles, terrain slopes under the constraining threshold and ocean currents.
- Currents in the sea.
- Operational costs of the harvester that could be considered.

5.10. Conclusion

The research question for this chapter were:

1. *What are the Key Performance Indicator (KPI)s of a mining field?*
2. *How can these Key Performance Indicators be calculated?*

In section 5.6 and 5.7 is has been shown that the PR that can be achieved in a mining field is a KPI by which the quality of a mining field can be judged. The equations laid out in this chapter show that it depends on the driving pattern, KPIs of the NC listed in table 5.1, and the Nodule Abundance (NA).

6

Field Shape and Obstacle Analysis

6.1. Introduction

In chapter 5, two driving patterns were approximated for the operation of the NC. The patterns can help assess which mining fields are most suitable by determining KPIs for a mining field. In this chapter, another method of assessing the suitability of a mining field is examined. The concept of mining fields has been inspired by agricultural fields. It is tested whether or not approximations that are made for agricultural fields also work for PN. The approximations could help in the delineation and determination of quality of mining fields. The method is this chapter is based upon the swathing driving pattern of the NC and the framework outlined in chapter 3.

The second part of this chapter analyzes the influence of obstacles in the operation of fields is tested. This is based on the discussion in section 4.7.2 which states that because of the resolution of 50 m, it is possible that there are obstacles inside the field. The overview of this chapter is shown in figure 6.1

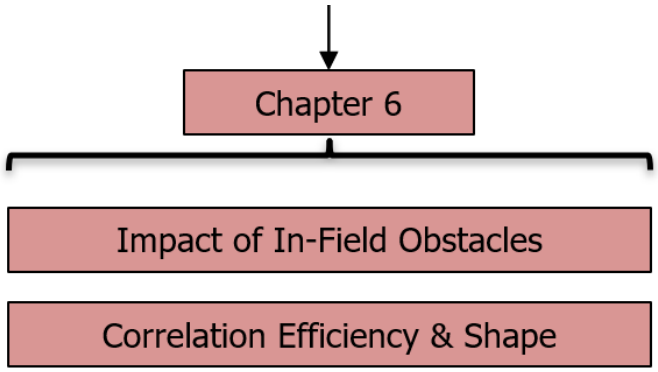

Figure 6.1: The thesis overview for chapter 6. The full overview is shown in figure 1.3

Oksanen and Visala [2009] have analyzed the Finnish agricultural fields to determine the impact of field shapes on the operation of the agricultural field machines. In their research they identified relevant shape indices and their correlation with field overhead time [Oksanen, 2013]. The overhead in this research refers to the unproductive time that is spent maneuvering, relative to the total time spent harvesting the field. So if the overhead is 10%, then 10% of the total time in the field is unproductive. The goal for this chapter is to check that there is a correlation between field shapes and overhead time that also applies to deep-sea mining fields. In that case, they could be used for future assessment of fields.

The method to assess the overhead for mining fields uses a model simulation of the deep-sea mining operation developed by Allseas. This model is computationally intensive, but can determine Key Performance Indicator (KPI)s when given a field, including the overhead time. This can be compared with the correlation with field shape from Oksanen and Visala [2009].

Another use of Allseas' mining simulation is to run fields with various conditions. One of which are is obstacles in the field. In chapter 4.7.2, it was discussed how the resolution of the data does not allow for

detecting smaller geological features and obstacles. They can cause the nodule collector to deviate from the ideal path in the field and potentially cause an overlap in areas covered by the collector. These negative effects may be the reason that an area is no longer profitably mineable. Using the mining simulator, different size and number of field obstacles are analysed.

6.2. Research Questions and Hypotheses

The goal of the research in this chapter is to find methods to approximate the overhead time of mining fields as defined by Oksanen [2013]. If these approximations are found to be valid, they can be used in the delineation of mining fields. The research questions that will be answered in this chapter:

1. *How do obstacles impact the operation of the nodule collector?*
2. *Can we use shape index correlations for the planning of deep-sea mining fields?*

The following are hypotheses for the research questions:

- Obstacles will increase the overhead of the mining fields since turnings are necessary to avoid obstacles and might also cause overlapping between paths of the machine.
- Having many smaller obstacles will have a more detrimental effect when compared to having a few larger obstacles. This is because a buffer zone must be created around obstacles, which inflates the radius of an obstacle by an absolute amount, which impacts the overall area more if there are more obstacles.
- Shape index correlations will also appear in the deep-sea mining fields, so we will be able to use them for the planning of deep-sea mining fields.
- Having a larger mining field makes shape indices less influential. This is because the time that is spent driving is a straight line is increased relative to the amount of time that is spent turning the collector.

6.3. Test Setup

Allseas has developed a high-fidelity model that plans the route of the collector inside the field and outputs several KPIs after running a simulation of the operation. The model assumes that the NC drives in a straight line and make 180 degree turns when we reach the field boundary. Obstacles are avoided by going around them (and not by making 180 degree turns). The base settings of the simulations are a field with rectangular shape, uniform nodule abundance of $17.5 kg/m^2$. The NC operates at a speed of $0.3 m/s$, a collecting efficiency of 80% and a turning radius of 30m. Each test run of the model will produce a number of KPIs that give information on how the NC behaved in the field. The main KPI is the average Production Rate (PR) in $[kg/s]$. Other KPIs can be found in the results in appendix B.

Two different tests are run to answer the research questions:

1. **Impact of obstacles in a field.** The field is covered for a certain percentage with several obstacles. Investigated is the difference in KPIs between large and small obstacles (that cover the same area of the field percentagewise). The location of the obstacles is arbitrary, but overlapping is prevented.
2. **Effect of field shapes.** Oksanen [2013] has published about the correlation between nine different shape indices and overhead time spent in an agricultural field. Fields with identical surface area, but different shapes are represented by a polygon. For every field the KPIs will be determined along with the following eight shape indices. For the calculation and description of each index, see appendix C.
   (a) Convexity.
   (b) Compactness.
   (c) Rectangularity.
   (d) Triangularity.
   (e) Ellipticity.
   (f) Ratio of principal moments.
   (g) Radius of the incircle.
   (h) 'Curb index'.

6.4. Results

6.4.1. Obstacle Fields

A simulation was run on 10 fields. The KPIs that the model output for each field with obstacles are depicted in table C.1. An example of the model output can be seen in figure 6.2.

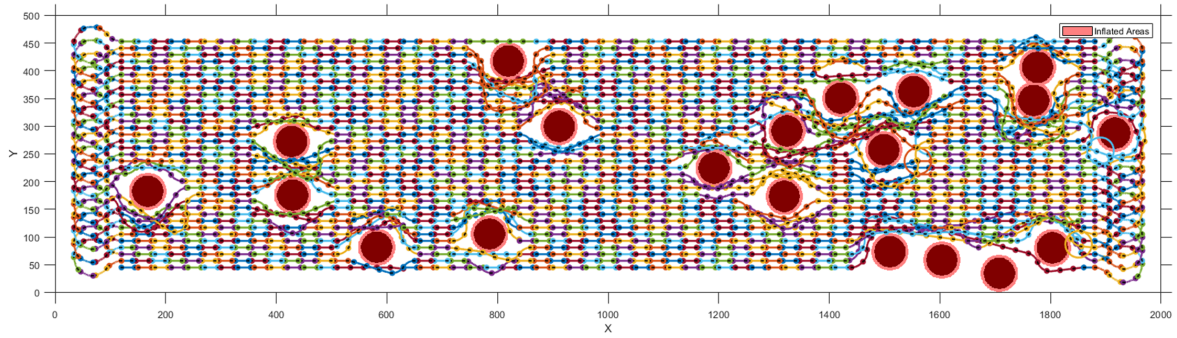

Figure 6.2: The output of the path planning model for obstacle field 4.

From the simulations is can be seen that obstacles cause the NC to deviate from the straight path. This path then overlaps with the lane next to it. These overlaps have a direct negative effect on the PR because nodules have previously been mined in this area. A linear correlation between the average Production Rate (PR) and areas losses due to overlapping can be found. Note that some area losses are inherent to the 180 degree turns at the end of swaths, as seen in figure 6.2. Therefore, area losses will never be zero in this simulation.

The following two variables are further examined for their effect on overlapping area, all depicted in figure 6.3.

1. **Total area coverage % of obstacles.** Depicted in figure 6.3, where the data points are depicted as orange squares. The interpreted trend in the data is encircled in orange and seems to indicate there is a linear relation with the area losses.
2. **Number of obstacles.** Depicted in figure 6.3, the number of obstacles shown on the secondary y-axis, with the data points indicated as blue triangles. The interpreted trend is encircled in blue, which indicates an exponential relationship between number of obstacles and overlapping area.

6.4.2. Different Field Shapes

Two sets of fields were analyzed: Convex fields and non-convex fields. The fields are displayed in appendix B in figure C.1 and C.2. For both sets of fields the KPIs and shape indices are also found in appendix B.

Using the shape indices described earlier, the overhead time for each field is estimated by using a correlation formula from Oksanen [2013]. This estimation is plotted against overhead time as calculated from the simulation. The results are shown in figure 6.4. There is no apparent correlation between the estimated overhead given by field shape correlations, and the overhead determined by the model.

6.5. Discussion

Only 11 simulations with obstacles were performed. The sample size seems therefore too small to draw very robust conclusions. Obviously having obstacles in the field is detrimental for the PR, but the exact formula can not confidently be deduced from the results.

The interpreted relationships with overlapping area line up with the hypothesis, although some data points have been left out of the encircled areas. Because of the random distribution of the obstacles, some unintended effect can occur. For example, if two obstacles are close together, they can form a choke point or wall take brings additional detrimental effects. If obstacles happen to be near the edge, the NC has an easier time passing around them.

As for the shape indices, they show no correlation with the simulations. This does not mean that the shape indices are wrong. They just do not fit the pathing in the simulation. The simulation differs significantly from the driving patterns used in Oksanen and Visala [2009], which is a combination of contouring and swathing in multiple directions.

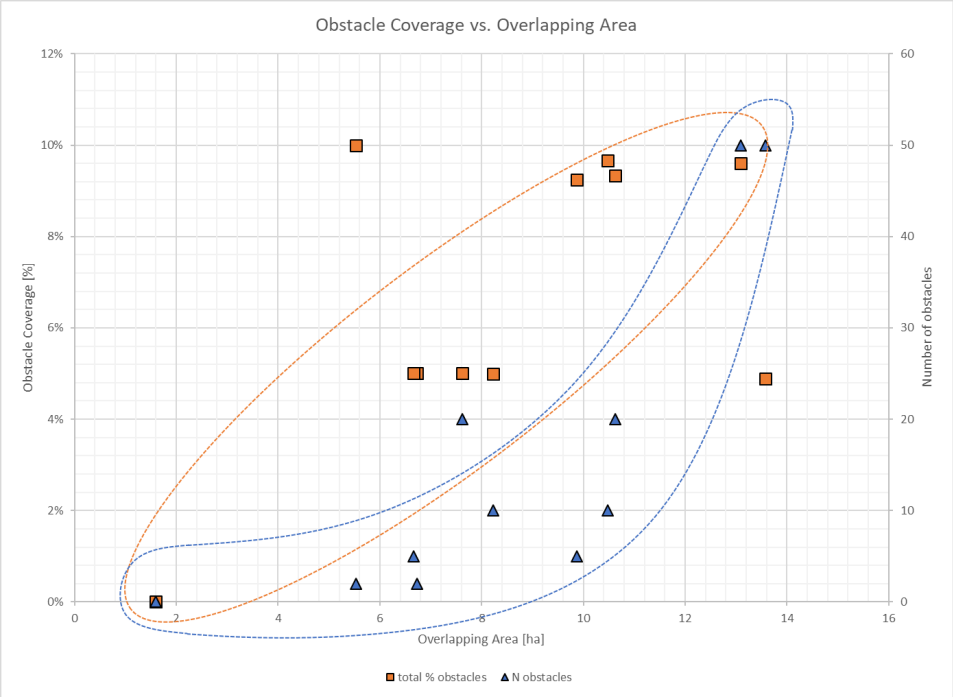

Figure 6.3: Results from the path planning model.Overlapped plotted against several obstacle parameters: area coverage of obstacles and number of obstacles. Note that the simulation without obstacles (Obstacle Coverage = 0%) overlaps for the two datasets.

6.6. Conclusion

1. *How do obstacles impact the operation of the nodule collector?* The impact of obstacles comes from the area losses from avoiding obstacles. The area coverage of obstacles shows a linear relationship with area losses. The number of obstacles shows an exponential relationship with area losses.
2. *Can we use shape index correlations for the planning of deep-sea mining fields?* Based on the simulations in this thesis, the shape indices of mining fields can not be used to approximate the operation of the NC in those fields.

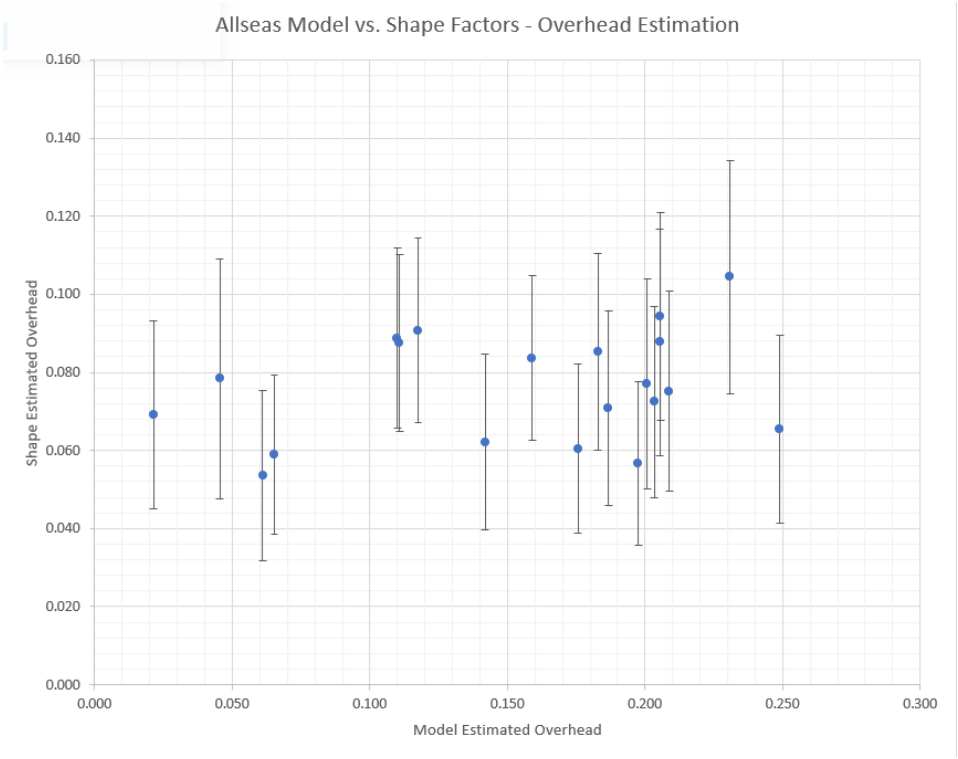

Figure 6.4: The overhead (percentage of unproductive time) as estimated from the shape indices (Y-axis) is plotted against the overhead found by the simulation (X-axis).

7

Synthesizing Mining Fields

7.1. Introduction

In chapter 4, the license area was analyzed and divided into multiple mining sites. The next step is to actually define the fields inside the mining site. To do this, SLD has been introduced in chapter 4.6 and two driving patterns of the NC have been approximated in chapter 5. To select good fields, KPIs of the mining operation inside fields are compared. The set of mining fields that is found to perform the best will be used for further analysis in chapter 8. The thesis process is shown in figure 7.1.

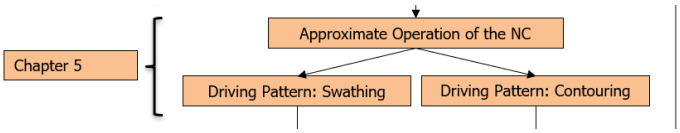

Figure 7.1: The thesis overview for chapter 7. The full overview is shown in figure 1.3

The area of the mining sites is defined previously (figure 4.5). Any point inside a site can be either part of a mining field, or not be mined at all. In other words, the mineable area of the mining site has to be decomposed into what are called fields. The site is completely covered and the fields don't overlap, so this is an *exact cellular decomposition* of the mining site [Latombe, 1991].

These fields can then be operated using different driving patterns, that were discussed in chapter 5. Because there are different ways of driving the nodule collector in a field, it is assumed that certain type of fields are more suited to one or the other. Therefore, two different methods of making fields are tested. The first method aims to make long fields. The second method aims to make fields with a more compact shape.

7.2. Objective and Research Questions

The objective of this chapter is the development of two methods for making mining fields and analyzing the approximation of two modes of operating those fields. The fields and operational methods are then compared. The research questions that will be answered in this chapter are:

1. *What is a suitable methods to define the mining fields?*
2. *What is the effect of different driving patters on the field Key Performance Indicators?*
3. *What are the sensitivity of Nodule Collector (NC) parameters with regards to mining Key Performance Indicator (KPI)s?*
4. *What are the important parameters for making fields with good Key Performance Indicator (KPI)s within a site?*

7.3. Methods for Making Long Fields

A method is proposed for decomposing a mining site into fields with a elongated shape. This method relies on the Straight-Line Distance (SLD) in a single direction. To illustrate the basis for the method, a sample

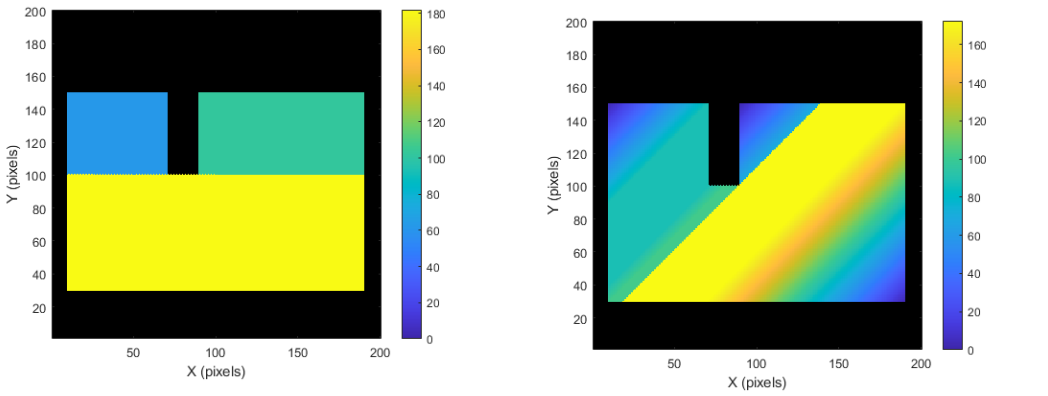

(a) Artificial field with the Straight-Line Distance (SLD) in the direction with the longest average distance (azimuth 90).

(b) Artificial field with the SLD in an arbitrary direction (azimuth 55)

Figure 7.2: An artificial field is shown with boundaries indicated in black.

site is depicted in figure 7.2, with the boundaries in black. In figure 7.2a, the SLD is left-to-right (azimuth 90), which is the direction in which the SLD is on average the longest in this sample site. in figure 7.2b, an arbitrary SLD azimuth is chosen (55 degrees north). In both cases, sharp transitions can be observed, caused by the protruding obstacle in the otherwise rectangular area. In the right figure, more gradual transitions can also be observed, caused by the difference in angle between the SLD and the area boundaries.

The sharp transitions are are perceived to be suitable boundaries for mining fields. This is because when using the swathing method, straight driving lanes are made in a certain direction, the length of which is indicated by the SLD. A sharp transition in SLD indicates an area where the the lanes are suddenly divided by an obstacle. A decision has to be made where to continue mining. Since the objective of a mining field is to have one continuous mineable area, this decision point at a sharp transition is a suitable boundary.

The sites, such as site 3 in figure 7.3, consist of raster points with information at each point. A method is proposed where raster points are combined into fields. The sharp transitions will be used as a boundaries of the fields. To do this, the transitions need to be defined. Two boundary criteria were tested:

Criteria 1: **Boundary based on gradient.** The first method uses the gradient which is defined as the absolute difference of SLD between raster points in two directions. Sharp transitions in SLD will show a high gradient. For site 3 this is shown on figure 7.3b. The threshold is based on the relative difference between the gradient and the SLD value at that pixel.

Criteria 2: **Boundary based on difference with Longest SLD.** The second method selects the longest Straight-Line Distance (SLD) available in the site. For site 3, this is plotted in figure 7.3a. When the difference with this value is too large, this is seen as a boundary of the field. The threshold is based on the relative difference between the longest SLD and the SLD value at the boundary.

In both cases, the correct value for the threshold that determines the boundaries is decided by sensitivity analysis. In the method to make fields, a field starts at one raster point and continually searches points surrounding points to add to the field. Roughly the following five steps are followed:

1. Start the field by selecting the point with the highest SLD that is available.
2. Set a threshold for the boundary, for example 20% of the largest SLD in the field.
3. Loop over the points surrounding the points in the field:
   (a) When the value (gradient or SLD) at that point is below the threshold, add the point to the field.
   (b) If the point exceeds the threshold, this point becomes a field boundary.
4. End the field when all the points surrounding the field are boundaries.
5. Move to the next field and repeat until all mineable areas in the site are part of a field.

Using this method, there are two adjustable parameters that affect the results. Firstly, the driving direction and the direction of SLD. This affects the SLD value at each point and therefore the results. And secondly, the threshold chosen for the field boundary.

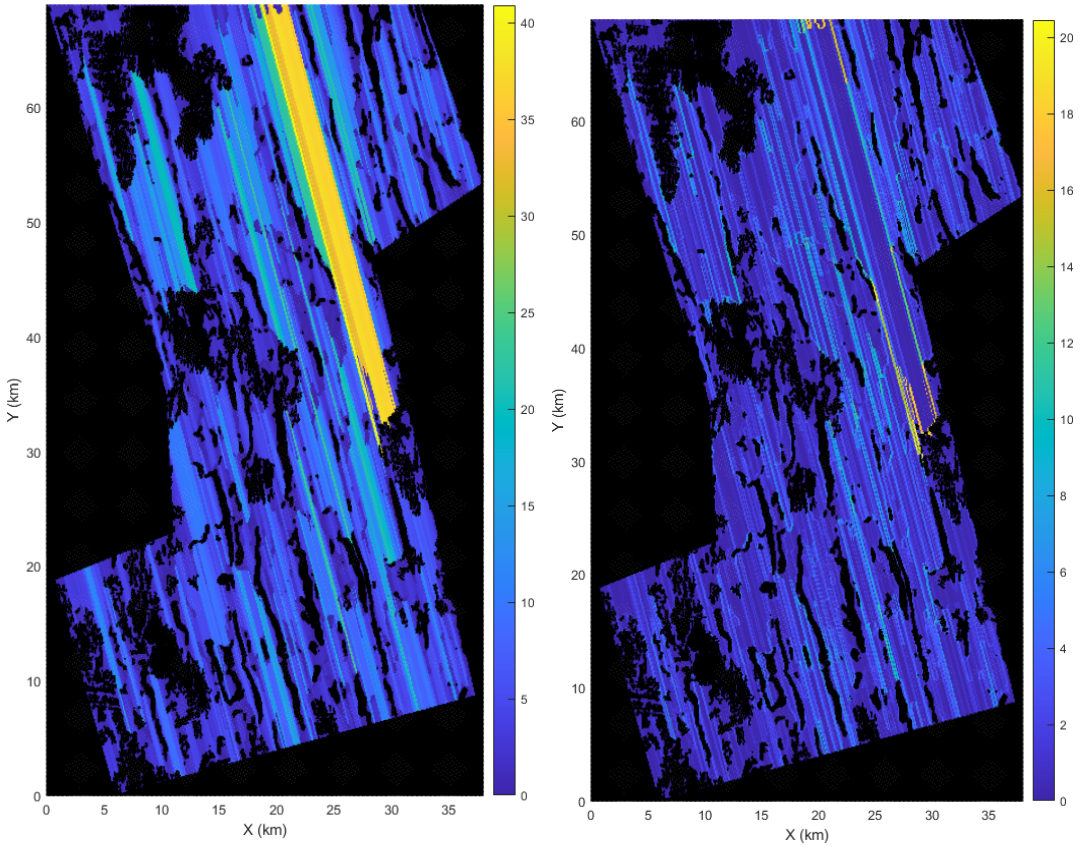

(a) The SLD in the best direction azimuth for site 3, which corresponds to the direction determined from figure 4.9.

(b) The gradient between raster points is shown, based on figure 7.3a

Figure 7.3: Site 3 is shown with hard constrained areas in black, previously shown in figure 4.8. The hard constrained areas correspond to the boundaries, slopes above thresholds, and nodule type 2 3.

Table 7.1: Results from making fields inside site 3 using two boundary criteria. Only the best solution that doesn't cross sharp boundaries is shown.

	Boundary Criteria 1	**Boundary Criteria 2**
Swathing Production Rate [kg/s]	85.27	96.25
Site coverage of largest 10% of fields [%]	91.2	91.1
Total number of fields in site 3	12472	3753

7.4. Resulting Long Fields

Fields are made using the method described previously. A sensitivity analysis is performed for the threshold of the two types of boundary criteria. The fields resulting from a threshold value must not cross sharp transitions. From the threshold values that comply with that, the value that results in the highest Production Rate (PR) when operating with a swathing driving pattern is chosen.

The results are shown in table 7.1. Boundary criteria 1 proved to be unreliable for selecting long fields. Many very small fields (less than 3 ha) were created, which depressed the resulting PR. Boundary criteria 2 was more successful in creating larger fields. The total number of fields is therefore lower as well.

The best solution uses boundary criteria 2 and contains 3753 fields inside site 3. Various statistics on the size distribution of the fields are shown in table 7.2. The largest 10% of the fields all have a surface area larger than 30ha and together cover 91.1% of the mineable area of site 3. The largest 10% of fields are plotted in figure 7.4a.

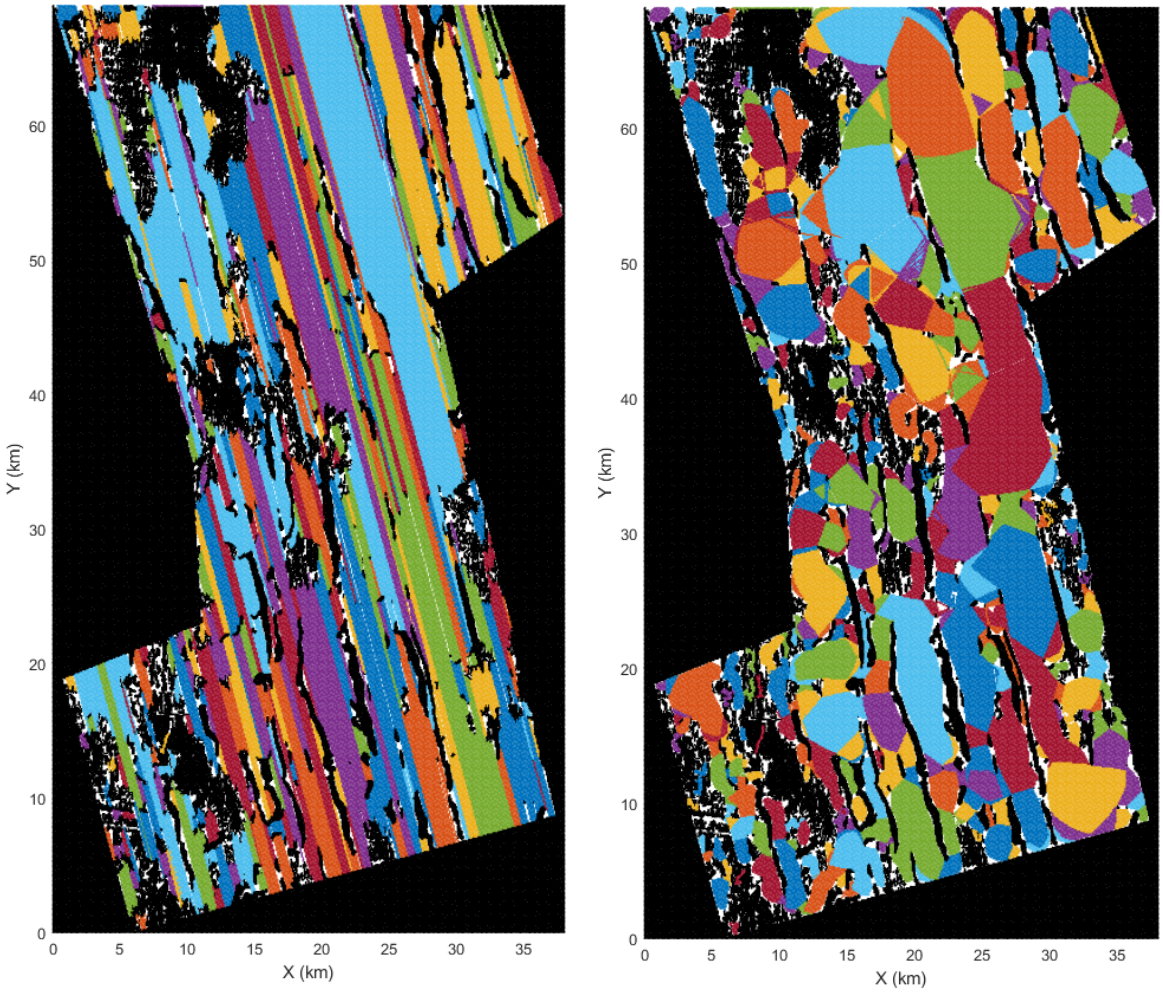

(a) The largest 10% of long fields resulting from the solution described in section 7.4.

(b) The largest 10% of compact fields resulting from the solution described in section 7.4.

Figure 7.4: Both plots showing the largest 10% of fields in site 3 with each field given a random colour. Areas in black are constrained. Areas in white are either unmined or in the smallest 90% of in terms of size.

Table 7.2: Summary statistics of the field sizes for the two sets of fields (units = ha).

	Long Fields	**Compact Fields**
Number of fields	3753	4267
Mean size	37.8	33.2
Minimum size	1	1
Maximum size	13187	5245
1st Quartile	1	1
2nd Quartile	2	2
3rd Quartile	6	7
Standard Deviation	309.2	216.8
Skewness	26.3	15.2

7.5. Method for Making Compact Fields

Using the assumptions outlined in the section 5.7, it becomes clear that a for a field to be suitable for contouring, the outline of the field shouldn't have very sharp corners. Additionally, since unproductive time is added for each loop, each loop should ideally be as large as possible, so the fields should be as large as possible.

Another criteria that follows from our approximation, that is less obvious, is that a field should not contain any bottlenecks: parts of the field that are thinner than the rest. This is because as loops around the edge of the field are completed, the bottlenecks will close, splitting the field in two. This process is schematically shown in figure 7.5.

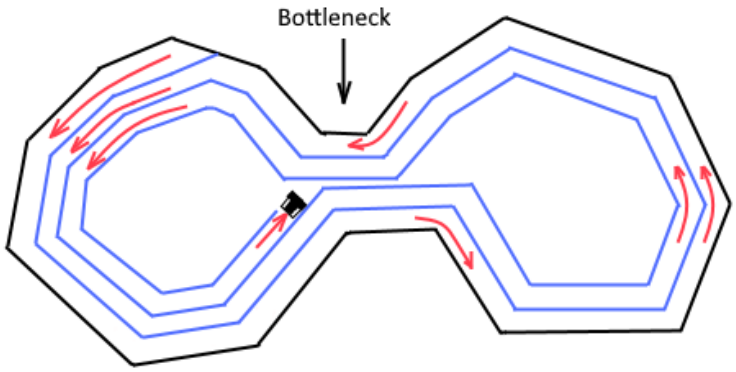

Figure 7.5: A schematic illustration of a field with a bottleneck. The nodule collector runs into it's own track on the third loop.

Following these criteria, the proposed method for making compact fields relies on the minimum Straight-Line Distance (SLD). For site 3, a plot of this was shown previously in figure 4.9 or enlarged the appendix in figure B.3. A low minimum SLD can be used to indicate a "bottleneck". Following the criteria we set out, areas with a high minimum SLD, (without bottlenecks) are perceived to be suitable for contouring.

For combining raster points into compact fields,the same procedure is followed as when making long fields. Except in this case, the minimum SLD is used instead of the SLD in one direction. The point with the highest minimum SLD is chosen as the starting point for the first field. Points surrounding the starting point are evaluated: when their minimum SLD value is within the threshold, it is added to the field.¨The threshold used in this case is the relative difference between the longest SLD in the field and the boundary.

7.6. Resulting Compact Fields

When long fields were made, it was easy to visually assess when the threshold was too large, because the fields would extend across clear boundaries that would violate the assumptions of swathing. For contouring it is less obvious. Although the fields should not include bottlenecks, it is hard to avoid them as the fields get smaller. When choosing the correct threshold, the larger fields have been the main focus of scrutiny. A threshold of 50% and lower were deemed to have large fields with an adequate shape. The same KPI were

analysed as previously when making long fields: the production rate achieved in the whole site.

The solution that was deemed the best result from the threshold of 50% are depicted in figure 7.4b. The statistics on the size distribution of the 4267 fields are shown in table 7.2.

7.7. Comparing Driving Patterns

There are now two sets of fields, resulting from section 7.4 and 7.6. In this section both are compared using swathing and contouring. A third option is also analyzed where contouring is combined with swathing. Because of the size distribution of the fields potentially affecting results, it has been chosen to show results both for all fields, as well the 100 largest fields in the set.

When making the fields for the site, the important KPI was the production rate that could be achieved. However, since production rate depends on nodule abundance, it is intrinsic to site 3. For comparing different driving methods, the dependency on nodule abundance is removed by introducing a different KPI: the unproductive time per unit area covered. All driving patterns add unproductive time for maneuvering. The pattern that adds on average the least per unit area should be more efficient and result in a higher production rate under the same nodule abundance conditions. Lastly, the production rate does not measure the total tonnage of nodules that is recovered from the ocean floor. Therefore, the total area coverage in the various methods are compared.

In figure 7.6 the added maneuvering time per hectare of mined area is shown. Long shaped fields consistently outperform the compact fields. When comparing driving methods the results show that out of all driving patterns contouring adds the least unproductive maneuvering time for area covered.

When comparing driving patterns between all fields and the largest 100 fields, the differences are quite large, indicating the detrimental effect of smaller fields on the unproductive time.

Swathing outperforms the combined method when considering all fields. When only considering the largest 100 fields, the combined method is better than swathing. The cause of this trend is likely because the combined method is largely dependent on the area coverage of the contouring method. For smaller fields, the unmined area in contouring is relatively large compared to the size of the field. In the combined method this area is mined using swathing, which can be inefficient if there are a lot of small fields.

Figure 7.7 shows the percentage coverage (or area efficiency) of site 3. Note that for all cases shown the lane spacing is zero. This means that when swathing or using the combined method, the whole field is mined. The results for contouring show that a higher percentage of area coverage is reached when mining the long shaped fields, compared to the compact fields, both for the 100 largest fields as for all fields. This is a result that goes against the hypothesis that compact fields would be more suitable for contouring. The cause might be that even though the fields generated are more compact, the corner angles are not necessarily less tight. As can be seen in figure 7.4b, most fields have a round shape, there are fields with triangular shape and tight corners.

7.8. Sensitivity Analysis of Nodule Collector Parameters

Figure 7.8 shows the impact of three parameters on the added maneuvering time. Since the speed of the NC has no influence, it is not listed. From the graph it can be seen that under none of the listed circumstances swathing outperforms contouring. Turning radius seems to have little effect on the added maneuvering time of contouring, although the area that is covered is reduced.

Table 7.3 shows that the unproductive time is really only a small percentage of the total time spent in the field. The most important parameters are therefore the parameters that reduce the mining time: The speed of the NC and the effective width of the NC. From figure 7.8 it is shown that increasing the width also decreases the total maneuvering time, so if a choice needs to be made between the two, increasing the width should have priority. However, the advantages are offset in the case that an increase in width also leads to an increase in maneuvering time.

7.9. Assessing the Reproducibility of Field Methods

It is important to determine if the method proposed for making fields and the optimal thresholds, are also viable for other areas, and not just site 3. Therefore, the same methods for making fields, using the same settings are replicated on site 7. Site 7 was made from the previous division made in figure 4.5.

For the long fields, the method generated 2718 fields to fill up the site. The largest 100 fields are depicted in figure 7.9a. The fields comply with the constraints listed in section 7.3, and look promising. For the compact

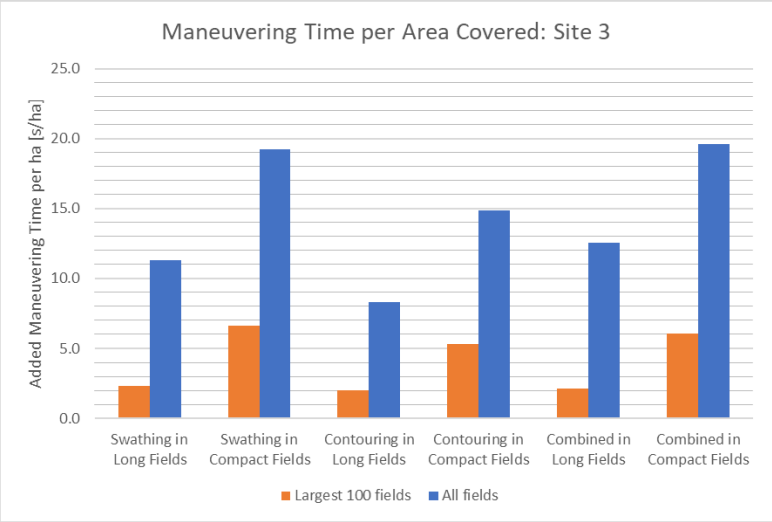

Figure 7.6: Maneuvering time per hectare for two sets of fields in site 3: long and compact fields. Three types of driving pattern are used: swathing, contouring and combined. Lastly, the production rates are compared between the largest 100 fields and all the fields combined (including the 100 largest).

Table 7.3: The unproductive time as a percentage of total time. Results for both sets of fields, for three driving patterns.

	Swathing in Long Fields	**Swathing in Compact Fields**	**Contouring in Long Fields**	**Contouring in Compact Fields**	**Combined in Long Fields**	**Combined in Compact Fields**
All fields	1.11%	1.23%	0.54%	0.96%	1.23%	1.26%
Largest 100 fields	0.15%	0.43%	0.13%	0.34%	0.14%	0.39%

fields, the method generated 3482 fields to fill up the site. The largest 100 are depicted in figure 7.9b. There are some oddly shaped fields that potentially contain bottlenecks and therefore do not comply with the constraints listed in section 7.5. Adjustments to the threshold improved the results slightly, although bottlenecks remained in some of the fields. It is possible that this area is not well suited to making compact fields. The reason for that might be that site 7 is less constrained and contains wide open areas. As discussed in section 4.7.4, the minimum SLD performs less in open areas.

With these two sets of fields, the maneuvering times per hectare are calculated for each driving method. It can be observed that the same pattern is present as in figure 7.6. The actual values are lower in each case, but this is because the fields sizes and shapes are different. The presence of the same pattern means that the results are reproducible.

Fields for a closeup of the area, which is inside site 7, are presented in the appendix figure E.1.

7.10. Discussion

7.10.1. Fields

The fields as they are created in this chapter rely solely on the SLD. Nodule abundance was described as an indicator for high quality mining areas (chapter 4), but is not taken into account directly when making the fields. There are two possibilities for still including this information into the fields:

- Indicate areas as hard-constrained so they cannot be part of a field. This was done in this thesis through the excluding of nodule type 2 3.
- Exclude fields after they are made, so only mineable fields are left.

7.10.2. Effect of Field Size Distribution

The two sets of fields contain thousands of fields: 3753 long and 4267 compact fields. In both sets, the 100 largest fields cover already around 70% of the mineable area in the site. The size distribution shows a very

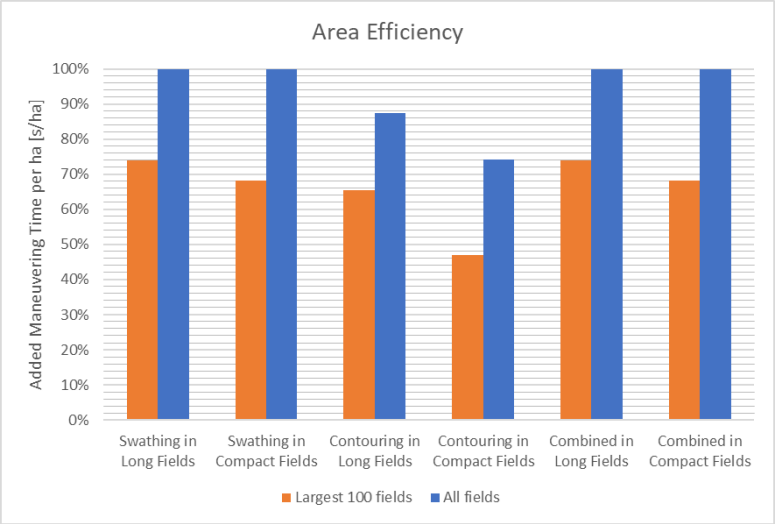

Figure 7.7: Area efficiency of site 3 for two sets of fields in site 3: long and compact fields. Three types of driving pattern are used: swathing, contouring and combined. Lastly, the production rates are compared between the largest 100 fields and all the fields combined (including the 100 largest).

high number of fields of just 1 or 2ha, which corresponds to 1 or 2 raster points. In the plots showing the field results (7.4a and 7.4b), it can be seen that the small fields are mainly around the constrained areas where the SLD is low.

For all results there is a big difference between considering all fields or just the 100 largest. The smaller fields negatively impact the production rate. This is because the small size means that more time is needed for maneuvering relative to mining. For swathing, the opposite side of the field is reached quickly when the field is smaller. For contouring, each loop covers less area and thus requires more maneuvering time according to our assumptions. It is very possible that some of the smaller fields will therefore be not mineable. It highlights the necessity of a follow-up step where it is determined which fields must be mined and which ones should be left untouched.

Contouring very small fields has another detrimental effect: A turning radius of 30m means that the area efficiency of such small fields becomes very low. This explains the bad performance of the contouring method with regards to area efficiency when considering all the fields. It does not explain why contouring performs so much worse in the compact fields compared to the long fields. This is potentially a result of the resolution of the data. The original data has a resolution of 50m, but for computational reasons, this has been increased to 100m. This means that fields boundaries cannot really be well rounded, except for really large fields. This potentially means that the polygon that describes the field also contains sharp turns, which are troublesome for the NC. In reality, these sharp turns are completely unnecessary. The compact fields, and more specifically their area efficiency, are therefore potentially misleading for contouring.

7.10.3. Effect of Directionality

The method gives results that make very sensible long fields. A downside of the approach is that all the fields in the site are in the same direction. This is not necessarily a negative aspect, but it does highlight the importance of proper site selection. If two areas have a different ideal swathing direction, they should not be included in the same site.

Another interesting point is the impact of the site boundaries on the ideal swathing direction. As an example see figure 7.2a, where the longest SLD direction follows the longest edge of the field. In , the directionality of the geological structures is very clear and the site boundaries follow that directionality. This can be clearly seen in the fields for site 5 (figure B.7), which is must larger than site 3 with different shape boundaries, but still shows the same longest SLD direction in figure B.9.

7.11. Conclusion

The research questions that were asked for this chapter are:

1. *What is a suitable method to define the mining fields?* A method based on the SLD for fields with a long

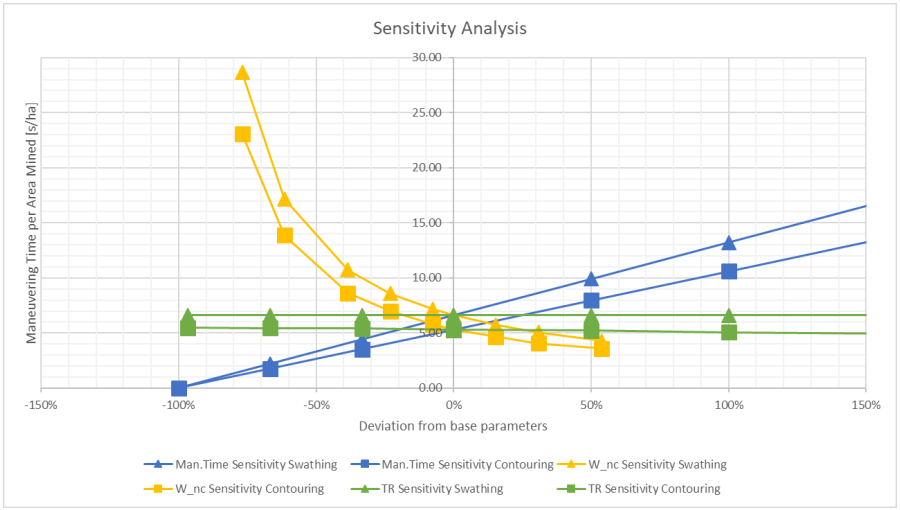

Figure 7.8: The sensitiviy of the three paramaters on the added maneuvering time per area mined. The base parameters are listed in table 5.1.

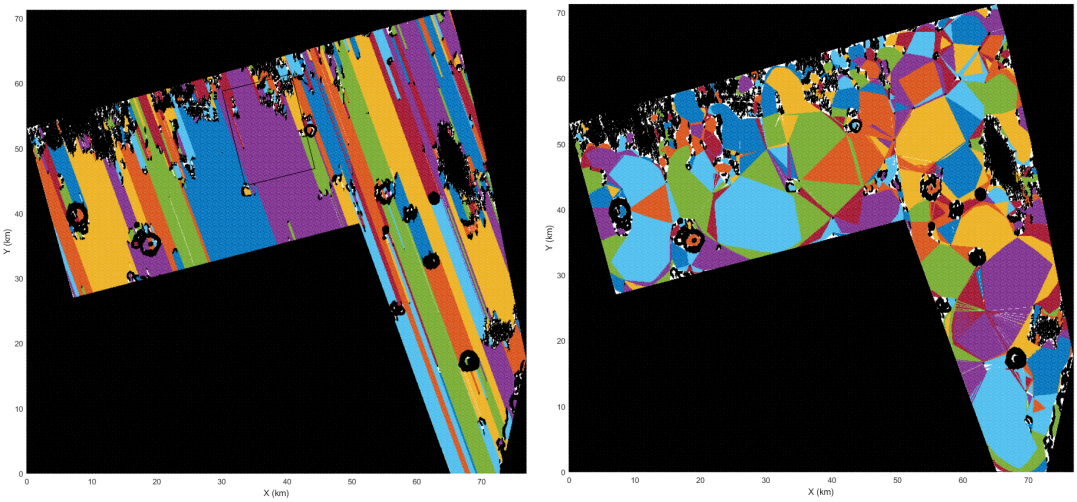

(a) The 100 long fields with the largest surface area in site 7. Together covering 0.92%

(b) The 100 compact fields with the largest surface area in site 7. Together covering 0.80%.

Figure 7.9: Fields in site 7. Each field has a different colour. Constrained areas are in black. White areas are unmined in the largest 100 fields.

shape, and a method based on the minimum SLD for fields with a more compact shape. Comparison of driving patterns in both show that long fields outperform the compact fields in all driving patterns.

2. *What is the effect of different driving patters on the field Key Performance Indicators?* The effect of driving pattern on PR is relatively small. Contouring adds less unproductive time than swathing. However, this pattern has a lower area efficiency. Combining contouring with swathing is a method with a high area efficiency and low unproductive time, but only when considering large fields. If small fields are considered and a high area efficiency is required, swathing gives the best results.
item *What are the sensitivity of Nodule Collector (NC) parameters with regards to mining Key Performance Indicator (KPI)s?* The Production Rate (PR) is most influenced by the speed and width of the NC, but an increase in width is most beneficial because it also reduces the unproductive time.
3. *What are the important parameters for making fields with the best Key Performance Indicator (KPI)s within a site?* The size of the fields influences the unproductive time. It is beneficial to make the fields as large as possible.

8

Long-term Sequencing

8.1. Introduction

In this chapter, a method is outlined for determining the sequence of fields. The sequence is made using a set of long fields inside site 3, that resulted from the work in chapter 7. For the overview of this chapter, see figure 8.1.

Figure 8.1: The thesis overview for chapter 8 The full overview is shown in figure 1.3

Up to this point in the thesis, the time aspect of the mining operation has only come in the form of comparing production rates between fields and driving methods. Looking at results from individual fields gives only a short-term impression of the value inside a given area. To make a longer-term approximation, the mining sequence needs to be considered. For the application in this thesis that would be the sequence in which the fields are mined. In this chapter a method is proposed to determine that sequence. The method needs to account for additional constraints such as processing capacity and mining targets. In addition, depending on the distance between viable mining areas, the travelling time can make an impact on the mining time.

8.2. Objectives and Research Questions

The objective of this chapter is to determine a good method for determining the sequence of mining fields, taking into account constraints. The research questions answered in this chapter:

1. *How can a sequence of mining fields be determined that accounts for constraints?*
2. *What is the impact of inter-field traveling time on the mining operation?*
3. *Which aspects are most important when deciding upon a mining sequence for the fields?*
4. *How can land-based mine planning methods be adapted to suit deep-sea mine planning planning?*

8.3. Method for Field Sequence

It has been discussed previously that the resource type is different from terrestrial mining. The Open-Pit Production Scheduling (OPPS) commonly deals with 3-dimensional block models. The goal is then to plan each block into a specific time period. At this stage of the thesis however, the goal is to plan mining fields instead of blocks. Fields can still be represented by the value of the material contained inside them and the cost of mining them, just like the blocks. The crucial difference between the two has to do with the travelling time, which requires the exact sequence to be known.

In the OPPS, the blocks are scheduled into periods, usually years. The exact sequence of the blocks can be calculated later. In the current problem, taking into account the travelling time between the fields, makes it necessary that the exact sequence is known for calculating the total time. This shows parallels to the Travelling Salesman Problem (TSP), where a traveller must find the shortest distance for visiting several cities. A

formulation of the problem that comes close to the field sequence problem is the selective TSP as described by Laporte and Martello [1990]. Because the selective TSP is NP-hard, and extra constraints are added, it is assumed that computing a solution using exact algorithms within reasonable time is not possible for a large number of fields.

In terrestrial mining, the same problem is encountered and metaheuristics are used. For solving the field sequence problem, a GA was chosen.

8.4. Constraints and Assumptions

There are many constraints possible for planning a mining operation, depending on the specific conditions. In this thesis the constraints are limited to aspects that are within the scope. They are all hard constraints, which means that if they are not complied with, the mining sequence is not valid. The constraints considered are as follows:

- **Mining rate**. There is only one NC which can only cover a certain area per unit time.
- **Operating hours**. The number of hours that the NC can be operated every year.
- **Tonnage targets**. For a time span there can be a target set for the required nodule tonnage. This sets a lower limit to the nodule tonnage. For site 3, the lower limit is set to 2.0 Mt per year.
- **Processing capacity**. Per unit time there can be a constraint for the capacity of the processing plant or storage facilities. This applies an upper limit to the nodule tonnage mined in a certain time. This constraint is not applied to the GA in this thesis.

The assumptions made are that there is only one NC mining one field at a time. A field must be completed before moving on to the next. In this chapter only fields from within one site are considered. It could be possible to go back-and-forth between two sites, but this is not considered.

8.5. Calculating Inter-Field Travel Times

The inter-field travelling takes time away from the operating hours. Minimizing it will help to comply with the constraints. The calculation follows the following steps: For each possible pair of fields, the distance between each of the vertices is determined. The shortest distance is selected to represent the distance between the two fields. This means that if fields are adjacent, the distance is zero. The time to travel between the two fields is dependent of the speed of the NC. This means that it is assumed that the NC travels at a constant speed in a straight line in-between the two fields. This provides an approximation for the travel time, although there are two downsides to this:

1. It assumes that the NC drives to the next field. Although other means of transportation, for example hoisting the NC and dropping it, would also take time.
2. It does not take into account non-traversable parts of the mining site. However, calculating the path around obstacles for each possible pair of mining fields would require too much computational power.
3. It does not take into account the position of the NC within the field. The end position of the NC after mining the field, or the starting position for the NC to mine the field are assumed to be at the ideal location of the field.

8.6. Accounting for the Time Value of Money

The goal of the mining operation is not only to comply with all the constraints. The operation is driven by profit. However, in this thesis no approximation of value of nodules is made, nor the costs of mining. To decide which sequence is better, it is still possible to account for some economical principles.

An important aspect in project finance is the time value of money [Brealey et al., 2012]. In general, investments become worth more over time. Money invested now could grow to a larger amount over several years. Therefore, if you could choose to have money now, or have the same amount of money later, it is preferable to have it earlier so that it can be invested. To represent that money becomes worth less over time, a discount ratio is used. This ratio reduces the value of a future cash flow and is used to calculate its Present Value (PV). The further in the future a cash flow is, the more is it discounted. The sum of all discounted future cash flows is the Net Present Value (NPV) of a project.

When planning a mining project, the time value of money is also used. Similar to any other project, it is preferable to extract the most value as early as possible. This value can be in the form of gold, copper or any

other commodity. Applying this principle to the mining sequence for PN would mean that it is beneficial to extract nodules as soon as possible. The PN are profitable if the constraints are obeyed, but exactly how much is not determined in this thesis. But no matter the actual value of the nodules, it would still be discounted the same. Therefore, instead of discounting the cash flows resulting from the nodules, the nodule tonnage itself is discounted for every year in the future. This will be referred to as the Discounted Nodule Tonnage (DNT).

The DNT can be used to select a sequence. Sequences that result in mining more nodules earlier on, will have a higher DNT. The aim is to have the sequence minimize the inter-field travelling time, and prefer to mine the field with high PR early. All the while, the constraints have to be obeyed.

8.7. Genetic Algorithm for Sequencing

The GA starts by determining the travel time between every pair of fields. For a large number of fields, the number of pairs grows exponentially so the travel times are calculated beforehand. Other known parameters before beginning the GA are the time needed and the total nodule tonnage for mining each field.

The GA works by following these steps:

1. **First Generation**. A starting population of solutions is generated where each solution represents a possible mining sequence. A solution is encoded by giving each field a unique identification (ID) number. One solution is a sequence of these IDs, where every ID occurs once (no duplicates). The starting population consists of 500 solutions, each of which is unique and random. The size of the population stays the same for each generation.

2. **Sequence to Schedule**. Each mining sequence is converted into a schedule for each year, that incorporates the travel times, mining times, the available operating hours per year and mining rate of the NC. The nodule tonnage is calculated from the schedule and discounted for each year to give the DNT.

3. **Constraints**. Any constraints are handled next by introducing a penalty in DNT for violating them. The magnitude of the penalty can vary depending on the severity of the constraint. For a hard constraint, the penalty sets the DNT to a level that is not viable for mining. Violation of soft constraints incur a lower penalty.

4. **Predator Function**. The DNT then serves as a measure of how good the solution is. A higher DNT means that the solution mines more nodules, and violates less constraints. The predator function then eliminates solutions with a low DNT. The predator functions as follows:

   (a) The DNT value is normalized to range from 0 representing the minimum DNT value, to 1, the maximum DNT value in the population.
   (b) For each solution, a random number is drawn between 0 and 1.
   (c) When the random number is higher than the normalized DNT value, the solution is eliminated. This method always eliminates the worst solution and always keeps the best solution. Better solutions have also have a bigger chance to survive this way. The not-eliminated solutions will be called "the survivors".

5. **Next Generation**. The surviving solutions form the basis for the next generation of solutions. To make the next generation, first the best 10% of the surviving population are directly put into the next generation in order to preserve the best solutions. Next, two processes are used to fill up to the 500 solutions in the population: crossover and mutation.

   - **Crossover**. In this process two parents solutions are randomly selected from all the survivors (including the top 10%). The first parent supplies the first part of the solution sequence up until a randomly decided break point. The second parent supplies the part of the sequence after the break point. This method of combining parent solutions means that there can be duplicates and missing fields. The duplicate fields are removed from the solution and are replaced by the missing fields that are not present in the solution. The missing fields are sorted by their position in the parent solutions. The first duplicate will be filled by the missing field that was mined earliest in the parent sequence.
   - **Mutation**. After crossover, there is a 5% chance that a mutation of the new solution happens. In the GA used here, two bits in the sequence are swapped with each other. The bits have varying length and do not overlap.

6. **Stopping Criteria**. The GA always stops when the maximum number of iterations (generations) is reached. Another criteria is if there has been no improvement in DNT over a certain number of generations. In the case that the stopping criteria are not met, the next generation is now complete and undergoes steps 2 to 6 again.

8.8. Results

8.8.1. Field Sequence for Site 3

The sequence for the largest 100 fields in site 3 is shown in figure 8.2. The total time for mining these fields is slightly over 7 years. In table 8.1 the total tonnages for each year can be seen. The minimum nodule target of 2 Mt per year is always, reached, except for the final year of operation in site 3. The nodule target turned out to not be a limiting constraint. Furthermore, the nodule tonnage is higher in the earlier years, tapering off.

In table 8.2 the various aspects that cost time this sequence are listed. The maneuvering time is low relative to the total time for the 100 fields that were considered for this sequence. Inter-field travel time is around 2% in the final sequence of fields. The different driving patterns make only several hundreds of a percent difference with respect to time spent on maneuvering or inter-field travel time.

Fields and sequences were also made for site 5, 7 and the PMT area. For site 5 a sequence was made using 250 fields. Visualizations are included in appendix E.

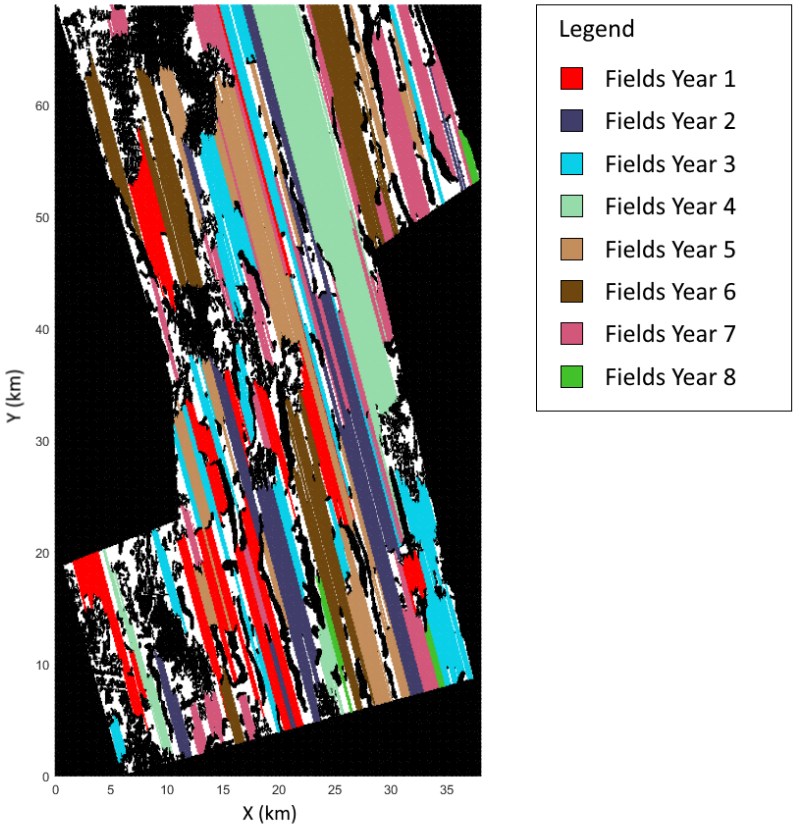

Figure 8.2: Sequence results for site 3.

8.8.2. Comparison with Other Sequencing Methods

To indicate the advantage that using the Genetic Algorithm has, the resulting DNT from the site is compared to other sequences that could be applied.

- Mining the largest field first. These fields have a low unproductive time, generally high PR and because of their size, they are closer to other fields.

Table 8.1: Statistics about the yearly nodule tonnages in the sequence resulting from the GA.

Number of fields	100
Total nodules [Mt]	15.57
Year 1 [Mt]	2.30
Year 2 [Mt]	2.26
Year 3 [Mt]	2.23
Year 4 [Mt]	2.18
Year 5 [Mt]	2.18
Year 6 [Mt]	2.18
Year 7 [Mt]	2.10
Year 8 [Mt]	0.14

Table 8.2: The time in hours dedicated to various aspects that cost time for site 3 for the sequence of fields displayed in figure 8.2.

Time in Hours	**Swathing**	**Contouring**	**Combined**
Mining time	44717	36800	44717
Maneuvering time	68	46	61
Inter-Field Travel Time	881	752	881
Percentage of total Time	**Swathing**	**Contouring**	**Combined**
Mining time	97.9%	97.9%	97.9%
Maneuvering time	0.15%	0.12%	0.13%
Inter-Field Travel Time	1.93%	2.00%	1.93%

- Mining the field with the highest production rate first. This can have a positive effect because more nodules are mined earlier.
- Mining the field with the highest nodule tonnage first.
- A random sequence.

The results are shown in figure 8.3. Sorting by production rate performs a little better than the other alternative sorting methods. A random sequence performs very close to the same level and even outperforms sorting by size and nodule tonnage in some cases. The genetic algorithm outperforms the other sequences by about 4%, although the difference is smaller when contouring. These results are due to a reduction in travelling time between fields.

Contouring shows a lower nodule tonnage than the other two methods because of the lower area coverage. When the timescale becomes increasingly large, this effect could be offset by the discounting. The timescale is not large enough when only considering side 3.

8.9. Discussion

One aspect that is not taken into account is how the operational hours affect the mining. It is possible that after mining a field, the NC is hoisted up for maintenance and afterwards directly dropped into the next field, which would cost essentially zero operational hours and results in zero travelling time.

The genetic algorithm does not have to option to exclude fields in the form described in this chapter. This makes sense because no costs are described for the mining operation, therefore it cannot be decided if a field is positive in terms of monetary value. Also, using the base settings the nodule target turned out to not be a constraining factor since it was achieved for every year. If the nodule target becomes a constraining factor, the option to leave out fields should be included in the sequence algorithm. An effect of leaving all fields in, is that the less productive, smaller fields are moved towards the back of the sequence calculated for the PMT area, shown in appendix D. The areas towards the north are later in the sequence, very likely because the travel times are higher and the fields are smaller. It should be evaluated if these fields are worth mining.

The time required to calculate the distances between 100 fields and determine the sequence using a genetic algorithm took around 30 minutes on a computer with a 2.60 GHz CPU. For a solution with 250 fields around the PMT area, shown in appendix D, the required time was around 2 hours for 789 iterations. The script was made in MATLAB. Using a stronger processor and efficient programming, the time can undoubt-

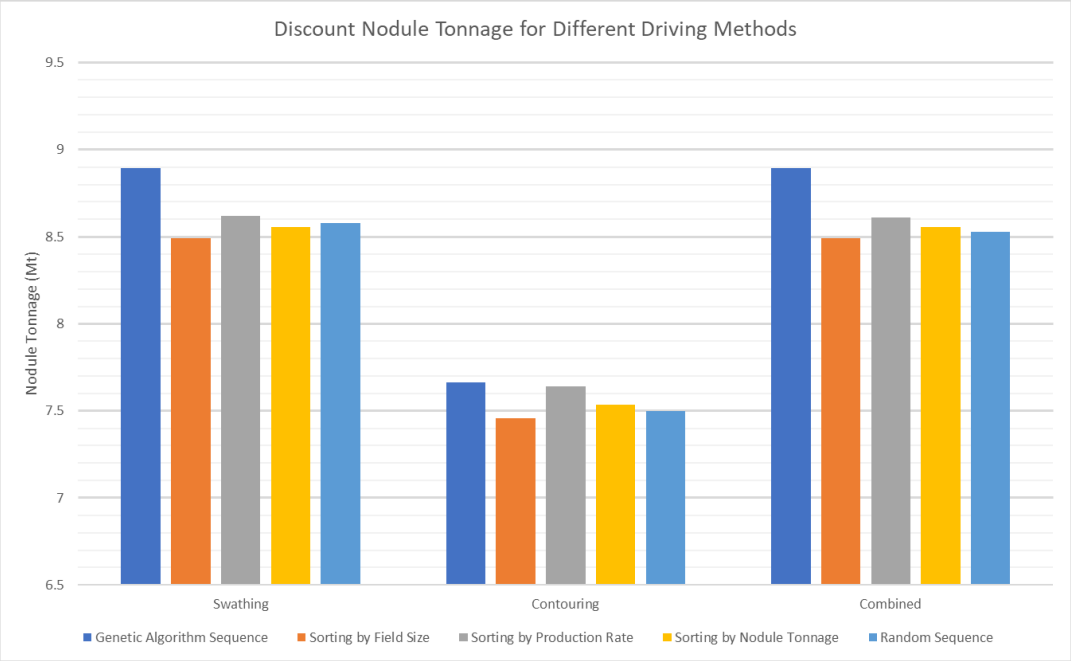

Figure 8.3: Discounted Nodule Tonnage for the different sequences of fields and different driving methods.

edly be brought down.

8.10. Conclusion

1. *How can a sequence of mining fields be determined that accounts for constraints?* In this chapter a genetic algorithm is used to determine a sequence for up to 250 fields using constraints for mining rate, operational hours and nodule targets. The limits of this algorithm were not reached in this thesis and larger solutions using more constraints are most likely possible.
2. *What is the impact of inter-field traveling time on the mining operation?* In the sequences shown from site 3, the travel time accounts for around 2% of the total time in the field.
3. *Which aspects are most important when deciding upon a mining sequence for the fields?* The travel time had a big impact on the final sequence. Preferring fields with a higher PR is also beneficial.
4. *How can land-based mine planning methods be adapted to suit deep-sea mine planning planning?* The formulation of the field sequence problem is different from the Open-Pit Production Scheduling (OPPS) problem. Due to accounting for travelling time between fields, the formulation is closer the Travelling Salesman Problem (TSP). Description of constraints can be adapted from terrestrial mining since various constraints are shared.

9

General Discussion

This thesis has contributed to developing a method for deep-sea mining with the new or innovative elements:

1. **Method for selecting mining sites.**
2. **Introducing the straight-line distance.**
3. **Making fields out of the straight line distance results.**
4. **Genetic algorithm for mining field sequence.**

The site selection was done by hand and the method is therefore not deterministic. The base rule that the selection was based upon was that mining fields cannot cross site boundaries. The boundaries of mining fields are either the site boundaries or constrained areas. For delineating a mining site, the main focus should therefore be on all factors constraining general mineability. The method is then applicable to any setting or framework, as long as the constraints for the NC and mining operation are well defined beforehand. What is unfortunate is that the SLD could not be applied to the entire license area due to computational constraints.

The development of the SLD metric is arguably the most important contribution of this thesis. Notably its use in excluding areas from mining. Previously Volkmann [2018] used a neighborhood filter to identify continuous mining areas, essentially the same purpose that the SLD can be used for. The difference comes from that by using the SLD, a quantative analysis can be made to determine if the area is too confined.

In section 5.5, the SLD is combined with the NA from the resource assessment and the parameters of the NC. The resulting PR cutoff graph gives a first approximation for the tonnages that can be mined at a required mining rate. An added benefit is that also the total time needed for mining can be quickly found from the graph. If this method would be applied to different license areas or frameworks, the SLD can still provide an estimation of mineability. Results of the fields show that even when the driving pattern is contouring, the long fields still perform very well. The SLD should therefore still provide a good approximation even for swathing. As long as the NC functions roughly the same way as the one described in the framework in this thesis.

In chapter 7, the definition of mining fields has been done in two different ways, using three different driving patterns. From the results of the sensitivity analysis of the NC parameters (table 7.3), it can be seen that no matter which driving method is applied, the unproductive time is relatively small. The license area is 75000 km^2, which is larger than the Netherlands and Belgium combined. If any of the larger open areas are selected, it makes intuitive sense that the time spent maneuvering is small. Even if the total turning circle of the NC is 60m wide. The largest impact for the mining operation is therefore the decision to exclude certain areas from mining, whether it is because of slope angles or nodule types. The SLD provides a very useful tool for excluding areas from mining. The fields and field sequence in the framework of this thesis will not make or break the profitability of the mining operation.

Overal, the model behaves as expected with regards to the deliniation of mining fields. The very low impact of different driving patterns and travel time was perhaps unexpected. The mining time is just always magnitudes larger than the maneuvering time.

The method seems very useable for the development of a realistic mining plan. This is necessary for the definition of reserves and something that deep-sea mining companies eventually must do. Of course, there are factors left out of scope that could negatively impact the operation. Most notably constraints related to the soil/surface quality, detailed technical constraints and environmental impact related constraints. Other limitations come from computational limitations of the SLD. For future use, this must definitely be improved.

10

Conclusions and Recommendations

The performed research has resulted in the following conclusions:

1. High quality mining areas can be identified by: the absence of hard-constraints such as slope and nodule type, a high nodule abundance, and large SLD which indicates efficient driving conditions for the collector.
2. Mining sites should be selected by taking into account the fact that mining fields cannot cross site boundaries due to the predefined hierarchy. Therefore site boundaries are adequately placed next to low quality mining areas.
3. Mining fields can be created using a method outlined in chapter 7. Fields with elongated shape are reliant upon the SLD, using sharp transitions in SLD values as a boundary. Fields with compact shape are created based upon the minimum SLD following a similar procedure.
4. The PR that can be achieved in a mining field is an adequate KPI to judge its quality. The PR depends on the driving pattern, the nodule abundance and the parameters of the NC.
5. Based on the simulations in this thesis, the shape indices of mining fields can not be used to approximate the operation of the NC in those fields.
6. Comparisons show that long fields outperform the compact fields in all driving patterns. The effect of driving pattern on PR is relatively small. Contouring adds less unproductive time than swathing. However, contouring has a lower area efficiency. It should be considered to use a combination of contouring and swathing based on the size of a field, with larger fields preferring a combination of both, and small fields preferring swathing.
7. From a sensitivity analysis of the parameters of the NC, the PR of a field is most influenced by the speed and width of the NC, but an increase in width is most beneficial because it also reduces the unproductive time spent in the field.
8. Obstacles in a mining field negatively impact the area efficiency and therefore the PR. The number of obstacles has a more severe effect than the size of the obstacles.
9. The formulation of the field sequence problem is different from the Open-Pit Production Scheduling (OPPS) problem because of the field sequence accounts for travelling time. The formulation of the field sequence is closer the Travelling Salesman Problem (TSP). Description of constraints can still be adapted from terrestrial mining.
10. A genetic algorithm can be used to determine a sequence for at least 250 fields using constraints for mining rate, operational hours and nodule targets. The travel time has a big impact on the final sequence.

10.1. Recommendations

The following are several points of recommendation for future work:

- *Kriging Methods.* In this thesis OK was used to reproduce results from a technical report. It has been shown however, that incorporation of backscatter data can improve the results. In this thesis is was only applied after the kriging to exclude nodule type 2 3.

- *Improving methodology.* As described in the discussion of chapter 4,the SLD methodology as described in this thesis is limited in computational performance. For future work, it would be helpful if the SLD could be calculated for larger areas at a good enough resolution. This might involve more computing power, more time or finding a different approach for calculating the same metric.
- *Maneuverability assumptions.* For the pilot mining test, it should be determined if the assumptions made in this thesis with regards to the maneuverability of the NC are valid. These assumptions are: static turning time for moving to the next swath and a maximum turning radius for which mining can still be done. Eventually it might be possible to test the approximation of adding unproductive time for each loop compared to driving straight.
- *Nodule type 2 & 3.* For the pilot mining test it would also be very relevant to test if mining nodule type 2 3 is truly so unproductive that they should be excluded from the mine planning. In general is must be established how different nodule abundances result in different collecting efficiencies.
- *Sea Currents.* Underwater weather conditions and currents could play a large role in the mining operation. The SLD can potentially play a role in analyzing what the effect are of adjusting driving direction based on currents.
- *Applying costs and revenues.* The determination of the mining sequence currently discounts the nodule tonnage. For a more accurate evaluation of which mining fields are worth mining, costs of the mining operation and revenues from the nodules can be used. Then it can also be decided to exclude fields from the mining sequence.
- *Direct planning and scheduling.* In this thesis the mining fields were defined and then the sequence was determined. It might be beneficial to apply direct planning, where based on various constraints, blocks are directly scheduled into a time period, more similar to the OPPS problem. It would be harder to account for the travelling time, but from the results presented in chapter 8, it is around 2% of the total in-field time.

Bibliography

Agarwal, B., Hu, P., Placidi, M., Santo, H. and Zhou, J. [2012], *Feasibility study on manganese nodules recovery in the Clarion-Clipperton Zone*, Vol. 2 of *The LRET Collegium 2012 Series: Seabed Exploitation, 2*, University of Southampton.

Alipour, A., Khodaiari, A., Jafari, A. and Tavakkoli-Moghaddam, R. [2017], 'A genetic algorithm approach for open-pit mine production scheduling', *International Journal of Mining and Geo-Engineering* **51**(1), 47–52.

Allseas SA (Allseas) [2020], 'Press Release: Allseas acquires ship for deep-sea polymetallic nodule collection in partnership with DG', Allseas Website.
URL: *https://allseas.com/wp-content/uploads/2020/03/2020-0302-Allseas-acquires-ship-for-deep-sea-polymetallic-nodule-collection-in-partnership-with-DeepGreen.pdf*

AMC Consultants (AMC) [2016], NI 43-101 Technical report. TOML Clarion Clipperton Zone project, Pacific Ocean, Technical report, Nautilus Minerals. DOI: 10.13140/RG.2.2.23742.08000.

AMC Consultants (AMC) [2019], 'NI 43-101 Technical Report: NORI Area D Clarion Clipperton Zone Mineral Resource Estimate'. Retrieved Februari 17, 2020.
URL: *https://www.sedar.com/DisplayCompanyDocuments.do?lang=ENissuerNo=00044394*

Bickford, M. [2013], *The Impact of the Geological Sciences on Society*, Vol. 501, Geological Society of America, p. 16.

Birdal, T. [2020], 'MATLAB Script: Maximum Inscribed Circle using Distance transform', MATLAB Central file exchange. Retrieved March 20, 2020.
URL: *https://www.mathworks.com/matlabcentral/fileexchange/30805-maximum-inscribed-circle-using-distance-transform*

Brealey, R., Myers, S., Allen, F. and Mohanty, P. [2012], *Principles of corporate finance*, Tata McGraw-Hill Education.

Broadus, J. [1987], 'Seabed materials', *Science* **235**(4791), 853–860.

Canadian Institute of Mining, Metallurgy and Petroleum (CIM) [2014], 'Cim definition standards - for mineral resources and mineral reserves', CRIRSCO Website.
URL: *http://www.crirsco.com/docs/cim_definition_standards_20142.pdf*

Denby, B. and Schofield, D. [1994], 'Open-pit design and scheduling by use of genetic algorithms', *Transactions of the Institution of Mining and Metallurgy. Section A. Mining Industry* **103**.

Diener, J. [2020], 'MATLAB Script: 2D minimal bounding box', MATLAB Central File Exchange. Retrieved August 10, 2020.
URL: *https://www.mathworks.com/matlabcentral/fileexchange/31126-2d-minimal-bounding-box*

DSMC and MiningWatch [2020], 'Predicting the impacts of mining deep sea polymetallic nodules in the pacific ocean: A review of scientific literature'.
URL: *https://miningwatch.ca/publications/2020/5/19/predicting-impacts-mining-deep-sea-polymetallic-nodules-pacific-ocean-review*

Dullaert, W., Sevaux, M., Sorensen, K., Springael, J. et al. [2007], 'Applications of metaheuristics', *European Journal of Operational Research* **179**(3), 601–604.

Ecorys [2014], Study to investigate state of knowledge of Deep Sea Mining, Technical report, European Commission - DG Maritime Affairs and Fisheries.
URL: *https://webgate.ec.europa.eu/maritimeforum/en/node/3732*

ESRI [2020], 'Area showing approximately the Clarion-Clipperton Fracture Zone'. Viewed on 16 September 2020.
URL: *https://www.arcgis.com/home/webmap/viewer.html?webmap=12fee4cade434080bb7c36357c6b94c5*

European Commission (EC) [2017], '2017 list of Critical Raw Materials for the EU', European Commission Website.
URL: *https://ec.europa.eu/growth/sectors/raw-materials/specific-interest/critical$_e$n*

Franco-Sepulveda, G., Del Rio-Cuervo, J. and Pachón-Hernández, M. [2019], 'State of the art about metaheuristics and artificial neural networks applied to open pit mining', *Resources Policy* **60**, 125–133.

Glasby, G. [2000], 'Lessons learned from deep-sea mining', *Science* **289**(5479), 551–553.

Global Sea Resources (GSR) [2020*a*], 'Press Release: GSR completes two key assessments of its polymetallic nodule collector technology', GSR Website.
URL: *https://www.deme-gsr.com/news/article/update-patania-ii-trial/*

Global Sea Resources (GSR) [2020*b*], 'Press Release: Update: Patania II trial', GSR Website.
URL: *https://www.deme-gsr.com/news/article/update-patania-ii-trial/*

Golder Associates (Golder) [2013], Updated NI43-101 Technical Report: TOML Clarion-Clipperton Zone Project, Technical report.
URL: *https://www.sedar.com/DisplayCompanyDocuments.do?lang=ENissuerNo=00044394*

Goovaerts, P. et al. [1997], *Geostatistics for natural resources evaluation*, Oxford University Press on Demand, chapter 4–5, pp. 75–138.

Green, J. and Vogt, D. [2009], Robot miner for low grade narrow tabular ore bodies: the potential and the challenge, 3rd Robotics and Mechatronics Symposium (ROBMECH 2009). Conference Paper.

Hein, J. and Koschinsky, A. [2014], 'Deep-ocean ferromanganese crusts and nodules', *Geochemistry of Mineral Deposits: Treatise of Geochemistry, 2nd Edition* **13**, 273–291.

Hein, J., Koschinsky, A. and Kuhn, T. [2020], 'Deep-ocean polymetallic nodules as a resource for critical materials', *Nature Reviews Earth & Environment* pp. 1–12.

Hein, J., Mizell, K., Koschinsky, A. and Conrad, T. [2013], 'Deep-ocean mineral deposits as a source of critical metals for high-and green-technology applications: Comparison with land-based resources', *Ore Geology Reviews* **51**, 1–14.

International Seabed Authority (ISA) [2010], *A Geological Model of Polymetallic Nodule Deposits in the Clarion-Clipperton Fracture Zone*, ISA technical study, International Seabed Authority.

International Seabed Authority (ISA) [2018*a*], 'Clarion-clippterton fracture zone exploration areas for polymetallic nodules', ISA Website.
URL: *https://www.isa.org.jm/map/clarion-clipperton-fracture-zone*

International Seabed Authority (ISA) [2018*b*], 'Fact Sheet: Contractors for Seabed Exploration', ISA Website.
URL: *https://isa.org.jm/files/files/documents/isacont-update.pdf*

Khan, A. and Niemann-Delius, C. [2015], Application of particle swarm optimization to the open pit mine scheduling problem, *in* 'Proceedings of the 12th International Symposium Continuous Surface Mining-Aachen 2014', Springer, pp. 195–212.

Knobloch, A., Kuhn, T., Rühlemann, C., Hertwig, T., Zeissler, K. and Noack, S. [2017], Predictive mapping of the nodule abundance and mineral resource estimation in the clarion-clipperton zone using artificial neural networks and classical geostatistical methods, *in* 'Deep-Sea Mining', Springer, pp. 189–212.

Kuhn, T., Wegorzewski, A., Rühlemann, C. and Vink, A. [2017], Composition, formation, and occurrence of polymetallic nodules, *in* 'Deep-sea mining', Springer, pp. 23–63.

Kumral, M. and Dowd, P. [2005], 'A simulated annealing approach to mine production scheduling', *Journal of the Operational Research Society* **56**(8), 922–930.

Lamghari, A. and Dimitrakopoulos, R. [2012], 'A diversified tabu search approach for the open-pit mine production scheduling problem with metal uncertainty', *European Journal of Operational Research* **222**(3), 642–652.

Lamghari, A. and Dimitrakopoulos, R. [2020], 'Hyper-heuristic approaches for strategic mine planning under uncertainty', *Computers & Operations Research* **115**, 104590.

Laporte, G. and Martello, S. [1990], 'The selective travelling salesman problem', *Discrete applied mathematics* **26**(2-3), 193–207.

Latombe, J. [1991], Exact cell decomposition, *in* 'Robot Motion Planning', Springer, pp. 200–247.

Lee, G., Kim, J., Chi, S., Ko, Y. and Ham, D. [2008], 'Examination of correction factor for manganese nodule abundance using the free fall grab and box corer', *The Sea: Journal of the Korean Society of Oceanography* **13**(3), 280–285.

Lee, M., Cho, S., Choi, J., Kim, H., Hong, S. and Lee, T. [2012], 'Metamodel-based multidisciplinary design optimization of a deep-sea manganese nodules test miner', *Journal of Applied Mathematics* **2012**.

Lerchs, H. and Grossman, F. [1965], 'Optimum design of open-pit mines', *Trans CIM* **68**, 17–24.

Leuangthong, O., Neufeld, C. and Deutsch, C. [2003], 'Optimal selection of selective mining unit (smu) size', *University of Alberta* . Published on University of Alberta Website.
URL: *http://www.ccgalberta.com/ccgresources/report05/2003-116-smuselect.pdf*

Marin, J. [1984], 'Computing columns, footings and gates through moments of area', *Computers Structures* **18**(2), 343–349.

Mero, J. [1965], *The mineral resources of the sea*, Oceanography Series, Elsevier Publishing Co.

Mewes, K., Mogollón, J., Picard, A., Rühlemann, C., Kuhn, T., Nöthen, K. and Kasten, S. [2014], 'Impact of depositional and biogeochemical processes on small scale variations in nodule abundance in the clarion-clipperton fracture zone', *Deep Sea Research Part I: Oceanographic Research Papers* **91**, 125–141.

Monnet, A. and Ait Abderrahim, A. [2016], Report on major trends affecting future demand for critical raw materials, Technical report, LGI Consulting. SCRREEN Project.

Mucha, J. and Wasilewska-Błaszczyk, M. [2020], 'Estimation accuracy and classification of polymetallic nodule resources based on classical sampling supported by seafloor photography (pacific ocean, clarion-clipperton fracture zone, iom area)', *Minerals* **10**(3), 263.

Mucha, J., Wasilewska-Blaszczyk, M., Kotlinski, R. et al. [2013], Variability and accuracy of polymetallic nodules abundance estimations in the iom area-statistical and geostatistical approach, *in* 'Tenth ISOPE Ocean Mining and Gas Hydrates Symposium', International Society of Offshore and Polar Engineers.

Oksanen, T. [2013], 'Shape-describing indices for agricultural field plots and their relationship to operational efficiency', *Computers and electronics in agriculture* **98**, 252–259.

Oksanen, T. and Visala, A. [2009], 'Coverage path planning algorithms for agricultural field machines', *Journal of field robotics* **26**(8), 651–668.

Park, S., Yeu, T., Yoon, S., Hong, S. and Sung, K. [2011], A study of sweeping coverage path planning method for deep-sea manganese nodule mining robot, *in* 'OCEANS'11 MTS/IEEE KONA', IEEE, pp. 1–5.

Poniewierski, J. [2019], Block model knowledge for mining engineers - an introduction, Technical report, Deswik. DOI: 10.13140/RG.2.2.11503.69281.

Rahn, M., Kukla, P. and Lottermoser, B. [2019], Deep-sea mining of seafloor massive sulfides and seafloor manganese nodules: deposit modelling and market potential, Technical report, Lehrstuhl für Geologie und Paläontologie und Geologisches Institut.

Rosin, P. [2003], 'Measuring shape: ellipticity, rectangularity, and triangularity', *Machine Vision and Applications* **14**(3), 172–184.

Schulz, J., DeYoung Jr, J., Seal II, R. and Bradley, D. [2017], Critical mineral resources of the United States—Economic and environmental geology and prospects for future supply, Technical report, United States Geological Survey. https://doi.org/10.3133/pp1802.

Schwanghart, W. [2020], 'Matlab script: Experimental (semi-) variogram', MATLAB Central File Exchange. **URL:** *https://www.mathworks.com/matlabcentral/fileexchange/20355-experimental-semi-variogram*

Sharma, R. [2017*a*], Assessment of distribution characteristics of polymetallic nodules and their implications on deep-sea mining, *in* 'Deep-Sea Mining', Springer, pp. 229–256.

Sharma, R. [2017*b*], Deep-sea mining: Current status and future considerations, *in* 'Deep-sea mining', Springer, pp. 3–21.

Sharma, R., Sankar, S., Samanta, S., Sardar, A. and Gracious, D. [2010], 'Image analysis of seafloor photographs for estimation of deep-sea minerals', *Geo-marine letters* **30**(6), 617–626.

Shishvan, M. and Sattarvand, J. [2015], 'Long term production planning of open pit mines by ant colony optimization', *European Journal of Operational Research* **240**(3), 825–836.

Singh, T. and Sudhakar, M. [2017], Statistical properties of distribution of manganese nodules in indian and pacific oceans and their applications in assessing commonality levels and in exploration planning, *in* 'Deep-Sea Mining', Springer, pp. 213–228.

Sparenberg, O. [2019], 'A historical perspective on deep-sea mining for manganese nodules, 1965–2019', *The Extractive Industries and Society* **6**(3), 842–854.

UNOET [1987], *Delineation of Mine-Sites and Potential in Different Sea Areas*, Vol. 4, Graham Trotman Ltd., London.

Volkmann, S. [2018], Blue Mining — Planning the Mining of Seafloor Manganese Nodules, Technical report, Fachgruppe für Rohstoffe und Entsorgungstechnik. DOI: 10.18154/RWTH-2018-230772.

White, M., Manocchio, A., Lowe, J., Johnston, M., Sant, T. et al. [2011], Resource drilling of the solwara 1 seafloor massive sulfide (sms) deposit, *in* 'Offshore Technology Conference', Offshore Technology Conference.

Yamazaki, T. and Sharma, R. [2000], 'Morphological features of co-rich manganese deposits and their relation to seabed slopes', *Marine georesources & geotechnology* **18**(1), 43–76.

A

Appendix: World Map of PN Areas

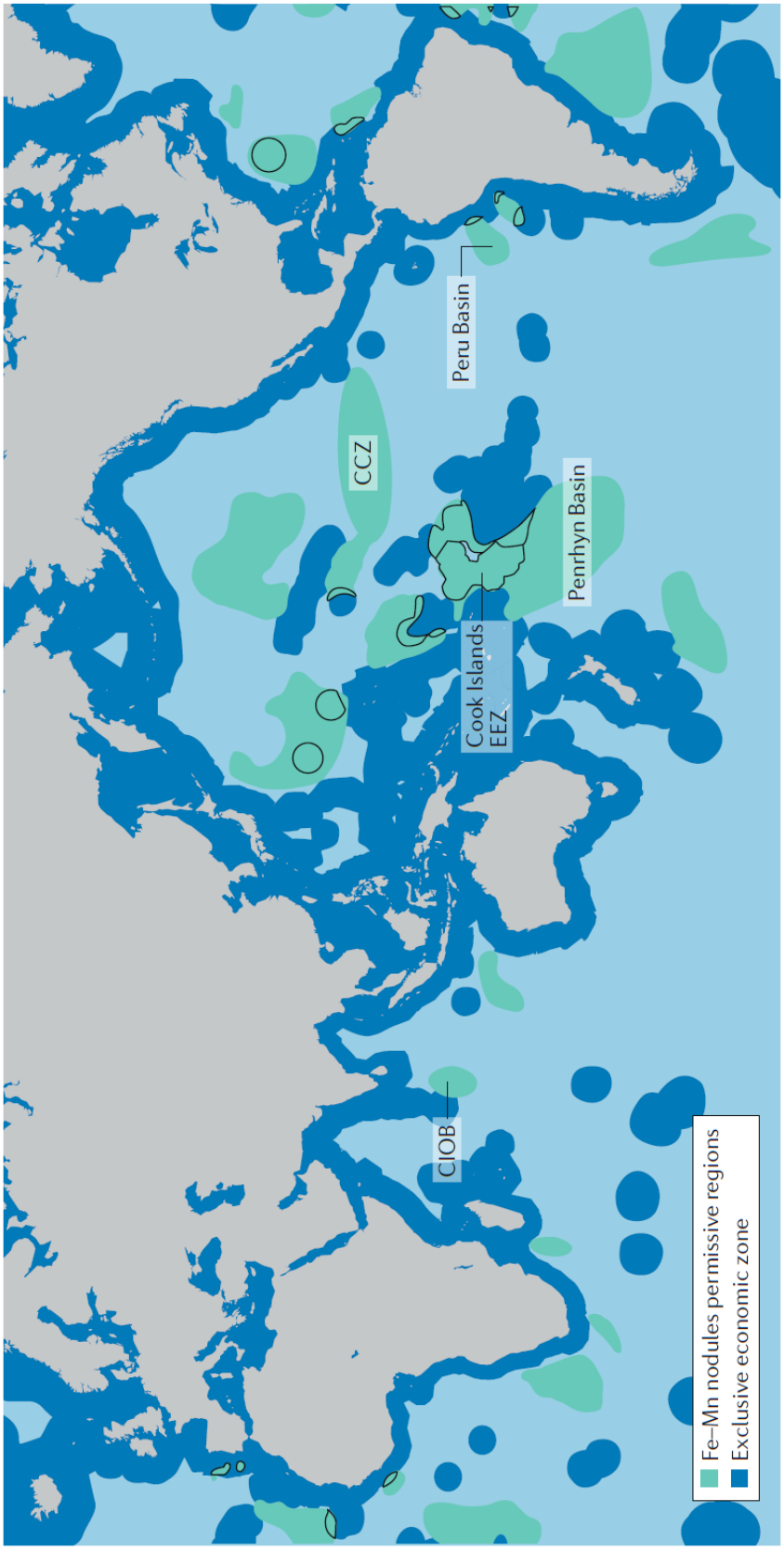

Figure A.1: Global permissive areas for development of abyssal plain manganese nodules. Exclusive economic zones (EEZs) are indicated as well as the most well known areas with PN are in the CCZ, Peru Basin, Penrhyn Basin, and the Central Indian Ocean Basin (CIOB). From Hein et al. [2020]

B

Appendix: SLD Plots

This appendix included the enlarged plots from site 3, and the SLD plots from site 5, 7, and 8.

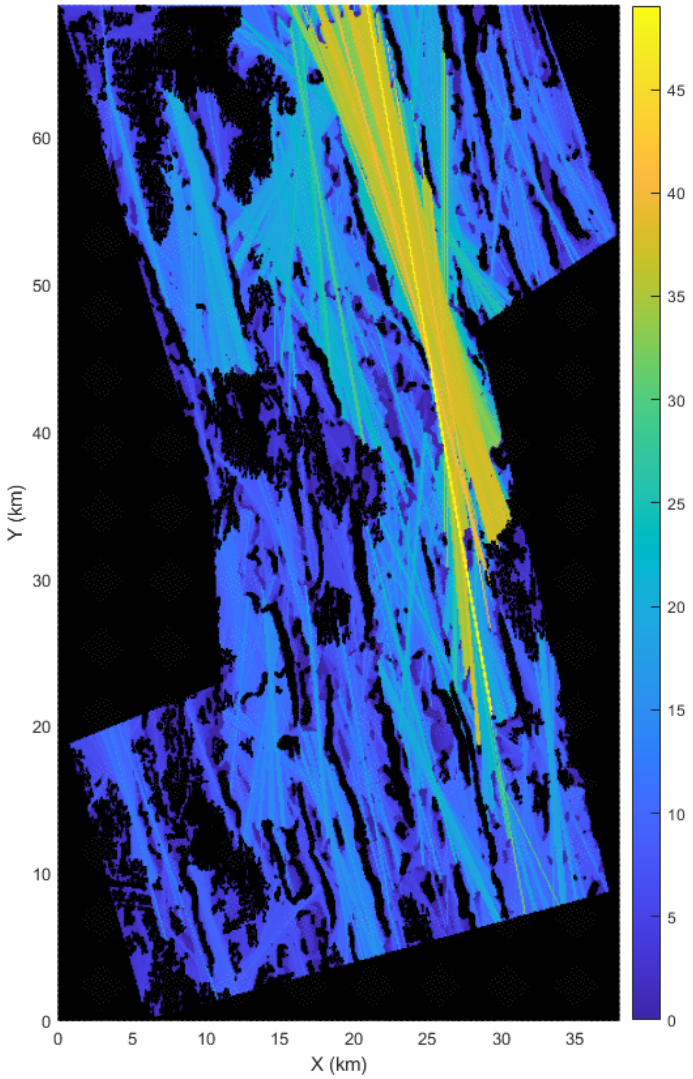

Figure B.1: The maximum SLD for site 3. The constrained pixels include slope constraints and nodule type constraints, shown in figure 4.8.

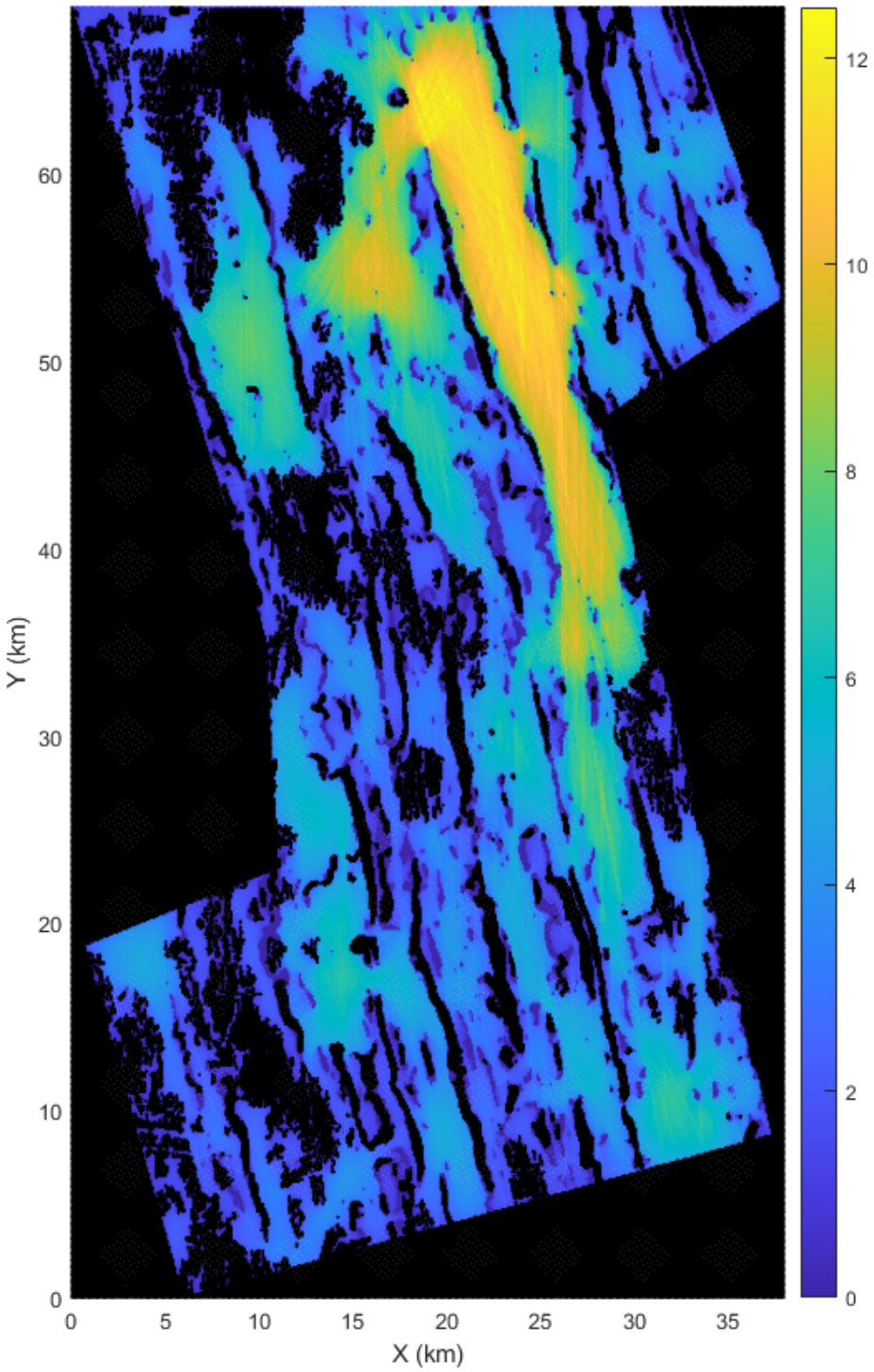

Figure B.2: The mean SLD for site 3 in each direction. The constrained pixels include slope constraints and nodule type constraints, shown in figure 4.8.

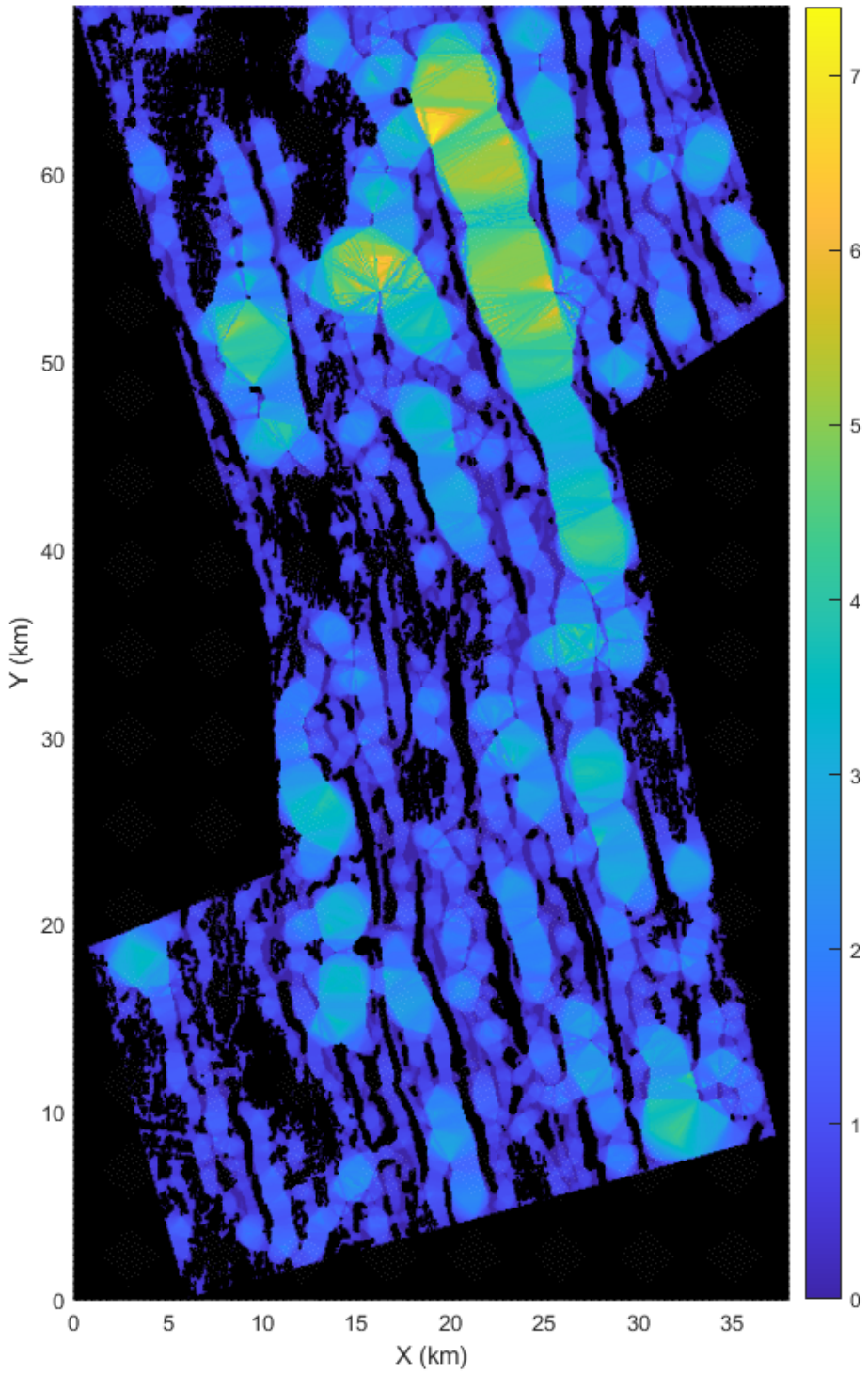

Figure B.3: The minimum SLD for site 3. The constrained pixels include slope constraints and nodule type constraints, shown in figure 4.8.

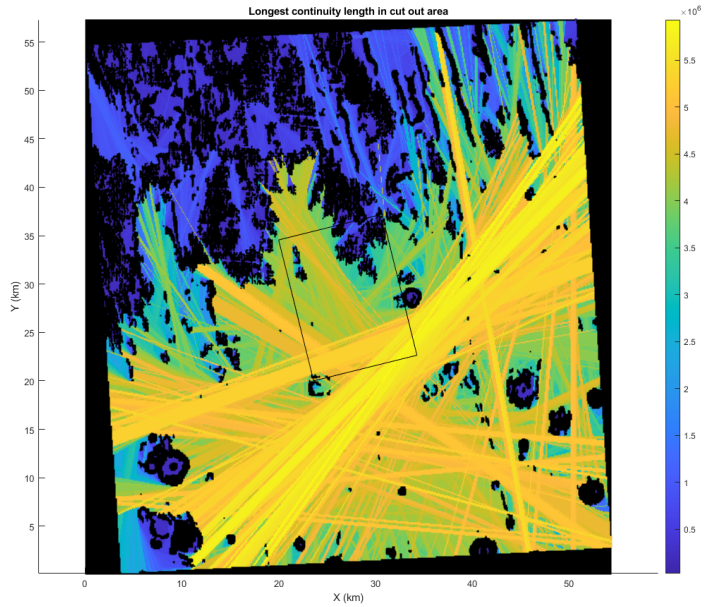

Figure B.4: The maximum SLD for the Area. The constrained pixels include slope constraints and nodule type constraints, shown in figure 4.8.

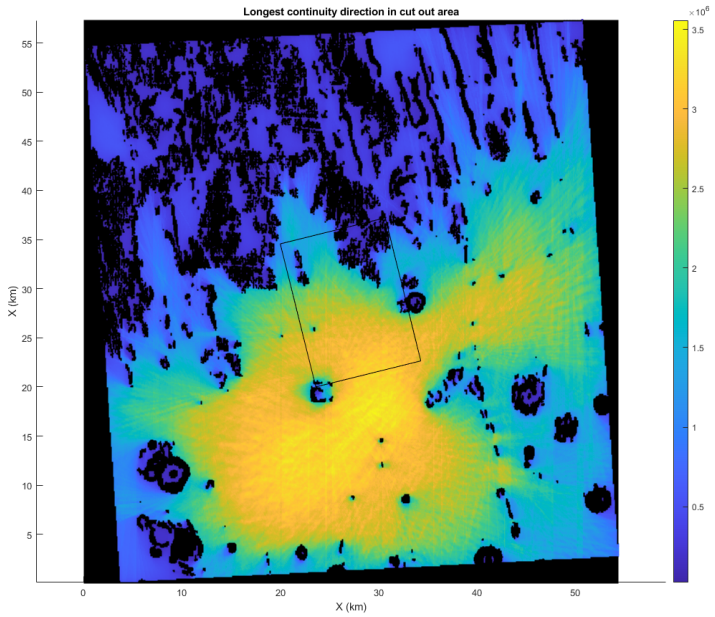

Figure B.5: The mean SLD for the Area in each direction. The constrained pixels include slope constraints and nodule type constraints, shown in figure 4.8.

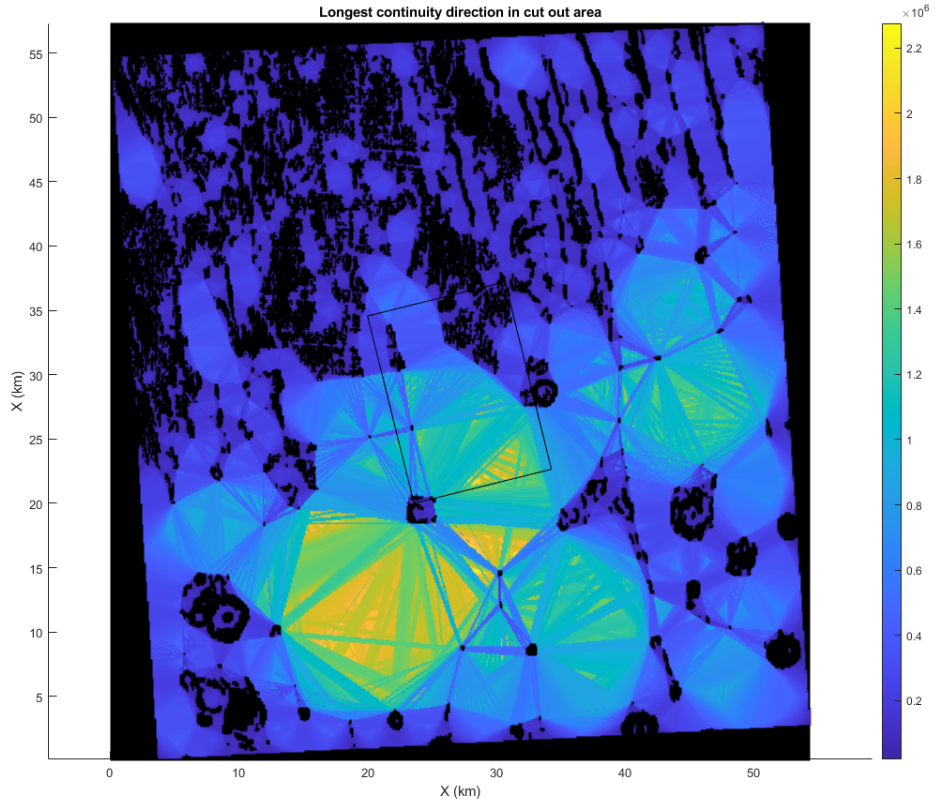

Figure B.6: The minimum SLD for the Area. The constrained pixels include slope constraints and nodule type constraints, shown in figure 4.8.

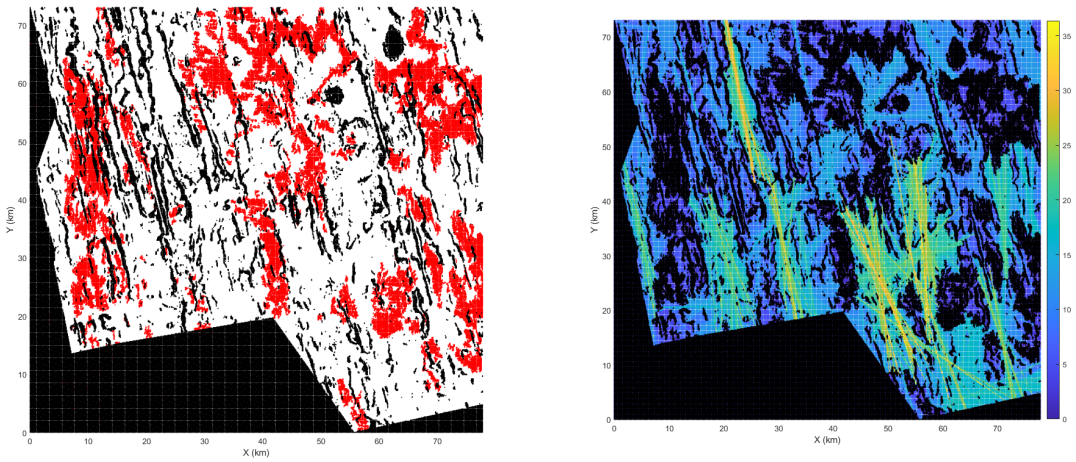

Figure B.7: On the left the constrained areas of site 5. Nodule type 2 & 3 indicated in red. Boundaries and slopes above threshold in black. On the left the maximum SLD

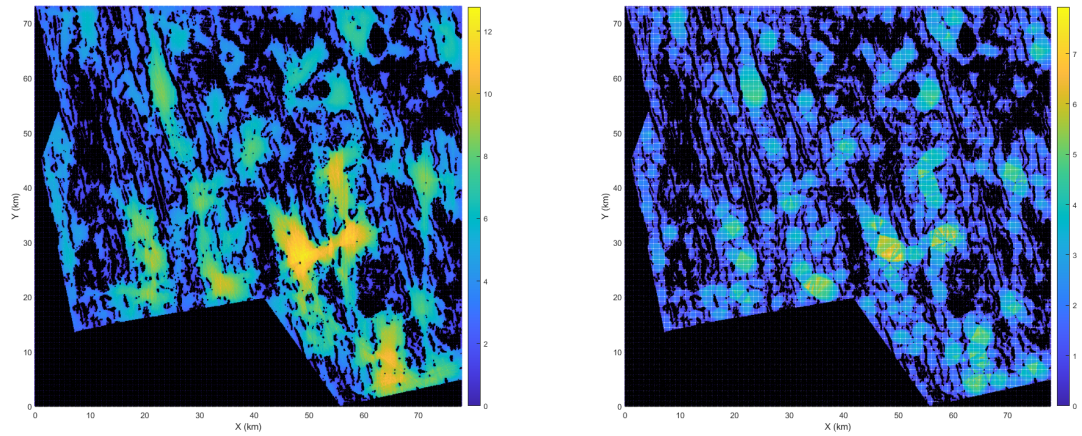

Figure B.8: On the left the mean SLD of site 5. On the right the minimum SLD (any direction) of site 5.

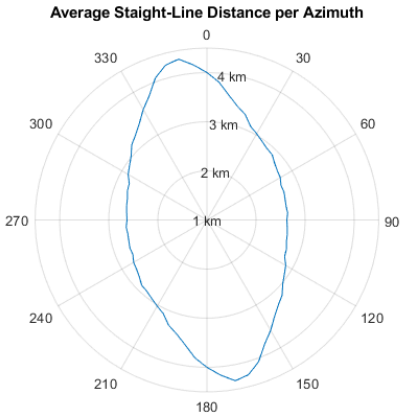

Figure B.9: The average SLD in each azimuth for site 5.

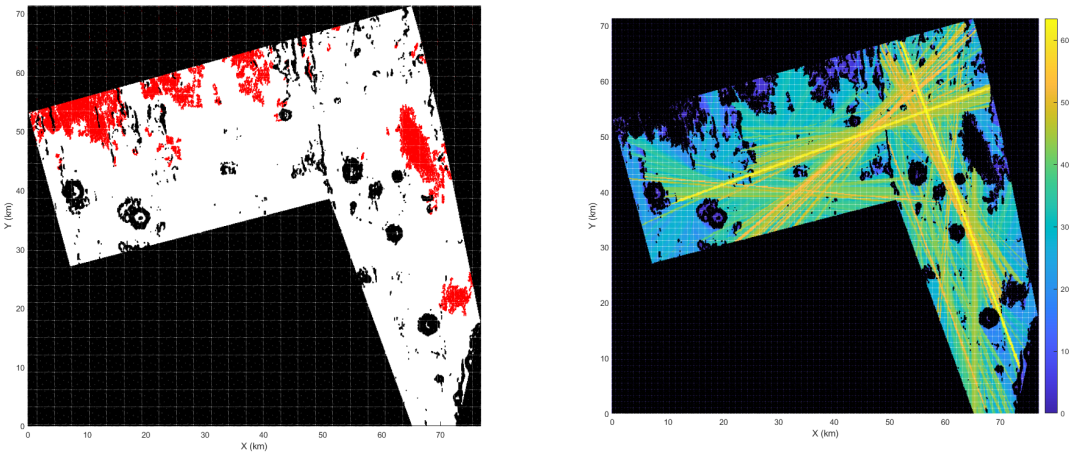

Figure B.10: On the left the constrained areas of site 7. Nodule type 2 & 3 indicated in red. Boundaries and slopes above threshold in black. On the left the maximum SLD

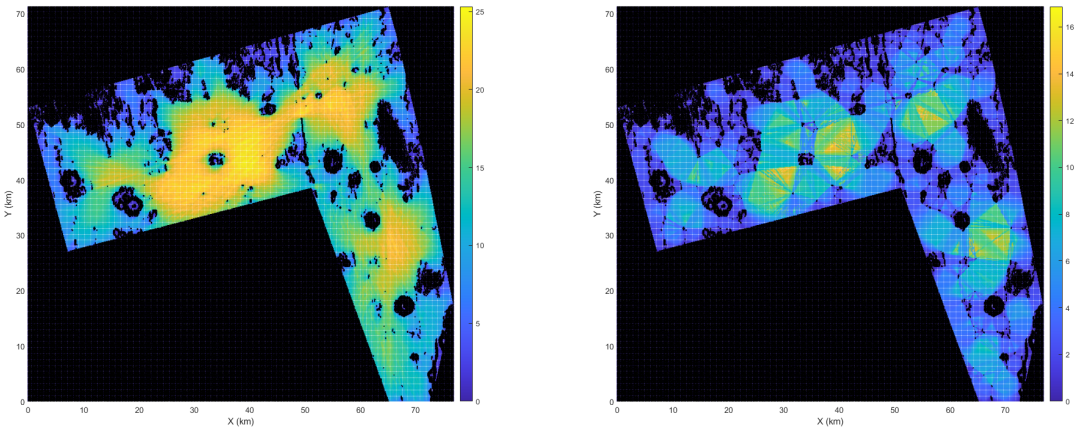

Figure B.11: On the left the mean SLD of site 7. On the right the minimum SLD (any direction) of site 7.

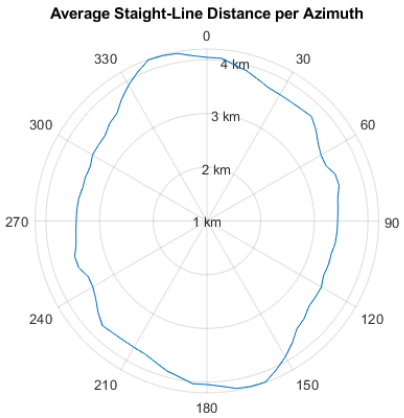

Figure B.12: The average SLD in each azimuth for site 7.

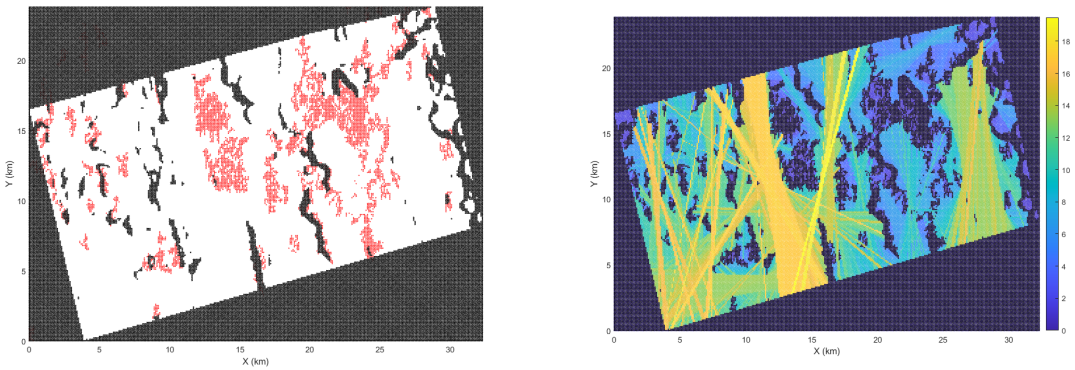

Figure B.13: On the left the constrained areas of site 8. Nodule type 2 & 3 indicated in red. Boundaries and slopes above threshold in black. On the left the maximum SLD

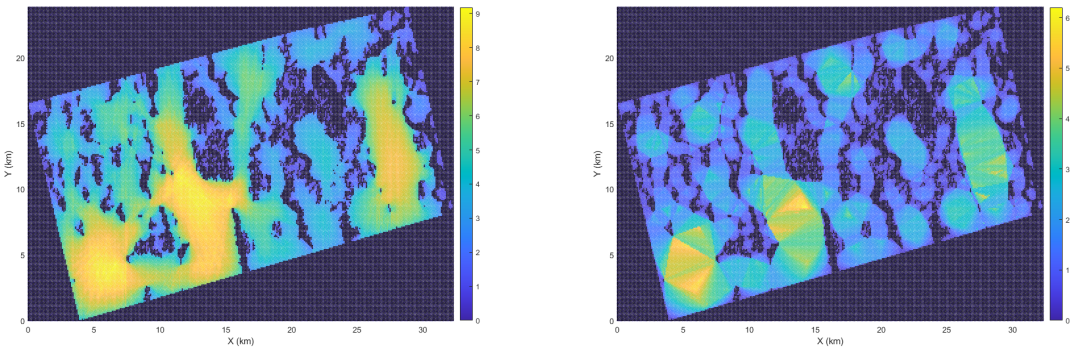

Figure B.14: On the left the mean SLD of site 8. On the right the minimum SLD (any direction) of site 8.

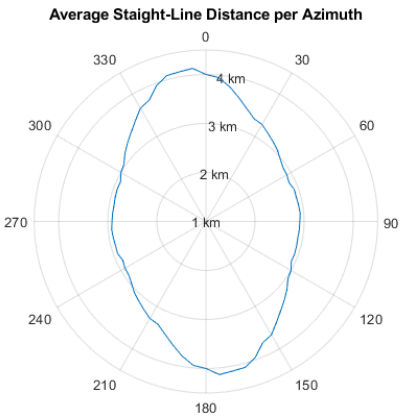

Figure B.15: The average SLD in each azimuth for site 8.

C

Appendix: Tables from Field Shape Analysis

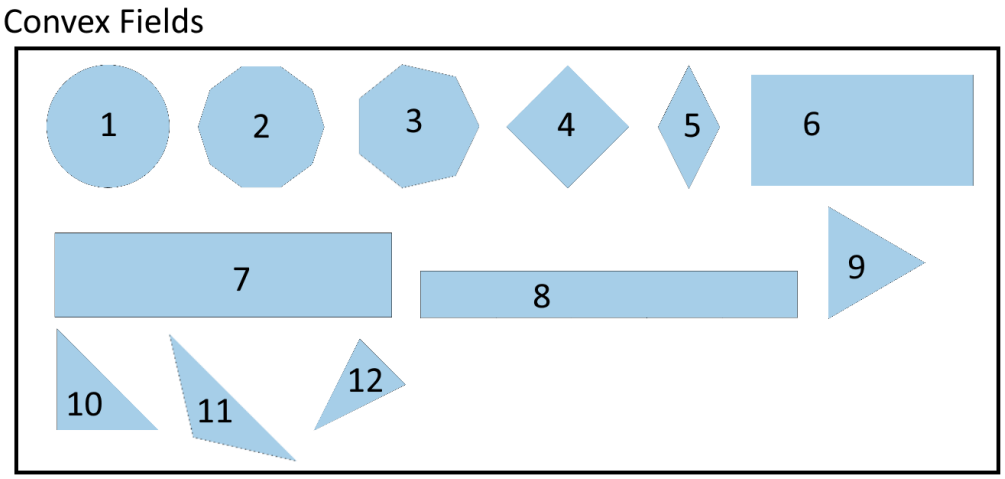

Figure C.1: The shape of all 12 convex fields that were analyzed for their shape indices.

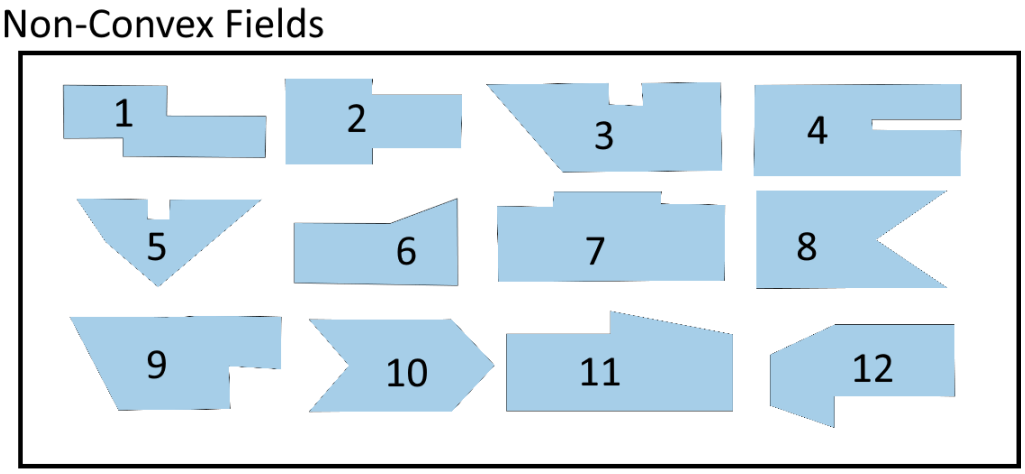

Figure C.2: The shape of all 12 non-convex fields that were analyzed for their shape indices.

	Field Base	Field 1	Field 2	Field 3	Field 4	Field 5	Field 6	Field 7	Field 8	Field 9	Field 10
Obstacle field coverage [%]	0.0%	5.0%	5.0%	5.0%	5.0%	4.9%	10.0%	9.3%	9.7%	9.3%	9.6%
Number of obstacles [−]	0	2	5	10	20	50	2	5	10	20	50
Average Production [kg/s]	19.0	16.6	16.7	16.1	16.5	14.9	17.1	15.6	15.4	15.6	14.6
Average Mining Rate [m^2/s]	1.8	1.7	1.7	1.7	1.7	1.6	1.7	1.7	1.7	1.7	1.6
Average Velocity [m/s]	0.29	0.28	0.29	0.29	0.29	0.28	0.29	0.29	0.29	0.28	0.28
Displacement [km]	69.3	73.1	72.9	74.1	73.7	86.5	66.9	74.7	74.6	78.1	79.1
Total duration [hrs]	65.4	71.4	70.9	72.2	71.6	85.9	64.1	72.6	72.7	76.5	78.8
Effective area covered [m^2]	4.00E+05	3.71E+05	3.71E+05	3.62E+05	3.66E+05	3.84E+05	3.46E+05	3.49E+05	3.43E+05	3.62E+05	3.44E+05
Area losses [m^2]	1.60E+04	6.73E+04	6.66E+04	8.22E+04	7.62E+04	1.36E+05	5.53E+04	9.87E+04	1.05E+05	1.06E+05	1.31E+05
Number of 180 degree turns [−]	35	35	35	35	35	35	35	35	35	35	35
Total nodules mined [t]	4.46E+03	4.27E+03	4.27E+03	4.19E+03	4.25E+03	4.62E+03	3.95E+03	4.09E+03	4.03E+03	4.28E+03	4.15E+03
Total nodules in-field [t]	1.75E+04	1.75E+04	1.75E+04	1.75E+04	1.75E+04	1.75E+04	1.75E+04	1.75E+04	1.75E+04	1.75E+04	1.75E+04
Spacing between lanes [m]	1	1	1	1	1	1	1	1	1	1	1

Table C.1: The KPI's for the field analysis of the obstacle fields. The average mining rate includes losses due to turning and excludes overlapping. Area losses are due to overlapping or turning

	Field 1	Field 2	Field 3	Field 4	Field 5	Field 6	Field 7	Field 8	Field 9	Field 10	Field 11	Field 12
Average Production [kg/s]	16.9	16.8	16.5	17.3	14.2	17.2	17.0	16.9	17.1	17.3	17.8	16.8
Average Mining Rate [m^2/s]	1.7	1.7	1.7	1.7	1.6	1.7	1.7	1.7	1.7	1.7	1.7	1.7
Average Velocity [m/s]	0.29	0.29	0.29	0.29	0.28	0.29	0.29	0.29	0.29	0.29	0.29	0.29
Displacement [km]	69.1	153.0	81.1	143.7	75.8	111.6	120.3	134.9	111.2	128.1	117.6	133.8
Total duration [hrs]	66.4	146.2	77.4	136.8	74.7	106.3	114.6	129.0	105.7	121.7	111.4	128.2
Effective area covered [m^2]	3.45E+05	7.56E+05	3.89E+05	7.33E+05	3.13E+05	5.64E+05	6.03E+05	6.71E+05	5.55E+05	6.50E+05	6.18E+05	6.64E+05
Area losses [m^2]	6.93E+04	1.62E+04	9.69E+04	1.29E+05	1.42E+04	1.05E+05	1.19E+05	1.38E+05	1.13E+05	1.19E+05	8.77E+04	1.39E+05
Total nodules mined [t]	4.03E+03	8.83E+03	4.59E+03	8.52E+03	3.82E+03	6.55E+03	7.02E+03	7.85E+03	6.51E+03	7.57E+03	7.12E+03	7.76E+03
Total nodules in-field [t]	1.75E+04	1.75E+04	1.75E+04	1.75E+04	1.75E+04	1.75E+04	1.75E+04	1.75E+04	1.75E+04	1.75E+04	1.75E+04	1.75E+04
Spacing between lanes [m]	1	1	1	1	1	1	1	1	1	1	1	1

Table C.2: The KPI's for the field analysis of the non-convex fields. The average mining rate includes losses due to turning and excludes overlapping. Area losses are due to overlapping or turning

	Field 1	Field 2	Field 3	Field 4	Field 6	Field 7	Field 9	Field 10
Average Production [kg/s]	17.5	17.6	17.5	16.7	18.3	18.4	15.9	16.1
Average Mining Rate [m^2/s]	1.7	1.7	1.7	1.7	1.7	1.7	1.6	1.6
Average Velocity [m/s]	0.29	0.29	0.29	0.28	0.29	0.29	0.28	0.28
Displacement [km]	53.1	51.8	48.2	34.6	34.6	16.2	22.6	20.3
Total duration [hrs]	51.4	50.0	46.6	34.0	33.1	15.5	22.5	20.2
Effective area covered [m^2]	2.87E+05	2.80E+05	2.59E+05	1.79E+05	1.95E+05	9.14E+04	1.10E+05	1.01E+05
Area losses [m^2]	3.18E+04	3.08E+04	3.04E+04	2.85E+04	1.27E+04	5.58E+03	2.55E+04	2.07E+04
Total nodules mined [t]	3.25E+03	3.16E+03	2.93E+03	2.05E+03	2.19E+03	1.02E+03	1.29E+03	1.17E+03
Total nodules in-field [t]	1.75E+04	1.75E+04	1.75E+04	1.75E+04	1.75E+04	1.75E+04	1.75E+04	1.75E+04
Spacing between lanes [m]	6	6	6	6	6	6	6	6

Table C.3: The KPI's for the field analysis of the convex fields. The average mining rate includes losses due to turning and excludes overlapping. Area losses are due to overlapping or turning

	Field 1	Field 2	Field 3	Field 4	Field 5	Field 6	Field 7	Field 8	Field 9	Field 10	Field 11	Field 12
Area [m^2]	698378	1210600	648581	1326900	543206	840763	1012600	1050604	885220	992374	946380	992215
Convexity	0.83	0.89	0.95	0.95	0.94	0.90	0.96	0.81	0.93	0.88	0.94	0.88
Compactness	0.39	0.46	0.50	0.38	0.42	0.57	0.58	0.43	0.55	0.58	0.58	0.57
Rectangularity	0.72	0.81	0.80	0.94	0.50	0.76	0.91	0.81	0.77	0.77	0.83	0.71
Triangularity	0.85	0.84	0.85	0.86	0.90	0.83	0.73	0.92	0.83	0.81	0.75	0.79
Ellipticity	0.80	0.81	0.81	0.79	0.62	0.82	0.93	0.74	0.82	0.84	0.91	0.87
ROPM	0.28	0.43	0.41	0.45	0.52	0.41	0.38	0.63	0.50	0.62	0.38	0.42
curb ratio	0.08	0.05	0.07	0.06	0.09	0.06	0.05	0.06	0.06	0.06	0.06	0.06
radius of the incircle [m]	234	427	265	393	240	314	330	408	354	400	328	308
Shape Estimated Overhead	0.077	0.069	0.065	0.061	0.078	0.071	0.057	0.094	0.073	0.085	0.062	0.075
Shape Est Overhead Std	0.027	0.024	0.024	0.022	0.031	0.025	0.021	0.027	0.025	0.025	0.023	0.026
Model Estimated Overhead	0.201	0.021	0.249	0.176	0.045	0.187	0.198	0.206	0.203	0.183	0.142	0.209

Table C.4: The shape factors and resulting overhead estimation of the non-convex fields. Includes the comparison with the Allseas model estimation.

	Field 1	Field 2	Field 3	Field 4	Field 6	Field 7	Field 9	Field 10
Area [m^2]	781616	732270	681309	498002	500000	250000	323352	320000
Convexity	1.00	1.00	1.00	1.00	1.00	1.00	1.00	1.00
Compactness	1.00	0.97	0.93	0.79	0.70	0.50	0.60	0.54
Rectangularity	0.79	0.77	0.74	1.00	1.00	1.00	0.50	0.50
Triangularity	0.68	0.69	0.69	0.75	0.75	0.75	1.00	1.00
Ellipticity	1.00	1.00	0.99	0.91	0.91	0.91	0.68	0.68
ROPM	1.00	1.00	1.00	1.00	0.50	0.25	1.00	0.58
curb ratio	0.05	0.05	0.05	0.07	0.07	0.12	0.09	0.10
radius of the incircle [m]	498	475	449	354	251	126	249	235
Shape Estimated Overhead	0.088	0.089	0.091	0.084	0.059	0.054	0.104	0.088
Shape Est Overhead Std	0.023	0.023	0.024	0.021	0.020	0.022	0.030	0.029
Model Estimated Overhead	0.111	0.110	0.118	0.159	0.065	0.061	0.231	0.205

Table C.5: The shape factors and resulting overhead estimation of the convex fields. Includes the comparison with the Allseas model estimation.

D

Appendix: Methods for Calculating Shape Indices

Eight shape indices are calculated in this thesis. The methods are described fully in Oksanen [2013], Oksanen and Visala [2009], and Rosin [2003].

1. **Convexity**. The area of the field is compared to the area of the convex hull.
2. **Compactness**. This index describes how circular the area is, calculated by the following formula where A is the area of the field and P is the perimeter or circumference.

$$\text{Compactness} = 4\pi \frac{A}{P^2} \tag{D.1}$$

3. **Rectangularity**. This index describes how rectangular the area is. This is determined by calculating the minimum bounding rectangle using an algorithm from Diener [2020]. The ratio between the area of the original region and the area of the bounding rectangle gives the index for rectangularity.
4. **Triangularity**. This index and the following use moments for 2-dimensional polygons. The moment of order p and q can be calculated by integrating over the polygon's interior, equation D.2. For this thesis the algorithm from Marin [1984] is used.

$$m_{pq} = \int\int x^p x^q \, dx dy \tag{D.2}$$

   For calculating the triangularity, the moment invariant method is used from Rosin [2003], equation D.3

$$I_1 = \frac{m_{20} m_{02} - m_{11}^2}{m_{00}^4} \tag{D.3}$$

   The triangularity is calculated as:

$$T = \begin{cases} 108 I_1 & \text{if } I_1 \leq \frac{1}{108} \\ \frac{1}{108 I_1} & \text{otherwise} \end{cases} \tag{D.4}$$

5. **Ellipticity**. The Ellipticity is using the same moment invariant.

$$E = \begin{cases} 16\pi^2 I_1 & \text{if } I_1 \leq \frac{1}{16\pi^2} \\ \frac{1}{16\pi^2 I_1} & \text{otherwise} \end{cases} \tag{D.5}$$

6. **Ratio of principal moments**. This is the ratio between the first principal moment and second principal moment. For rectangular shapes this is the aspect ratio between the two sides.
7. **Radius of the incircle**. Calculated by using an image transform algorithm from Birdal [2020].
8. **'Curb index'**. Introduced by Oksanen [2013]. The outside of the field is offset inwards. This is the so-called 'curb'. This simulates the effect of driving one time around the field with a harvester. The 'curb index' is the area of the field compared to compared to the area of the field without the curb.

E

Appendix: Additional Fields with Sequences

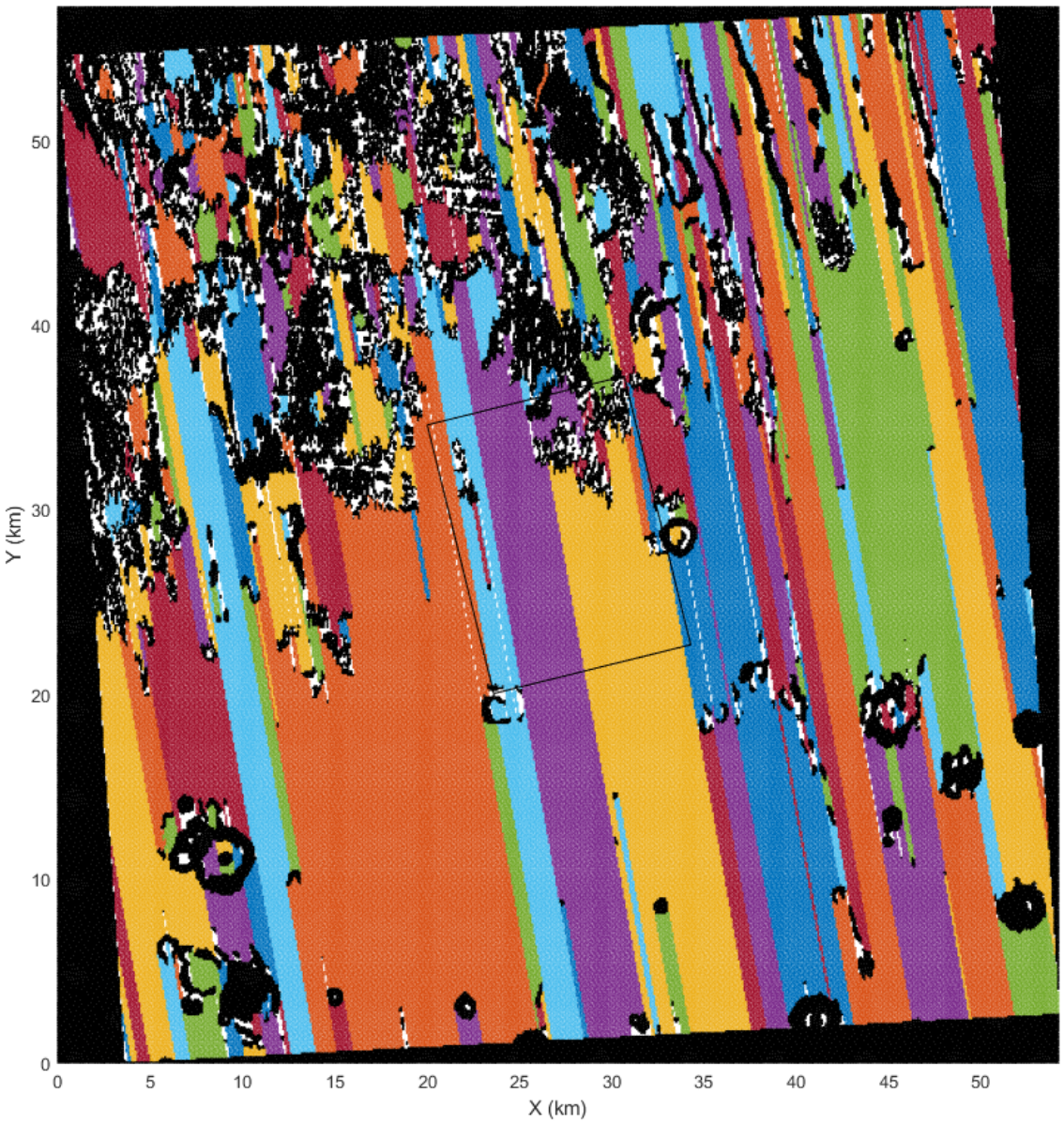

Figure E.1: Fields around the PMT area (indicated with black lines).

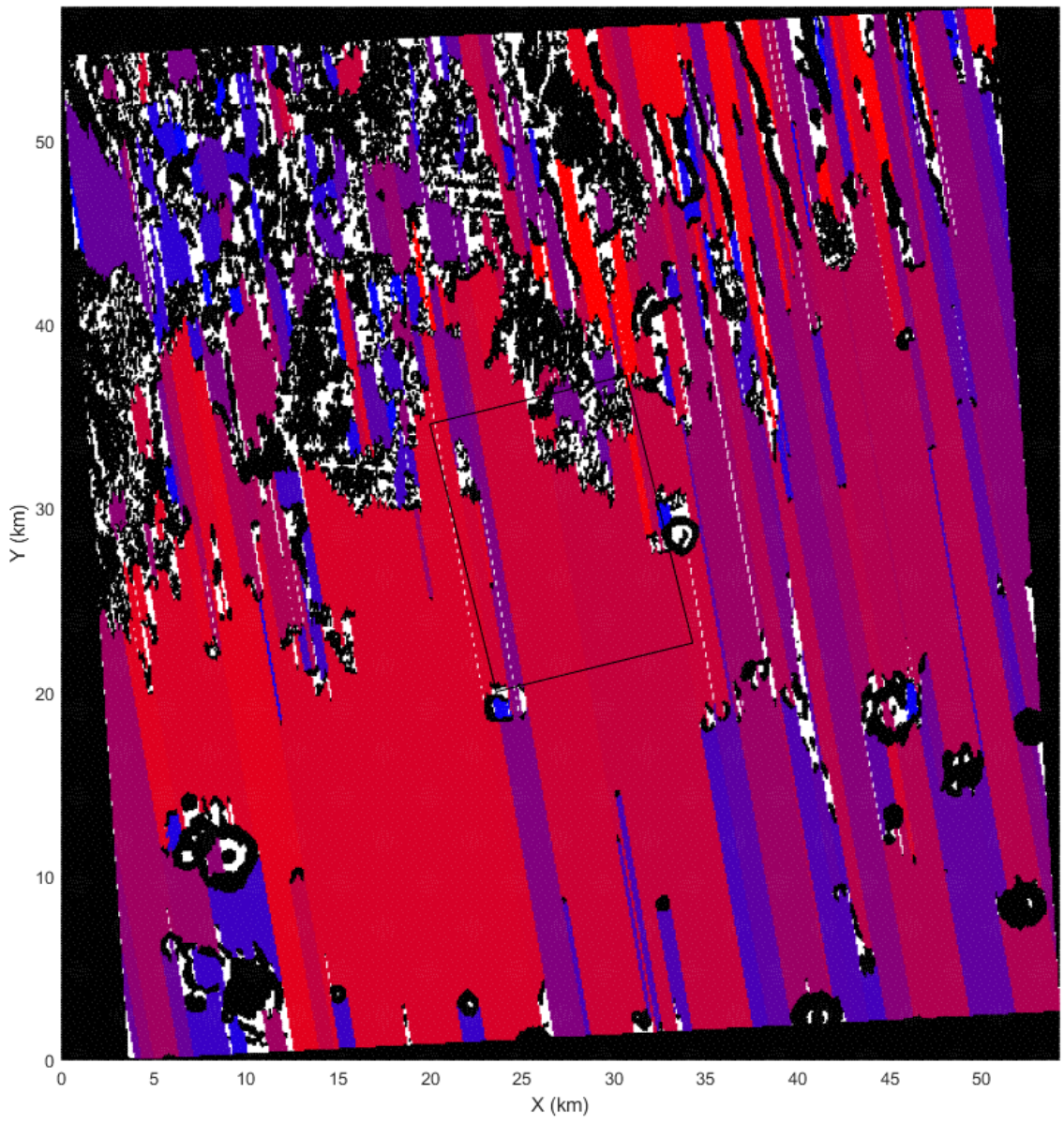

Figure E.2: Sequence of the fields around the PMT area. Colour code is that red is first and blue later.

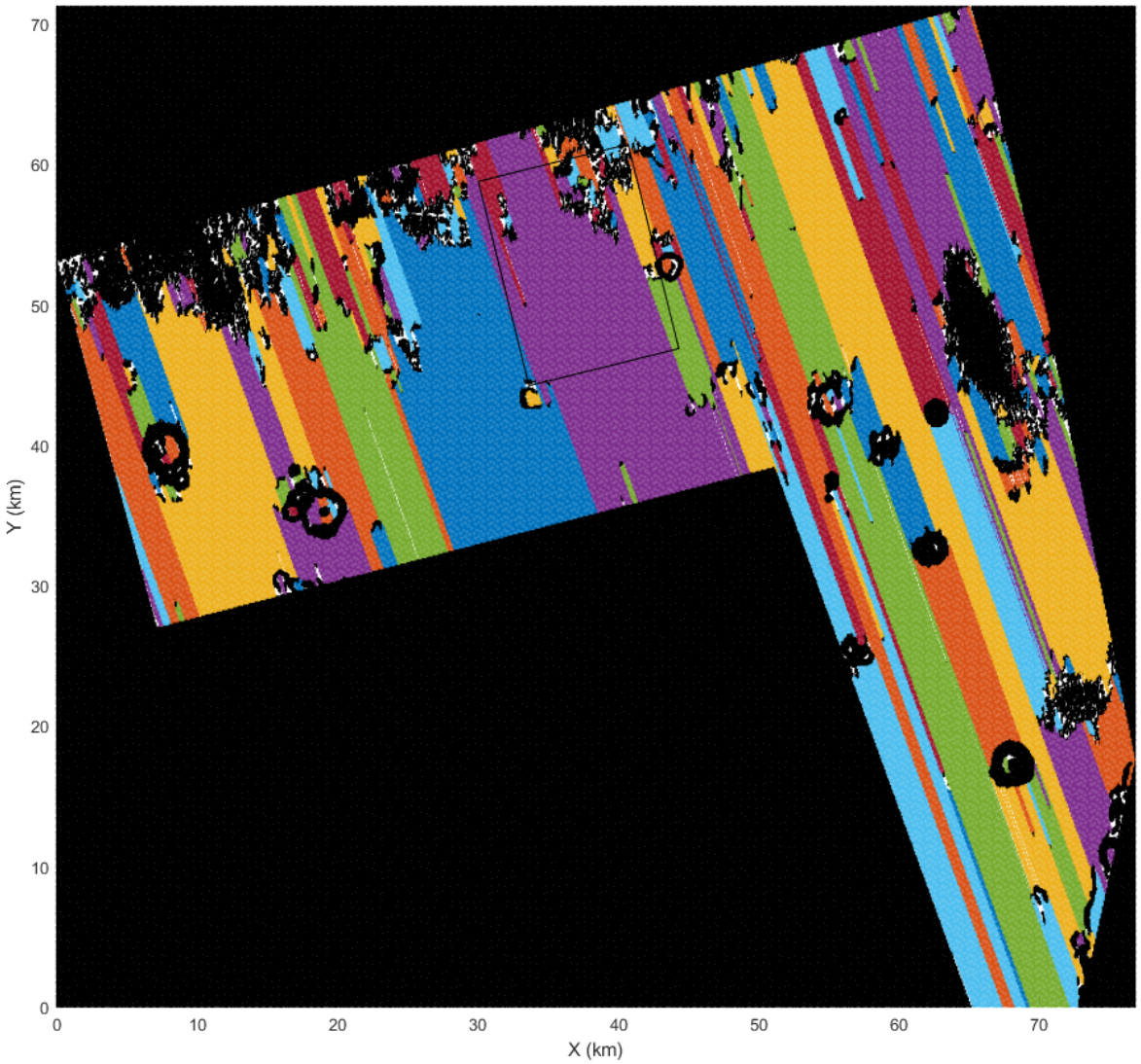

Figure E.3: The long fields generated for site 7. PMT area is indicated in black lines.

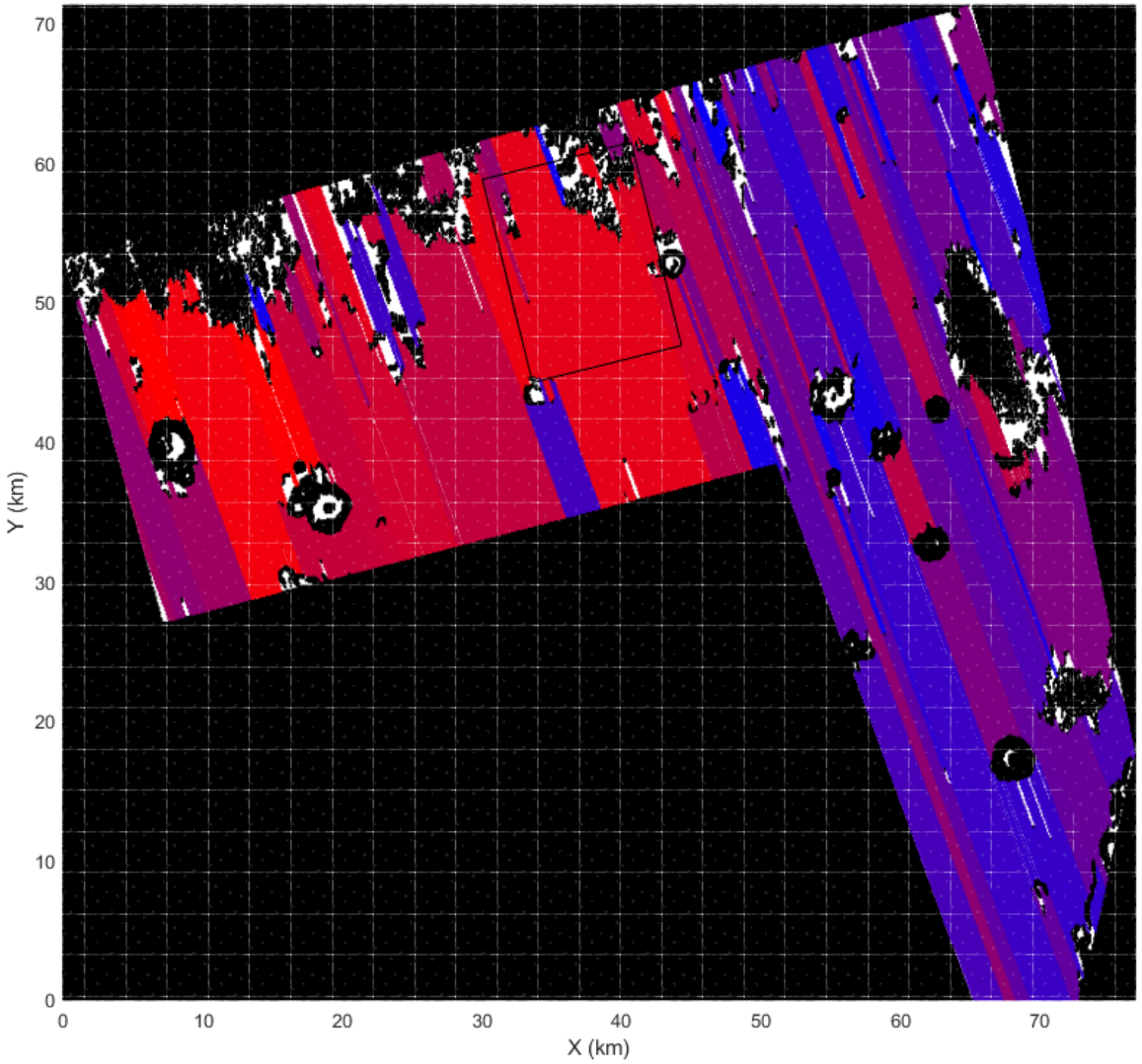

Figure E.4: The fields generated for site 7 displayed in sequence.Colour code is that red is first and blue later.